January 2011

Opposing Crosstalk between Rho1 and Cdc42 in Epithelial Morphogenesis

Steve Warner
Washington University in St. Louis

WASHINGTON UNIVERSITY IN ST. LOUIS

Division of Biology and Biomedical Sciences

Molecular Cell Biology

Dissertation Examination Committee:
Gregory Longmore, Chair
Thomas Baranski
Kendall Blumer
Kathryn Miller
Andrey Shaw
James Skeath

OPPOSING CROSSTALK BETWEEN RHO1 AND CDC42 IN EPITHELIAL MORPHOGENESIS

by

Stephen James Warner

A dissertation presented to the
Graduate School of Arts and Sciences
of Washington University in
partial fulfillment of the
requirements for the degree
of Doctor of Philosophy

May 2011

Saint Louis, Missouri

ABSTRACT OF THE DISSERTATION

Opposing crosstalk between Rho1 and Cdc42 in epithelial morphogenesis

by

Stephen James Warner

Doctor of Philosophy in Biology and Biomedical Sciences
(Molecular Cell Biology)

Washington University in St. Louis, 2011

Professor Gregory Longmore, Chairperson

Epithelial cells line all surfaces of the body exposed to external environments where they perform critical roles for maintaining homeostasis. In addition, epithelial cells are implicated in several disease processes and are the most common cell type implicated in cancer. Therefore, understanding the regulation of epithelial cell development and function has important implications for adult homeostasis and disease states. The Rho family of small GTPases functions in a wide array of cellular processes in epithelial cells. However, in mammals Rho subfamilies have multiple members, often with overlapping roles, complicating the precise determination of Rho protein function in epithelial cells, especially *in vivo*. In *Drosophila*, two Rho subfamilies have only one member, Rho1 and Cdc42, which allows for straightforward loss-of-function analysis, *in vivo*. To determine the role of Rho1 and Cdc42 in *Drosophila* epithelia, we used mosaic clonal analysis and targeted RNA interference expression to perform loss-of-function studies with Rho1 and Cdc42 during pupal eye and larval imaginal disc morphogenesis. First, clonal analysis in

the post-mitotic *Drosophila* pupal eye epithelium demonstrated that Rho1 was required to maintain AJ integrity independent of its role in sustaining apical cell tension. Rho1 depletion disrupted adherens junctions only when depleted in adjacent cells. Rho1 maintained AJs by inhibiting DE-cadherin endocytosis in a Cdc42/Par6-dependent manner. In contrast, depletion of Rho1 in single cells decreased apical tension, and Rok and Myosin were necessary downstream of Rho1 to sustain apical cell tension. Second, clonal analysis in the pupal eye epithelium further demonstrated that Cdc42 was also critical in limiting apical cell tension. It did so by localizing Par6/aPKC to AJs, where this complex limited Rho1 activity, and thus, acto-myosin contractility. Lastly, studies in larval imaginal discs identified Cdc42 and the Par polarity complex as novel regulators of apoptosis-induced compensatory proliferation. Depletion or disruption of this complex from AJs induced JNK-dependent apoptosis and compensatory proliferation. This was mediated by increased Rho1-Rok activation downstream of Cdc42 depletion, and Rok's regulation of Myosin activity but not F-actin activated JNK. Therefore, opposing crosstalk between Rho1 and Cdc42 dictates epithelial cell shape, junctions, and compensatory proliferation during morphogenesis.

Acknowledgements

I would like to thank my mentor, Greg Longmore, for all his support and encouragement during the past two years, especially for his willingness to support and contribute to a direction of research divergent from that of his lab. I also thank the members of the Longmore lab for technical assistance and advice and for providing an enjoyable atmosphere in which to work.

I would like to thank Ross Cagan and the former members of the Cagan lab for support and assistance during the initial stages of this project, especially Sujin Bao who taught me the basics of *Drosophila* work. I am grateful for early advice and suggestions from Craig Micchelli, which helped shape the experimental designs and directions of these studies. I appreciate funding from the MSTP training grant and the NIH.

I acknowledge the members of my thesis committee, Jim Skeath, Tom Baranski, Ken Blumer, Kathy Miller, and Andrey Shaw for their advice and encouragement about my thesis as well as career directions. I would especially like to thank Jim Skeath for acting as the chair of my committee and for his generosity in providing reagents for the project. In addition, I am grateful to Andrey Shaw and the Department of Pathology for their willingness to provide a confocal microscope to use.

Furthermore, I thank my family and friends for encouragement throughout this work. I am especially grateful for my parents for their continued and unconditional support throughout all phases of my life. Lastly, I would like to thank my wife, Poppy, and my son, Logan, for always providing the highlights of my day.

Table of Contents

List of Figures

Chapter 2

Chapter 3

Chapter 4

List of Tables

Chapter 2

Chapter 3

Chapter 4

CHAPTER 1

Introduction

Epithelial cell biology

Epithelia are one of the four basic tissue types in body. An epithelium is composed of sheets of cells that line the internal and external surfaces of the body, and at these surfaces, epithelial cells perform several specialized functions, such as absorption, secretion, and protection. While epithelial cells are critical for these homeostatic functions, they are also implicated in several disease processes. Most notably, epithelial cells are the most common cell type implicated in cancer (Tanos and Rodriguez-Boulan, 2008).

One unique characteristic of epithelial cells that allows them to perform these specialized functions is distinct apical-basal polarity. Epithelial cells require contact with a basement membrane for survival, and the cell surface in contact with the basement membrane is termed the basal membrane. The portion of the epithelial cell juxtaposed to neighboring epithelial cells is the lateral membrane, and the apical membrane of an epithelial cell is exposed to the external or internal environment of the body. The apical-basal polarity of an epithelial cell is not only seen with regard to the cellular membrane but is also apparent intracellularly, with polarized locations of intracellular organelles and cytoskeleton. This polarized nature is required for epithelial cells to function properly, and disruption of epithelial cell polarity is often an early event in the development of epithelial tumors (carcinoma) (Tanos and Rodriguez-Boulan, 2008).

Important components of epithelial cells that help maintain their polarity, among other functions, are intercellular junctions. The two predominant intercellular epithelial junctions are adherens junctions (AJs) and tight junctions (TJs). AJs mediate cell-cell

adhesion between epithelial cells by linking to the actin cytoskeleton, while TJs limit paracellular diffusion between neighboring epithelial cells and diffusion of membrane constituents between the apical and basal-lateral membranes. While formation of AJs and TJs is important for the establishment of epithelial cell polarity in a nascent epithelium (Nejsum and Nelson, 2009; Tanos and Rodriguez-Boulan, 2008), the role of AJs and TJs in maintenance of epithelial polarity in a formed epithelium is not well known. Also, AJs and TJs are often disorganized in carcinoma development (Etienne-Manneville, 2008; Jeanes et al., 2008), and while the formation of nascent AJs and TJs has been well characterized (Knust and Bossinger, 2002; Yap et al., 2007), how AJs and TJs are maintained in a mature epithelium has received much less attention.

Drosophila epithelial morphogenesis

Because of its genetic tractability, *Drosophila* have emerged as an important model organism in many biological systems, including epithelial morphogenesis. *Drosophila* epithelia begin as primordial tissues specified in the embryo. In larval development, epithelial tissues undergo extensive proliferation and become imaginal discs, which develop as epithelial monolayer tissues that give rise to several adult structures, such as eyes, wings, legs, and antennae. During pupation, the final stages of development, these epithelial tissues mainly undergo differentiation as opposed to proliferation.

Drosophila epithelia have highly conserved AJs compared to mammals, with conservation in structure, function, and protein constituents (Knust and Bossinger, 2002).

The AJs in *Drosophila*, as in mammals, consists of a transmembrane protein as the core component, called Epithelial cadherin (E-cadherin), which binds to other E-cadherin molecules in neighboring cells. The intracellular side of E-cadherin is bound to proteins of the catenin family, namely α-catenin, β-catenin, and p120-catenin, which are thought to mediate linkage of E-cadherin to the actin cytoskeleton, to modulate E-cadherin binding strength, and to regulate E-cadherin membrane trafficking (Bryant and Stow, 2004; Gates and Peifer, 2005; Gumbiner, 2005). The mammalian TJ has a functionally homologous structure in *Drosophila* called the septate junction (SJ), and unlike the TJ, which lies apical to the AJ, the SJ lies basal to the AJ along the basal-lateral membrane (Furuse and Tsukita, 2006; Knust and Bossinger, 2002).

Analyses of epithelial morphogenesis during each of the three main stages of *Drosophila* development (embryo, larval, and pupal) have contributed to our understanding of epithelial biology. Specifically, studies in embryonic and larval epithelia have highlighted the importance of epithelial polarity regulation (Bilder, 2004). Three main protein complexes have been identified as being important for polarity regulation in *Drosophila* epithelia, and these polarity complexes are conserved in mammals. These include the Crumbs, the Par, and the Scribble polarity complex (Assemat et al., 2008). Disruption of epithelial polarity by mutating members from each of these complexes results in epithelial hyperproliferation (Bilder, 2004), and this link between epithelial polarity disruption and increased proliferation has subsequently been demonstrated in mammalian systems (Dow and Humbert, 2007). However, even though a

relationship between epithelial polarity and proliferation is well established, how epithelial polarity regulates proliferation is not well understood.

While embryonic and larval epithelia have been critical in demonstrating the functional importance of polarity establishment and maintenance, pupal epithelia have been useful for characterizing epithelial cell shape, adhesion, and intercellular junctions (Bao and Cagan, 2005; Carthew, 2005; Classen et al., 2005). The pupal eye develops as a post-mitotic monolayer neuroepithelium and is composed of an orderly array of approximately 800 individual units called ommaditidia (Cagan and Ready, 1989). Each ommaditidum is composed of 26 cells, consisting of a neuronal core with eight photoreceptor neurons and four lens-secreting cone cells. Each neuronal core is optically insultated from neighboring ommatidia by sets of pigment epithelial cells (PECs). Two primary PECs are immediately adjacent to the neuronal core, and six secondary PECs and three tertiary PECs form a hexagonal pattern around each ommatidium. Three mechanosensory bristles occupy alternating vertices of the hexagon. During the beginning of puparium formation, the PECs of the pupal eye cease proliferation and begin to undergo differentiation (Wolff and Ready, 1991). By 40 hours after puparium formation, PECs occupy their final position within the ommatidum and continue to differentiate (Cagan and Ready, 1989). At this stage, the PECs form a precisely ordered hexagonal pattern with extremely high fidelity. In this pattern, PECs have defined intercellular junctions (AJs and SJs) and repeating cell shapes, which facilitates identification of perturbations to these two properties.

The Rho GTPase Family

Rho GTPases are known for their regulation of actin cytoskeleton dynamics and have been demonstrated to function in several other cellular processes, including gene transcription, cell-cycle progression, vesicle transport, and polarity regulation (Hall, 2005). Rho proteins are members of the Ras superfamily of small GTPases, which function as molecular switches, alternating between a GTP-bound, active form and a GDP-bound, inactive form. Three classes of GTPase regulatory proteins modulate the activation status of Rho proteins. Guanine nucleotide-exchange factors (GEFs) promote Rho activation, while GTPase-activating proteins and guanine nucleotide-dissociation inhibitors (GDIs) inhibit Rho activation (Bos et al., 2007). When in the active, GTP-bound form, Rho proteins bind to effector proteins, which mediate downstream signaling events and cellular functions (Bishop and Hall, 2000).

In mammals, at least 20 Rho family protein members exist and are divided into eight subfamilies based on protein sequence similarity (Vega and Ridley, 2007). Three subfamilies, Rho, Rac, and Cdc42, have high conservation across species and have been studied extensively. Each of these subfamilies has multiple members, with the Rho subfamily containing RhoA, RhoB, and RhoC, the Rac subfamily containing Rac1, Rac2, Rac3, and RhoG, and the Cdc42 family containing Cdc42, TC10, TCL, Wrch1, and Chp/Wrch2. In addition, each of these individual Rho proteins often binds to and activates several effector proteins, creating signaling pathways with many potential permutations (Bishop and Hall, 2000).

With the potential for redundancy from multiple family members and effectors, one approach frequently used to facilitate functional studies of Rho proteins is expression of dominant-negative (DN) or constitutively active (CA) protein forms. DN proteins function by binding to GEFs and inhibiting effector activation, thereby acting as a sink for GEFs that activate a Rho protein. CA proteins are unable to hydrolyze GTP to GDP and so continuously activate effector proteins. However, because multiple Rho family members share both upstream GEFs and downstream effector proteins, DN and CA protein expression can affect the activities of several Rho proteins (Heasman and Ridley, 2008). Therefore, determining a Rho protein's function requires specific loss-of-function analyses, which is complicated in mammalian systems with multiple Rho family members.

As opposed to the 8 subfamilies containing at least 20 Rho proteins in mammals, *Drosophila* have only 3 subfamilies and 5 Rho proteins (Johndrow et al., 2004). The Rho subfamily contains only Rho1, the Cdc42 family contains only Cdc42, and the Rac subfamily contains Rac1, Rac2, and Mtl. Loss-of-function mutations have been generated for all 5 *Drosophila* Rho proteins and have contributed valuable insight into Rho protein function *in vivo*. While these loss-of-function studies have demonstrated the importance of Rho proteins in neurogenesis and embryogenesis, the role of these proteins in epithelial morphogenesis beyond the embryo stage has not been well characterized.

Rho GTPase function in epithelial junctions

The Rho GTPases have been shown to function in regulation of epithelial AJs and TJs. In mammalian tissue culture systems, both increased and decreased RhoA activation has been shown to disrupt AJs (Sahai and Marshall, 2002). Increased RhoA activation, leading to activation of the Rho effector, Rho-associated kinase (ROCK), and subsequent increased acto-myosin contractility resulted in disruption of AJs between cultured epithelial cells. In addition, inhibition of Rho subfamily activity with the cell-permeable botulinum toxin C3 also disrupted of AJs. This was a result of decreased activation of another RhoA effector, the diaphanous-related formin Dia1, which promotes linear F-actin polymerization. This study highlighted the importance of Rho in AJ regulation, at least in mammalian tissue culture systems.

A role for Rho family proteins in nascent AJ formation has also been demonstrated during *Drosophila* embryo dorsal closure, a process where lateral epidermal sheets fuse along the midline to cover the extraembryonic amnioserosa and seal a dorsal hole (Jacinto et al., 2002). Expression of DN and CA Rho proteins or loss-of-function mutations for Rho1, Cdc42, or Rac1/Rac2/Mtl have resulted in embryos with dorsal holes, implicating all three *Drosophila* Rho families in this process (Hakeda-Suzuki et al., 2002; Harden et al., 1999; Magie et al., 1999). It is thought that the ability of Rho proteins to regulate F-actin assembly in the lateral epidermal cells is responsible for the effects of interfering with Rho protein function on the dorsal closure process.

Rho1 has also been demonstrated to function in nascent AJ formation in earlier stages of *Drosophila* embryogenesis. As in mammalian tissue culture, the role of Rho1 in AJ formation is thought to be mediated through the Rho1 effector Dia and its ability to

promote F-actin polymerization (Homem and Peifer, 2008). Mammalian tissue culture systems and *Drosophila* embryogenesis provide useful model systems to study AJ formation in cells where AJs are continually being disassembled and formed as cells proliferate. However, whether Rho proteins regulate AJs in remodeling epithelial cells with formed AJs, similar to that which occurs in adult epithelia, has not been addressed.

Rho GTPase regulation of epithelial cell shape

Epithelial cells have diverse shapes, ranging from flat and long squamous cells to tall and thin columnar cells (Montell, 2008). These cell shapes are not only important for proper epithelial cell function, but a prominent characteristic of malignant epithelial cells is aberrant cell morphology (Clark et al., 2007). A major determinant of epithelial cell shape is the activity of the acto-myosin cytoskeleton, which can be modulated by affecting F-actin polymerization or myosin activity. Myosin activity is regulated by phosphorylation of the myosin light chain (MLC). Phosphorylation of MLC results in activation of myosin, which then pulls on F-actin cables to cause cell contraction (Conti and Adelstein, 2008). A major regulator of MLC phosphorylation is the Rho effector ROCK, which can either directly phosphorylate MLC or indirectly phophosphorylate MLC by phosphorylation and activation of MLC-kinase or phosphorylation and inactivation of MLC-phosphatase (Olson and Sahai, 2009). While the mechanism by which Rho/ROCK functions to regulate myosin activity and epithelial cell shape has been well characterized, how Rho/ROCK is regulated to control epithelial cell shape is not clear. As misregulation of epithelial cell shape is critical for migration and invasion of

malignant epithelial cells (Olson and Sahai, 2009), determining how epithelial cell shape is regulated may provide insight into this process.

Rho GTPase regulation of epithelial polarity

The role of Rho GTPases in epithelial polarity has recently been demonstrated using an *in vitro* system where Madin-Darby canine kidney (MDCK) epithelial cells are grown in three-dimensional cysts, spherical epithelial monolayers with a lumen. Formation of MDCK cysts requires proper epithelial polarity establishment (Montesano et al., 1991). Depletion of Cdc42 from MDCK cells impairs their ability to polarize and form cysts with a proper lumen, demonstrating that Cdc42 has important functions for epithelial polarity and morphogenesis into cysts (Martin-Belmonte et al., 2007). This study suggested that phosphatidylinositol 4,5-bisphosphate recruits Cdc42 to the apical membrane, and the apical localization of Cdc42 then controls epithelial polarity and cyst morphogenesis. However, how Cdc42 regulates epithelial polarity subsequent to its apical localization is not well known.

Rac1 has also been demonstrated to function in MDCK cystogenesis. Expression of Rac1-DN in MDCK cells results in inversion of cyst polarity, causing proteins normally localized to the apical membrane to localize to the basal membrane (O'Brien et al., 2001). A recent study suggests that the ability of Rac1-DN expression to cause inverted polarity of MDCK cysts is due to increased RhoA activation (Yu et al., 2008). Rac1-DN expression activated RhoA, which led to activation of ROCK I and myosin II and inversion of MDCK cyst polarity. However, how RhoA/ROCK I/myosin II activation

results in inverted polarity is not characterized. Furthermore, whether activation of RhoA signaling contributes to the polarity disruption following Cdc42 depletion is not known. In addition, while these studies were performed using an *in vitro* model of epithelial polarity and morphogenesis, if and how Rho GTPases function in epithelial polarity *in vivo* remains to be better characterized.

Thus far, the pleiotropic functions and multiple family members of Rho GTPases and their downstream effectors have impeded the precise determination of individual Rho protein function. The aim of this thesis was to use the array of genetic techniques and the well-characterized larval and pupal epithelial tissues in *Drosophila* to better understand the functions of Rho GTPases in epithelial morphogenesis.

CHAPTER 2

Distinct functions for Rho1 in maintaining adherens junctions and apical tension in remodeling epithelia

Chapter 2 represents a previously published article, entitled "Distinct functions for Rho1 in maintaining adherens junctions and apical tension in remodeling epithelia," which appeared in the Journal of Cell Biology, June 15, 2009, Vol. 185, pp. 1111-1125.

Distinct functions for Rho1 in maintaining adherens junctions and apical tension in remodeling epithelia

Stephen J. Warner and Gregory D. Longmore

Departments of Medicine and Cell Biology

Washington University, St. Louis, MO, 63110

Abstract

Maintenance and remodeling of adherens junctions (AJs) and cell shape in epithelia are necessary for the development of functional epithelia and commonly altered during cancer progression/metastasis. While formation of nascent AJs has received much attention, whether shared mechanisms are responsible for the maintenance and remodeling of AJs in a dynamic epithelia, particularly *in vivo*, is not clear. Using clonal analysis in post-mitotic *Drosophila* pupal eye epithelium, we demonstrate that Rho1 is required to maintain AJ integrity independent of its role in sustaining apical cell tension. Rho1 depletion in a remodeling, post-mitotic epithelium disrupts AJs but only when depleted in adjacent cells. Surprisingly, neither of the Rho effectors, Rok or Dia, is necessary downstream of Rho1 to maintain AJs, instead Rho1 maintains AJs by inhibiting DE-cadherin endocytosis in a Cdc42/Par6-dependent manner. In contrast, depletion of Rho1 in single cells decreases apical tension, and Rok and Myosin are necessary, while Dia function also contributes, downstream of Rho1 to sustain apical cell tension.

Introduction

A hallmark of epithelia is the presence of intercellular junctions. The two apical-most junctions are tight junctions and adherens junctions (AJs). AJs mediate adhesion between cells and, by coupling to the actomyosin cytoskeleton, provide for tension within epithelial sheets or between cells. The core component of AJs is E-cadherin, and proper localization and function of E-cadherin is critical for the development and morphogenesis of metazoans and maintenance of adult epithelia (Gumbiner, 2005).

Distinct E-cadherin adhesive functions are required during the formation and stabilization of newly forming or nascent AJs, as opposed to maintenance and remodeling of formed AJs (Capaldo and Macara, 2007). The former process has been extensively characterized using cell biological systems such as MDCK epithelial cells, where the formation of nascent AJs can occur between two single cells (Adams et al., 1998) or within a monolayer of cells in response to calcium (Gumbiner et al., 1988), and developmental systems such as *Drosophila* embryogenesis, where dorsal closure brings two epithelial sheets together to form nascent AJs (Jacinto et al., 2002). A less well understood process, in general, is the maintenance and remodeling of formed AJs as occurs in some adult tissue epithelium or during developmental morphogenesis. Adult, fully differentiated epithelia such as present in skin and intestine have stem cells that constantly replenish older epithelial cells as they are shed. To do so, these new epithelial cells need to remodel their junctions so as to migrate yet maintain junctions such that the epithelium remains intact and functional (Hollande et al., 2005; Niessen, 2007). Pathologically, misregulation and turnover of mature epithelial AJs are associated with

cancer metastasis (D'Souza-Schorey, 2005). Thus, determining how AJs in epithelia are maintained and remodeled will have important implications for epithelial morphogenesis during development, adult tissue homeostasis, and disease states.

Rho GTPases are molecular switches that regulate epithelial cell cytoskeletal dynamics and cell-cell adhesion (Braga et al., 1997; Harden et al., 1999; Takaishi et al., 1997; Yamada and Nelson, 2007). To do so active Rho proteins associate with effector proteins that mediate downstream signaling events to control specific cell responses. The ability of Rho proteins to activate different effectors is believed to be responsible for their functional diversity (Bishop and Hall, 2000), yet whether certain effectors can be assigned to specific roles and what those roles are, especially *in vivo,* is still uncertain.

In mammals the Rho subfamily of Rho GTPases consists of three members, RhoA, RhoB, and RhoC. All three members are expressed ubiquitously (Wennerberg and Der, 2004), bind similar downstream effectors, including ROCK1/2 and mDia1/2 (Wheeler and Ridley, 2004), and share similar functions, such as promoting stress fiber formation and adhesion maturation (Vega and Ridley, 2007). However, differences also exist. RhoB may have unique functions in endosome transport while RhoA and RhoC are more involved in generating actomyosin tension (Wheeler and Ridley, 2004). Because the common use of dominant mutant proteins likely affects more than one Rho protein, attempts have been made to uncover functional differences between Rho proteins by generating gene-specific mouse knockouts. The mouse knockout of RhoA is embryonic lethal (Wang and Zheng, 2007), while knockouts of RhoB (Liu et al., 2001) and RhoC (Hakem et al., 2005) develop normally. Thus, the presence of multiple

members of Rho in mammals has complicated the precise determination of their functions *in vivo*. In contrast, in *Drosophila* only one Rho member exists, Rho1, and studies in *Drosophila* have made significant contributions in determining Rho1's function in the development of several different tissues (Johndrow et al., 2004). In addition, several of the Rho effectors, including Rok (*Drosophila* ROCK) and Dia, have only one member in *Drosophila*, allowing for a more straightforward analysis of the specific contributions of these effectors to Rho function, *in vivo*.

The *Drosophila* pupal eye is a post-mitotic monolayer neuroepithelium that has been a useful model system in which to study epithelial morphogenesis (Tepass and Harris, 2007). It is composed of approximately 800 repeating units called ommatidia. Each ommatidium is composed of four cell types: eight photoreceptors, four glial-like cone cells, three mechanosensory bristles, and eleven pigment epithelial cells (PECs). Between 18 and 41 hours after puparium formation (APF), PECs undergo patterning into a hexagonal array that surrounds and optically insulates the neuronal core of each ommatidium (Cagan and Ready, 1989). During this morphogenic/maturation process, PECs remodel their AJs as cells reposition themselves relative to one another to achieve their proper niche and form the tissue architecture (Bao and Cagan, 2005; Larson et al., 2008). Concurrently, in order to preserve the integrity of the epithelium, PECs maintain their AJs. The final result is a predictable repeating pattern, with high fidelity, of mature epithelial cells with distinct cell shapes and AJs. We used the epithelium of the *Drosophila* pupal eye to ask whether and how the *in vivo* functions of Rho1 and its two

main downstream effectors, Rok and Dia, affect remodeling of formed AJs, as opposed to Rho1's role in the formation/stabilization of new AJs.

Results

Global depletion of Rho1 in a formed epithelium disrupts adherens junctions

To determine if and how Rho1 influences the maintenance of a remodeling epithelium *in vivo*, we genetically decreased Rho1 throughout the *Drosophila* pupal eye. Because null alleles of *Rho1* are homozygous lethal before pupal development, we generated GAL4-inducible RNAi transgenic lines targeting *Rho1*. Two RNAi lines, UAS-Rho1-RNAi1 and UAS-Rho1-RNAi2, produced similar phenotypes when expressed in the pupal eye, and UAS-Rho1-RNAi1 (referred to as Rho1-RNAi) was used for the rest of the study as it produced the stronger phenotype.

By 41 hours APF, the pigment epithelial cells (PECs) of the pupal eye are fully patterned and begin to undergo the final stages of differentiation (Figs. 1a, b). Expression of Rho1-RNAi throughout the pupal eye beginning at puparium formation (0 hours APF), using the eye specific promoter *GMR-gal4*, resulted in severe disruptions of AJs, as detected by immunostaining for DE-cadherin (*Drosophila* E-cadherin), Armadillo (*Drosophila* β-catenin), and α-catenin at 41 hours APF (Figs. 1c, d). Interestingly, only AJs between PECs were affected while AJs between a PEC and cone cell or between cone cells were not (Fig. 1d''), despite equivalent expression of Rho1 in PECs and cone cells (Fig. 10d) and equivalent RNAi depletion in both cell types (Figs. 10d, e). The ability of Rho1-RNAi to decrease expression of Rho1 was confirmed by immunofluorescence of larval wing discs, Western blot of pupal eyes at 41 hours APF, and immunofluorescence of pupal eyes at 21 hours and 41 hours APF (Fig. 10). To

demonstrate phenotypic specificity, co-expression of Rho1 with Rho1-RNAi reverted pupal eyes to wild type (Fig. 10c), while over-expression of closely related Cdc42 or Rac1 did not (data not shown). Finally, Rho1-RNAi phenotypes were enhanced in *Rho1* null heterozygous backgrounds, either with a deficiency deleting *Rho1* or *Rho1* null alleles (Figs. 11a-f). Because only a residual amount of Rho1 protein remains in pupal eyes expressing Rho1-RNAi (Fig. 10), removing a genomic copy of Rho1 may enhance the phenotype by decreasing the levels of Rho1 below a critical threshold earlier in development.

To determine when expression of the Rho1-RNAi, and thus depleted levels of Rho1, began to disrupt AJs in pupal eye development, we used live imaging of pupal eyes expressing Rho1-RNAi and α-catenin-GFP to label AJs (Larson et al., 2008). In control, wild type pupal eyes between 20 and 28 hours APF, AJs are maintained between PECs (Suppl. Movie 1). When Rho1-RNAi was expressed at puparium formation (0 hours APF), AJs were intact at 20 hours APF, then gradually became disrupted starting at 21 hours APF (Suppl. Movies 2 and 3). This suggested that Rho1 regulated AJs beginning at 21 hours APF.

Depletion of Rho1 in adjacent cells is required to disrupt AJs whereas decreased apical tension is cell autonomous

To determine whether AJ regulation by Rho1 was cell autonomous, or not, clones of PECs expressing Rho1-RNAi were generated using the Flp-out technique (Ito et al., 1997). Surprisingly, depleting Rho1 in a single PEC did not affect AJs (Fig. 2a) or the

polarized localization of DE-cadherin (Fig. 2c) but did result in enlarged apical cell area (Figs. 2a and c, as quantified in Table 1). However, in multiple cell Rho1-RNAi clones, AJs were disrupted, but only between adjacent clonal cells and not between wild type and clonal cells (Fig. 2b). Enlarged apical area was present in all Rho1 depleted clones regardless of the Rho1 status of neighboring cells (Fig. 2b). This clonal analysis indicated that a decrease in Rho1 in adjacent cells was necessary to disrupt AJs, whereas the ability of Rho1 to sustain apical cell area was a cell autonomous effect.

To confirm that the observed Rho1-RNAi clonal phenotypes were indeed the result of loss of Rho1 function, we used mosaic analysis with a repressible cell marker (MARCM) (Lee and Luo, 1999) to generate clonal cells homozygous for the *Rho1* null alleles $Rho1^{72F}$ and $Rho1^{72O}$. MARCM clones of $Rho1^{72F}$ and $Rho1^{72O}$ (hereafter referred to as $Rho1^{72}$) resulted in identical phenotypes but more severe than Rho1-RNAi (Figs. 2d, e, as quantified in Table 1) and depletion of Rho1 protein (Fig. 2d''). F-actin localization at the level of AJs was disrupted in $Rho1^{72}$ clones, consistent with Rho1's role in regulation of actin dynamics (Fig. 2e, as quantified in Table 2). Furthermore, $Rho1^{72}$ clones were rescued by expressing Rho1 in the clones and in some of these Rho1-rescued $Rho1^{72}$ clones decreased apical area was observed, likely due to high level, over-expression of ectopic Rho1 (Fig. 2f, as quantified in Table 1, and Fig. 2f').

Rho1 does not affect septate junction organization, despite disrupting adherens junctions

In *Drosophila*, the functional homolog of the vertebrate tight junction is the septate junction (SJ), which, in contrast to vertebrate epithelia, lies basal to the AJs (Furuse and Tsukita, 2006). Having demonstrated that a loss of Rho1 disrupts pupal eye AJs, we asked if a decrease in Rho1 affected SJs by analyzing the localization of Discs large (Dlg) and Coracle (Cor) in $Rho1^{72}$ MARCM clones. Between two clonal cells, where the AJs were clearly disrupted, Dlg and Cor localization was unaffected (Figs. 3a, b and Fig. 11g). Depletion of Rho1 in the pupal wing, as observed in the pupal eye, resulted in increased apical cell areas and disruption of AJs but not SJs (Figs. 3d, e). To determine if, in general, AJs can be disrupted without affecting SJs in the pupal eye, we generated MARCM clones with a null allele of *shotgun* (*Drosophila e-cadherin*), shg^{R69}. Similar to $Rho1^{72}$ clones, SJs remained intact in shg^{R69} clones (Fig. 3c). This result is similar to that observed in mammalian MDCK cells where depletion of E-cadherin in islands of cells with formed junctions did not affect tight junctions (Capaldo and Macara, 2007). Unlike the requirement for depletion of Rho1 in adjacent cells to disrupt AJs, depletion of DE-cadherin in a single cell disrupted AJs around that cell (Fig. 3c, arrowhead, Fig. 11h).

Rok and Myosin are not necessary for the maintenance or remodeling of formed AJs

Active Rho regulates cellular responses through binding to and activating downstream effector proteins/enzymes. Two major effectors of active Rho are the Rho kinases and Diaphanous proteins, both of which have only one member in *Drosophila*.

Rok is a serine/threonine kinase that activates the Myosin light chain (MLC), leading to increased Myosin activity and actomyosin contractility (Conti and Adelstein, 2008).

To determine the role of Rho1-Rok-Myosin axis in mature pupal eye epithelium morphogenesis, MARCM clones of the *rok*^{2} null allele, *spaghetti squash sqh*^{AX3}, a null allele of the *Drosophila* homolog of MLC, and *zip*^{1}, a null allele of *Drosophila* Myosin heavy chain *zipper*, were generated. In all instances single cell clones had an increased apical cell area similar to *Rho1*^{72} clones (Figs. 4a, c, d as quantified in Table 1). However, in contrast to *Rho1*^{72} clones, in multiple, neighboring null clones all AJs were completely intact (Figs. 4b, c, d). The *rok*^{2} and *Rho1*^{72} clonal cells exhibited an equivalent decrease of MLC phosphorylation (Figs. 11i, j, as quantified in Table 3), indicating that Rok activity was decreased equally in *rok*^{2} and *Rho1*^{72} clones. Decreased MLC activity in *sqh*^{AX3} clones was confirmed by immunofluorescence with a phospho-MLC antibody (Fig. 4c''). Absence of Myosin heavy chain in *zip*^{1} clones was confirmed by immunofluorescence (Fig. 4d''). These results indicated that the Rho1-Rok-Myosin axis was necessary to maintain appropriate apical cell tension but not required to maintain/remodel formed AJs.

Dia is not required to maintain or remodel AJs in vivo but cooperates with Rok to maintain apical cell tension

Another major effector of Rho is the formin protein Dia that promotes linear F-actin synthesis. In both vertebrate and *Drosophila* cells it has been shown to be important for nascent AJ formation (Carramusa et al., 2007; Homem and Peifer, 2008;

Kobielak et al., 2004; Sahai and Marshall, 2002). Therefore, we asked whether AJ disruption following Rho1 depletion was mediated by decreased Dia activity in remodeling epithelia.

Pupal eye epithelium AJs were unaffected in MARCM clones containing *dia*^{5}, a strong hypomorphic allele, despite a significant decrease in Dia protein levels (Fig. 5a). As this allele was recently found to be temperature sensitive (Homem and Peifer, 2008), we also generated clones that were shifted to the non-permissive temperature for 30 hours before dissection. This also had no affect on AJs organization (Fig. 12a). Since residual Dia protein remained in the *dia*^{5} clonal cells, we further decreased Dia levels in *dia*^{5} clones by expressing Dia-RNAi in *dia*^{5} MARCM clones. This resulted in essentially undetectable levels of Dia protein in the clonal cells (Fig. 5b''). Despite this, AJs were still unaffected (Fig. 5b). In a second approach we generated clones expressing Dia-CA (Somogyi and Rorth, 2004). When Dia-CA was expressed in adjacent cells, a strengthening of the AJs was not detected (Figs. 5c, d). As evidence that the Dia-CA protein was active, Dia-CA expressing cells developed a rounded morphology, especially primary PECs (Fig. 5c), and had increased intensity of apical F-actin staining (Fig. 5d). If Dia was acting downstream of Rho1 to regulate mature AJs, then expression of Dia-CA in *Rho1*^{72} MARCM clones should rescue the AJs defect. In *Rho1*^{72} clones expressing Dia-CA, AJs remained disrupted (Fig. 5e, as quantified in Table 4). In sum, these data indicated that Dia was not acting downstream of (not required for) Rho1 to maintain/remodel formed AJs.

Possibly the action of both major Rho effectors was required to remodel AJs in formed, remodeling epithelia. To test this possibility we made clones of cells depleted of both Dia and Rok by expressing Dia-RNAi in *rok*^{2} MARCM clones. Again, mature AJs were not affected in these clones, indicating that Dia and Rok do not cooperate to regulate AJs (Fig. 5f). Surprisingly, while cells depleted of Dia had no change in apical area (Fig. 5b, as quantified in Table 1), expression of Dia-RNAi in *rok*^{2} MARCM clones resulted in a greater increase in apical area compared to *rok*^{2} MARCM clones alone (Figs. 4b and 5f, as quantified in Table 1). These data indicated that Dia and Rok function cooperatively to sustain apical cell tension.

Rho1 regulates AJs through membrane trafficking of DE-cadherin

How then could a loss of Rho1 disrupt mature AJs? To determine if Rho1 affected DE-cadherin protein levels, we performed Western blot analysis of pupal eyes uniformly expressing Rho1-RNAi at 41 hours APF, when Rho1-RNAi caused strong AJ disruptions (Fig. 1c). The level of DE-cadherin in Rho1-RNAi expressing tissue relative to control tissue was not significantly different (Figs. 6a and b). Since Rho1-RNAi expression was driven only in the eye, the decrease in Rho1 protein with the Rho1-RNAi demonstrated the dissections were specific to the eye tissue (Fig. 6a).

We also used a genetic approach to address this question. If a loss of Rho1 leads to AJ disruptions strictly because of a decrease in DE-cadherin levels, then increasing DE-cadherin in these cells should rescue the AJs. We generated clones that expressed Rho1-RNAi and over-expressed DE-cadherin. Even with high levels of DE-cadherin in

cells with decreased Rho1, AJs were still disrupted, as determined by Armadillo localization (Fig. 6c). To control for the effects of DE-cadherin over-expression on AJs, we generated clones that over-expressed DE-cadherin alone and observed an increased Armadillo localization at the AJ between two clonal cells (Fig. 6d). Therefore, these results confirmed the Western blot analysis and indicated that the AJ disruptions from decreased Rho1 were not the result of decreased total levels of DE-cadherin in this epithelium.

Membrane trafficking of cadherins is another means by which AJ localization can be regulated (D'Souza-Schorey, 2005; Yap et al., 2007). E-cadherin has three general trafficking routes: delivery of newly synthesized E-cadherin from the Golgi complex to the plasma membrane, endocytosis and recycling of E-cadherin back to the plasma membrane, and endocytosis of E-cadherin with targeting to the lysosomes for degradation.

To determine whether Rho1 controls endocytosis/recycling of DE-cadherin, which involves endocytosis of DE-cadherin into Rab5-containing early endosomes and delivery of DE-cadherin back to the plasma membrane in Rab11-containing recycling endosomes (Yap et al., 2007), we first asked if blocking endocytosis of DE-cadherin in a Rho1 null clone could rescue the AJ disruption. Expression of a Rab5 dominant negative transgene (Rab5-DN) (Zhang et al., 2007) or Rab5-RNAi in $Rho1^{72}$ clones both reverted the AJ defect seen between two $Rho1^{72}$ clonal cells (Fig. 7: b versus a, Fig. 13a, Fig. 7c, and as quantified in Table 4). Importantly, these manipulations had no effect on the decreased apical tension resulting from Rho1 depletion (Fig. 7b, Fig. 13a, and as

quantified in Table 5). Clones expressing Rab5-DN or Rab5-RNAi alone did not affect DE-cadherin localization or apical area (Figs. 13b, c).

In another approach, expression of a constitutively active Rab5 (Rab5-CA) (Zhang et al., 2007) in the *Rho1*^{72} clones might be predicted to enhance/worsen the AJ defects in *Rho1* null adjoining cells. Expression of Rab5-CA in *Rho1*^{72} clones did not worsen the *Rho1*^{72} AJ phenotype between two clonal PECs (as quantified in Supplementary Information Table 4), but did disrupt AJs between a PEC and cone cell, a phenotype that was not observed in *Rho1*^{72} clones (Fig. 7d). Although clones expressing Rab5-CA alone had increased intracellular DE-cadherin, AJs were unchanged (Fig. 13d).

If depletion of Rho1 indeed results in increased endocytosis of DE-cadherin (i.e., Rho1 inhibits DE-cadherin endocytosis), then Rho1 depleted cells should exhibit increased internalization of DE-cadherin. To detect internalized DE-cadherin, we performed a DE-cadherin endocytosis assay using pupal eyes containing *Rho1*^{72} MARCM clones. *Rho1*^{72} clonal cells had increased intracellular DE-cadherin compared to surrounding wild type cells (Fig. 7e), representing increased internalization and/or decreased recycling of DE-cadherin with Rho1 depletion. In addition, pupal eyes expressing Rho1-RNAi had increased intracellular DE-cadherin, much of which co-localized with Rab5, compared to control pupal eyes (Figs. 4e, f). Consistent with a role for Rho1 in endocytosis of DE-cadherin, Rho1 protein co-localized with Rab5-positive, DE-cadherin containing endosomes (Fig. 7f).

To inhibit recycling of internalized endosomes we expressed Rab11-DN (Zhang et al., 2007) in the *Rho1*^{72} clones. While *Rho1*^{72} clones exhibit disrupted AJs only

between two clonal PECs, expression of Rab11-DN in the *Rho1*^{72} clones led to a worsening of the Rho1 null phenotype. In addition to frequent disruptions of AJs between *Rho1*^{72} clonal cells, disruption of AJs between *Rho1*^{72} clonal cells and wild type cells were now apparent (Fig. 7g). The effect of the Rab11-DN on the AJs was specific to the *Rho1*^{72} clones (i.e., loss of Rho1 activity) since neither clones expressing the Rab11-DN alone nor MARCM clones with the *Rab11*^{EP3017} loss-of-function allele had affects on the AJs (data not shown). Rab7-DN (Zhang et al., 2007), that blocks targeting of early endosomes to lysosomes, and Rab8-DN (Zhang et al., 2007), that inhibits transport of vesicles from the Golgi to the plasma membrane had no effects on the localization of DE-cadherin in *Rho1*^{72} clonal cells (Fig. 7h, as quantified in Table 4).

Rho1 regulation of AJs is Cdc42/Par6 dependent

The related GTPase, Cdc42, was recently demonstrated to promote endocytosis and recycling of DE-cadherin in *Drosophila* epithelia (Georgiou et al., 2008; Harris and Tepass, 2008; Leibfried et al., 2008). Since crosstalk between the activities of Rho GTPase family members is critical for the regulation of many cellular responses, such as cell-ECM and cell-cell adhesion, and cell migration, we asked whether Rho1 activity limits DE-cadherin trafficking in remodeling pupal epithelium by inhibiting Cdc42. In other words in the absence of Rho1 (*Rho1*^{72} clones) it is proposed that Cdc42 activity is enhanced and thus E-cadherin endocytosis increased. If so then depletion of Cdc42 in Rho1 null cells could rescue AJ disruptions. To test this we expressed a Cdc42-RNAi in *Rho1*^{72} clones. Like Rab5-DN and Rab5-RNAi, depletion of Cdc42 reverted the AJ

defects seen between two *Rho1*^{72} clonal cells (Figure 8a, as quantified in Table 4) but did not affect the increased apical area (Figure 8a, as quantified in Table 5). In another approach to address this question, we asked whether depletion of Cdc42 could rescue the AJ disruptions between two Rho1-RNAi expressing cells. When Rho1-RNAi was expressed in *Cdc42* LOF clones, AJs between clonal cells remained completely intact (Fig. 8b), indicating that Cdc42 was required for Rho1 depletion to disrupt AJs. The Cdc42 effector implicated in promoting DE-cadherin endocytosis is Par6 (Georgiou et al., 2008; Harris and Tepass, 2008; Leibfried et al., 2008). Expression of Rho1-RNAi in *par6* null clones had normal appearing AJs (Fig. 8c). Cdc42-RNAi, *Cdc42* LOF, or *par6* null clones alone did not fragment AJs (data not shown). Together, these data indicated that Rho1 maintained/remodeled AJs in formed epithelia by inhibiting endocytosis and recycling of DE-cadherin in a Cdc42/Par6-dependent manner.

Discussion

We have isolated two specific functions downstream of Rho1 in an *in vivo*, remodeling epithelium, as opposed to formation of nascent cell-cell adhesions. They are to sustain apical cell tension and maintain AJs. The former function is cell autonomous and requires Rok and Myosin with a supporting role from Dia, while the latter is not cell autonomous and involves inhibition of DE-cadherin endocytosis through Cdc42/Par6, independent of Rok or Dia. The ability to separate these two phenotypes downstream of Rho is consistent with the idea that Rho proteins achieve their functional diversity by activating several effectors.

Our results showing that Dia has no role in regulating AJs is contrary to several published studies, in both mammalian systems (Carramusa et al., 2007; Sahai and Marshall, 2002) and *Drosophila* (Homem and Peifer, 2008). Dia has been shown to also regulate Myosin in the control of cell contraction in the *Drosophila* embryo (Homem and Peifer, 2008; Mulinari et al., 2008) and larval eye epithelium (Corrigall et al., 2007). Although we show that Dia cooperates with Rok to regulate apical cell tension (Fig. 9), we saw no effect on apical cell shape upon Dia depletion alone in the pupal eye. One explanation for these discrepancies may be inherent differences between mammalian tissue culture systems and *in vivo Drosophila* systems, and/or between different stages of *Drosophila* development. Alternatively, while Rok and Dia are necessary for the formation of nascent AJs, other Formin proteins, or combination of different actin nucleating proteins maintain AJs. Another *Drosophila* Formin protein that could function with Rho to regulate the actin cytoskeleton is Dishevelled-associated activator of

morphogenesis (Daam) (Habas et al., 2001; Matusek et al., 2006). Loss-of-function and gain-of-function studies showed that Daam, like Dia, did not function to maintain/remodel AJs in pupal epithelium, however (Figs. 12b, c).

Our data indicates that Rho affects AJ turnover/remodeling by regulating E-cadherin endocytosis, in a Cdc42/Par6-dependent manner (Fig. 9). A role for Rho in endocytosis of growth factor receptors in cell lines has been previously reported (Ridley, 2006; Symons and Rusk, 2003), through its effects upon actin dynamics. In the Rho1 null pupal eye epithelial clones we observed a decrease in AJ-associated F-actin intensity, however, Dia-depleted cells (the major Rho actin effector) had unaffected AJs and F-actin intensity (Table 2). Rok can also regulate actin through LIMK-Cofilin, but pupal eye Rok null clones or pupal eyes homozygous for a strong hypomorphic allele of *Drosophila Limk*, $Limk^{EY08757}$ (Eaton and Davis, 2005) have intact AJs with no decrease in F-actin intensity (Table 2, and SW and GL unpublished data). These data suggest the possibility that Rho1 can regulate actin in a Dia- and Rok-independent manner.

Another possibility is that Rho1 regulates AJ turnover and E-cadherin endocytosis independent of, or in addition to, its effects upon actin dynamics. In support of this, we could uncouple disruption of F-actin structures from AJ disruption. Clones with a *chickadee* null allele (*Drosophila profilin*) have disrupted F-actin and a greater decrease in AJ-associated F-actin than Rho1 null cones (Table 2), yet AJs between Chickadee null cells are unaffected (Fig. 14a). Furthermore, an increase in cortical actin in two adjacent cells expressing Dia-CA was not sufficient to affect AJs. Finally, co-localization of Rho1 at DE-cadherin, Rab5 positive endosomes suggests that Rho1 may be directly involved in

endocytosis/recycling of DE-cadherin. Although another Rho effector, Protein kinase N (Pkn), has been implicated in vesicular transport (Mukai, 2003), expression of Pkn-RNAi in the pupal eye did not disrupt AJs despite disruption of cell patterning in a manner as or more severe than expression of Rho1-RNAi (Fig. 14b).

AJs were disrupted following Rho1 depletion only when two adjacent cells were depleted. While the mechanism behind this is still largely unknown, some insight may be gleaned from the effects of expressing Rab11-DN in the Rho1 null clones, which resulted in disrupted AJs between clonal and non-clonal cells. Perhaps Rab11 recycling endosomes compensate for increased endocytosis of DE-cadherin in the Rho1-depleted cell. If so this raises the possibility that Rho1 depletion stimulates recycling of Rab11 endosomes. Also, the maintenance of AJs between wild type and Rho1 null cells is distinct from the loss of AJs between wild type and DE-cadherin null cells. In the absence of Rho1, newly synthesized DE-cadherin localizes to the membrane but its regulation via endocytosis and recycling is altered. Between wild type and Rho1 null cells, binding in trans to DE-cadherin in the wild type cell could stabilize DE-cadherin delivered to the membrane of the Rho1 null cell and prevent/limit its endocytosis/recycling. In contrast, between two Rho1 null cells, the altered endocytosis/recycling of DE-cadherin in both cells results in loss of AJ maintenance.

Depletion of Cdc42 or Par6 rescued the AJ defects from Rho1 depletion, suggesting the effect of Rho1 depletion on AJs involves Cdc42/Par6-dependent regulation of DE-cadherin trafficking. Cdc42 and Par6 have recently been implicated in the regulation of DE-cadherin endocytosis and recycling (Georgiou et al., 2008; Harris

and Tepass, 2008; Leibfried et al., 2008) but by distinct mechanisms and in different tissues. Georgiou et al. and Leibfried at al. both propose a role for Cdc42/Par6 in promoting DE-cadherin endocytosis in pupal notum epithelium, while Harris and Tepass suggest Cdc42/Par6 regulates DE-cadherin trafficking indirectly by preventing Crumbs endocytosis in embryonic ventral neuroectoderm. Our data are consistent with the former results based on two points. First, both Cdc42-RNAi and Rab5-DN/Rab5-RNAi rescue the Rho1 AJ phenotype, supporting the notion that Cdc42 functions similar to Rab5 and promotes DE-cadherin endocytosis. Second, between two Rho1 null cells, where DE-cadherin is disrupted, Crumbs either co-localizes with fragmented DE-cadherin or is undisrupted (Fig. 14c). In contrast, when DE-cadherin null cells were analyzed, most clones exhibited disrupted Crumbs localization (Fig. 14d). This suggests that the primary defect from Rho1 depletion is AJ disruption, which likely then affects Crumbs localization, and that the proposed increase in Cdc42 activity resulting from Rho1 depletion is not acting through Crumbs to affect AJs. While our results are consistent with Georgiou et al. and Leibfried at al., the results from Harris and Tepass may reflect differences in the nature of the ventral neuroectoderm, which has distinct properties even from the dorsal neuroectoderm (Harris and Tepass, 2008). Determining how Rho1 regulates Cdc42 activity to maintain AJs and if Rho1 maintains AJs through Cdc42 in systems other than the pupal eye are important questions for future studies.

Materials and Methods

Drosophila stocks

All crosses and staging were performed at 25°C unless otherwise noted. w^{1118} or Canton-S was used as wild type. Stocks are described in Flybase (http://flybase.bio.indiana.edu). *GMR-gal4*, *tubulin-gal80*^{ts}, *Rho1*^{72F}, *Rho1*^{72O}, *rok*^{2} FRT19A, *dia*^{5} FRT40A, *Cdc42*^{4} FRT19A, UAS-Rho1, UAS-GFP, UAS-Rab5-DN, UAS-Rab5-CA, UAS-Rab11-DN, UAS-Rab7-DN, UAS-Rab8-DN, and *chic*^{221} were kindly provided by the Bloomington *Drosophila* Stock Center, *patched-gal4*, UAS-DE-cadherin, *wsp*^{3} FRT82B, and *shg*^{R69} FRT42D by R. Cagan (Mount Sinai, New York, NY), UAS-Dia-CA by M. Peifer (UNC, Chapel Hill, NC), *zip*^{1} FRT42D by T. Wolff (Washington University, St. Louis, MO), *sqh*^{AX3} by R. Karess (CNRS, Gif sur Yvette, France), *Daam*^{Ex68} FRT19A and UAS-Daam-CA by J. Mihály (Hungarian Academy of Sciences, Szeged, Hungary), UAS-Rok-CAT by G-C. Chen (Academia Sinica, Taipei, Taiwan), UAS-Dia-RNAi and UAS-Rab5-RNAi by the Vienna *Drosophila* RNAi Center (Vienna, Austria), *Rab11*^{EP3017} FRT82B by D. Ready (Purdue University, West Lafayette, IN), UAS-Rab5-GFP by M. González-Gaitán (University of Geneva, Switzerland), *par6*$^{\Delta 226}$ FRT19A by C. Doe (University of Oregon, Eugene, OR), and UAS-Pnk-RNAi by the National Institute of Genetics (Shizuoka, Japan).

Rho1-RNAi and Cdc42-RNAi lines were generated as previously described (Bao and Cagan, 2006) using fragments of *Rho1* and *Cdc42* amplified from Canton-S cDNA, respectively. UAS-Rho1-RNAi1 targets 325-786 bp and UAS-Rho1-RNAi2 targets 770-

1310 bp after the start codon of *Rho1*. UAS-Cdc42-RNAi targets the region 191 bp before to 278 bp after the start codon of *Cdc42*.

Clonal analysis and genetics

To generate Flp-out clones over-expressing a transgene, progeny from Act5C>y^+>gal4, UAS-GFP; hsFLP crossed to the following genotypes were heat-shocked for 30 minutes at 37°C as 3rd instar larvae or early pupae: (1) UAS-Rho1-RNAi/SM6a-TM6b, (2) UAS-Dia-CA, (3) UAS-Daam-CA, (4) UAS-Rho1-RNAi; UAS-DE-cad/SM6a-TM6b, (5) UAS-DE-cad, (6) UAS-Rab5-DN, (7) UAS-Rab5-RNAi, (8) UAS-Rab5-CA, and (9) UAS-Rab11-DN. Clones were marked by the presence of GFP.

MARCM clones were generated by heat-shocking 3rd instar larvae with the following genotypes for 1 hour at 37°C:

hsFLP, UAS-GFP; *Rho1*^{72O}, FRT42D/*tub-gal80*, FRT42D; *tub-gal4*/+

hsFLP, UAS-GFP; *Rho1*^{72F}, FRT42D/*tub-gal80*, FRT42D; *tub-gal4*/+

rok^{2}, FRT19A/hsFLP, *tub-gal80*, FRT19A; UAS-GFP, UAS-*lacZ*/+; *tub-gal4*/+

sqh^{AX3}, FRT19A/hsFLP, *tub-gal80*, FRT19A; UAS-GFP, UAS-*lacZ*/+; *tub-gal4*/+

hsFLP, UAS-GFP; *zip*^{1}, FRT42D/*tub-gal80*, FRT42D; *tub-gal4*/+

hsFLP, UAS-GFP; *dia*^{5}, FRT40A/*tub-gal80*, FRT40A; *tub-gal4*/+

hsFLP, UAS-GFP; *dia*^{5}, FRT40A/*tub-gal80*, FRT40A; *tub-gal4*/UAS-Dia-RNAi

rok^{2}, FRT19A/hsFLP, *tub-gal80*, FRT19A; UAS-GFP, UAS-*lacZ*/+; *tub-gal4*/UAS-Dia-RNAi

Daam^{Ex68}, FRT19A/hsFLP, *tub-gal80*, FRT19A; UAS-GFP, UAS-*lacZ*/+; *tub-gal4*/+

hsFLP, UAS-GFP; *chic*^{221}, FRT40A/*tub-gal80*, FRT40A; *tub-gal4*/+

hsFLP, UAS-GFP; *Rho1*^{72}, FRT42D/*tub-gal80*, FRT42D; *tub-gal4*/UAS-Rho1

hsFLP, UAS-GFP; *Rho1*^{72}, FRT42D/*tub-gal80*, FRT42D; *tub-gal4*/UAS-Dia-CA

hsFLP, UAS-GFP; *Rho1*^{72}, FRT42D/*tub-gal80*, FRT42D; *tub-gal4*/UAS-Rab5-DN

hsFLP, UAS-GFP; *Rho1*^{72}, FRT42D/*tub-gal80*, FRT42D; *tub-gal4*/UAS-Rab5-RNAi

hsFLP, UAS-GFP; *Rho1*^{72}, FRT42D/*tub-gal80*, FRT42D; *tub-gal4*/UAS-Rab5-CA

hsFLP, UAS-GFP; *Rho1*^{72}, FRT42D/*tub-gal80*, FRT42D; *tub-gal4*/UAS-Rab11-DN

hsFLP, UAS-GFP/UAS-Rab7-DN; *Rho1*^{72}, FRT42D/*tub-gal80*, FRT42D; *tub-gal4*/+

hsFLP, UAS-GFP; *Rho1*^{72}, FRT42D/*tub-gal80*, FRT42D; *tub-gal4*/UAS-Rab8-DN

hsFLP, UAS-GFP/UAS-Cdc42-RNAi; *Rho1*^{72}, FRT42D/*tub-gal80*, FRT42D; *tub-gal4*/+

Cdc42^{4}, FRT19A/hsFLP, *tub-gal80*, FRT19A; UAS-GFP, UAS-*lacZ*/UAS-Rho1-RNAi; *tub-gal4*/+

par6$^{\Delta 226}$, FRT19A/hsFLP, *tub-gal80*, FRT19A; UAS-GFP, UAS-*lacZ*/UAS-Rho1-RNAi; *tub-gal4*/+

Clones were marked by the presence of GFP. FRT sites were recombined onto *Rho1*^{72O} (42D), *Rho1*^{72F} (42D), *sqh*^{AX3} (19A), *chic*^{221} (40A) as previously described (Xu and Rubin, 1993).

Expression of either GFP alone or GFP and Rho1-RNAi with *patched-gal4* in the pupal wing was performed by crossing *patched-gal4*, UAS-GFP, *tub-gal80*^{ts}/SM6a-TM6b to *w*^{1118} or UAS-Rho1-RNAi/SM6a-TM6b at 18^{o}C. Progeny were shifted to 29^{o}C 3-4 days after egg laying and dissected at 18 hours APF.

Immunofluorescence

Pupal eyes or wings were dissected in PBS, fixed in 4% paraformaldehyde for 45 minutes, washed once in PBS-T (PBS/0.1% Triton X-100), washed twice in PAXD (PBS containing 1% BSA, 0.3% Triton X-100, 0.3% deoxycholate), and washed once in PAXDG (PAXD with 5% goat serum), all on ice. The tissue was then incubated overnight at 4^{o}C with primary antibodies diluted in PAXDG, washed three times in PBS-T, and incubated overnight at 4^{o}C with secondary antibodies diluted in PAXDG. After washing twice in PBS-T, the tissue was post-fixed in 4% paraformaldehyde for 25 minutes at room temperature, washed twice in PBS-T, and mounted in Vectashield mounting media (Vector Labs). Antibodies used were rat anti-DE-cadherin (1:20), mouse anti-Discs large (1:50), mouse anti-Rho1 (1:20), rat anti-α-catenin (1:50), mouse anti-Armadillo (1:50), mouse anti-Coralce (1:20) (all from the Developmental Studies Hybridoma Bank at the University of Iowa), rabbit anti-Zip (1:200, from T. Wolff, Washington University, St. Louis), rat anti-Crumbs (1:500, from U. Tepass, University of Toronto, Ontario, Canada), rabbit anti-Dia (1:500, from S. Wasserman, UCSD, San Diego, CA), and rabbit anti-phospho-Myosin Light Chain 2 (Ser19) (1:20, Cell Signaling). Rhodamine-phalloidin (1:500, Invitrogen) was added in the primary and secondary antibody incubations to visualize F-actin. Secondary antibodies were Alexa 488 and 568 (Invitrogen) and Cy5 (Jackson ImmunoResearch). Immunofluorescence was analyzed on a confocal Zeiss LSM 510 using a Zeiss Plan-Apochromat 63X 1.4 NA oil objective at room temperature with Zeiss LSM 510 software. Adobe Photoshop was used to minimally adjust brightness and contrast to whole images. Live imaging of

developing pupal eyes from either *GMR-gal4*, UAS-α-catenin-GFP/+ or *GMR-gal4*, UAS-α-catenin-GFP/UAS-Rho1-RNAi was performed as previously described (Larson et al., 2008) on a Zeiss Axioplan2 with a Zeiss Plan-Apochromat 63X 1.4 NA oil objective at room temperature using a CCD camera (Quantix Photometrics, Tuscon, AZ) and ImagePro Plus 5.1 software (MediaCybernetics, Bethesda, MD).

DE-cadherin endocytosis assay

Pupal eyes containing $Rho1^{72}$ clones were dissected and processed essentially as previously described (Le Borgne and Schweisguth, 2003). Following dissection, pupal eyes were incubated with anti-DE-cadherin antibodies for 45 minutes at 25°C and processed for immunofluorescence as described above. The lack of AJ staining in photoreceptors in Fig. 7g indicated that only surface DE-cadherin was labeled with antibody.

Western blot analysis

Pupal eyes 41 hours APF were dissected in PBS and transferred to RIPA buffer on ice. Lysates were run on a 10% SDS-polyacrylamide gel and transferred to nitrocellulose. Antibodies used were rat anti-DE-cadherin (1:100), mouse anti-α-tubulin (1:2000), mouse anti-Rho1 (1:100), and HRP-conjugated secondaries. Quantification was performed using ImageJ v1.38 with standard procedures.

Quantification and statistics

Images were analyzed using ImageJ v1.38 (NIH). Apical area indices were calculated as the ratio of a clonal cell apical area divided by an analogous, neighboring non-clonal cell apical area. F-actin indices were calculated as the ratio of phalloidin staining pixel intensity in a clonal cell divided by that in an analogous, neighboring non-clonal cell. Phospho-MLC indices were calculated as the ratio of phospho-MLC immunofluorescence pixel intensity in a clonal cell divided by that in an analogous, neighboring non-clonal cell. AJ indices were calculated as the ratio of the border length positive for DE-cadherin immunofluorescence divided by the total border length between two clonal cells. P-values were calculated using unpaired, two-sided Student's t-tests.

Acknowledgements

We thank R. Cagan for support during the initial stages of this work; J. Skeath, M. Peifer, T. Wolff, R. Karess, J. Mihály, G-C. Chen, C. Doe, D. Ready, U. Tepass, S. Wasserman, M. González-Gaitán, the Vienna *Drosophila* RNAi Center, the National Institute of Genetics, the Bloomington *Drosophila* Stock Center, and the Developmental Studies Hybridoma Bank for reagents; D. Larson for help with live imaging; and C. Micchelli for helpful discussions. This work was supported by grants NIH CA85839 and GM080673 to GDL.

Figures

Figure 1. Rho1 is required to maintain AJs in the pupal eye.

Confocal immunofluorescent localization of DE-cadherin (DE-cad) in wild type pupal eye (a and b). c = cone cell, b = bristle cell, 1^o = primary pigment epithelial cell (PEC), 2^o = secondary PEC, 3^o = tertiary PEC. The photoreceptors are basal to this optical section. Anterior is to the right in all images. This and subsequent pupal eyes are 41 hours APF unless otherwise noted. Confocal immunofluorescent localization of the AJ components DE-cadherin and Armadillo (Arm) (c) and Armadillo and α-catenin (α-cat) (d) in the pupal eye expressing Rho1-RNAi using *GMR-gal4* (GMR>Rho1-RNAi). Arrows identify AJs between primary PEC and cone cells, and arrowheads identify AJs between cone cells. Scale bars represent 10 μm.

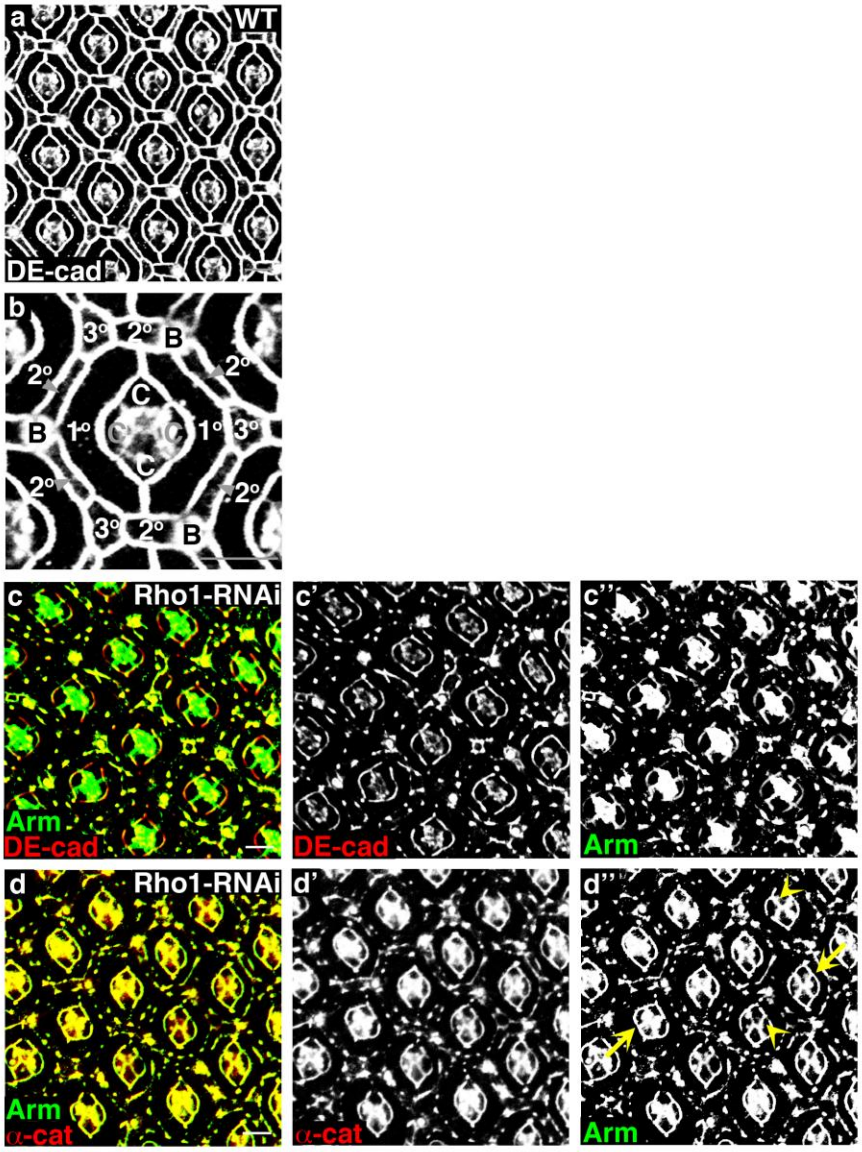
a
WT
DE-cad
b
3°
2°
B
2°
2°
C
B
1°
1°
3°
C
2°
2°
3°
2°
B
c
Rho1-RNAi
Arm
DE-cad
c'
DE-cad
c''
Arm
d
Rho1-RNAi
Arm
α-cat
d'
α-cat
d''
Arm

Figure 1

Figure 2. Depletion of Rho1 in adjacent cells is required to disrupt AJs but decreased apical tension is cell autonomous.

Confocal immunofluorescent localization of DE-cadherin in a single PEC clone (a and a') and multiple cell clones (b and b') expressing Rho1-RNAi (marked with GFP). Arrows in b' identify intact AJs between a clonal cell and wild type cell. Arrowheads identify disrupted AJs between two adjacent clonal cells. Apical (c) and lateral (c') optical sections of DE-cadherin immunofluorescent localization in Rho1-RNAi clonal cell. Yellow line (c) identifies where lateral section (c') was taken. Asterisks mark analogous cells in adjacent ommatidia. Arrow (c') identifies Rho1-RNAi clone. Confocal immunofluorescent localization of DE-cadherin (d and d') and Rho1 (d'') in $Rho1^{72}$ (Rho1 null) MARCM clones (clonal cells are GFP positive). Arrows identify clonal cells, and arrowheads identify disrupted AJs between clonal cells. Confocal immunofluorescent localization of DE-cadherin (e, e', and e'') and phalloidin staining (F-actin) (e'' and e''') in $Rho1^{72}$ MARCM clones. Arrows identify clonal cells, and arrowheads identify disrupted AJs between two clonal cells. Confocal immunofluorescent localization of DE-cadherin (f and f') and Rho1 (f'') in $Rho1^{72}$ MARCM pupal eye clones over-expressing Rho1. Arrows identify cells with rescued apical profiles while arrowheads identify rescued AJs between clonal cells. Scale bars represent 10 μm.

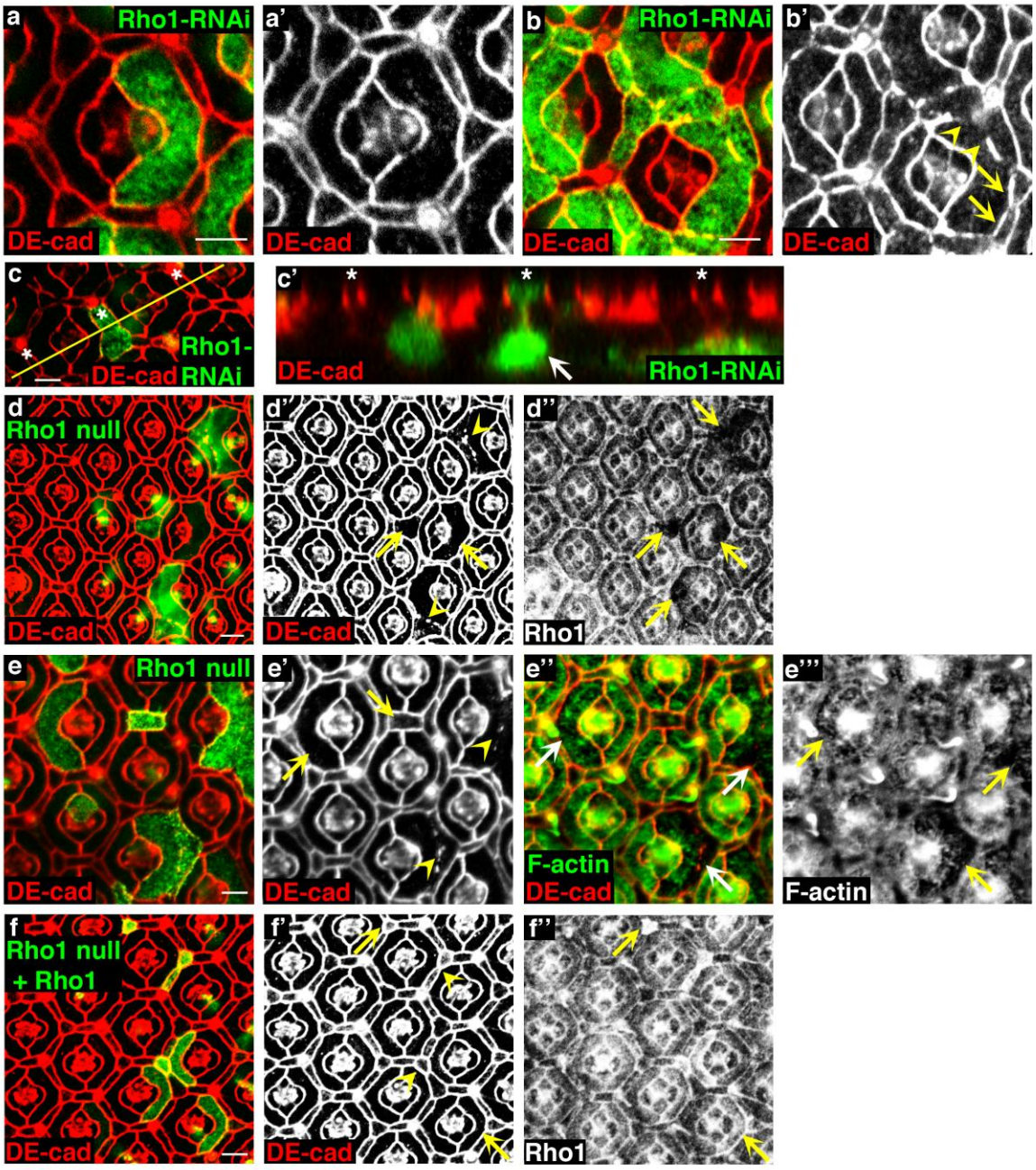
a
Rho1-RNAi
DE-cad
a'
DE-cad
b
Rho1-RNAi
DE-cad
b'
DE-cad
c
Rho1-RNAi
DE-cad
c'
DE-cad
Rho1-RNAi
d
Rho1 null
DE-cad
d'
DE-cad
d''
Rho1
e
Rho1 null
DE-cad
e'
DE-cad
e''
F-actin
DE-cad
e'''
F-actin
f
Rho1 null
+ Rho1
DE-cad
f'
DE-cad
f''
Rho1

Figure 2

Figure 3. Rho1 specifically regulates AJs but not SJs in formed, remodeling pupal epithelium

Confocal immunofluorescent localization of DE-cadherin (a and a') and Discs large (Dlg) (a and a'') in *Rho1*^{72} MARCM clones. Arrowheads identify AJs (a') and SJs (a'') between clonal cells. Confocal immunofluorescent localization of DE-cadherin (b, b', b'') and Discs large (b, b', b''') in apical (b) and lateral (b'-b''') optical sections of *Rho1*^{72} MARCM clones. Yellow line (b) identifies where lateral section (b', b'', and b''') was taken. Yellow asterisk identifies a *Rho1*^{72} MARCM clone, while white asterisk identifies an analogous non-clonal, wild type cell. Arrows identify AJs (b'') and SJs (b''') of the *Rho1*^{72} clonal cell that neighbors another clonal cell on the right and a non-clonal cell on the left. Confocal immunofluorescent localization of DE-cadherin (c and c') and Discs large (c and c'') in *shg*^{R69} (DE-cad null) MARCM clones. Arrows identify multiple cell clones, and arrowhead identifies a single cell clone. Confocal immunofluorescent localization of DE-cadherin (d and d'') and Discs large (d and d''') in pupal wing epithelial cells expressing GFP using *patched-gal4*. Confocal immunofluorescent localization of DE-cadherin (e and e'') and Discs large (e and e''') in pupal wing epithelial cells co-expressing GFP and Rho1-RNAi using *patched-gal4*. Scale bars represent 10 μm.

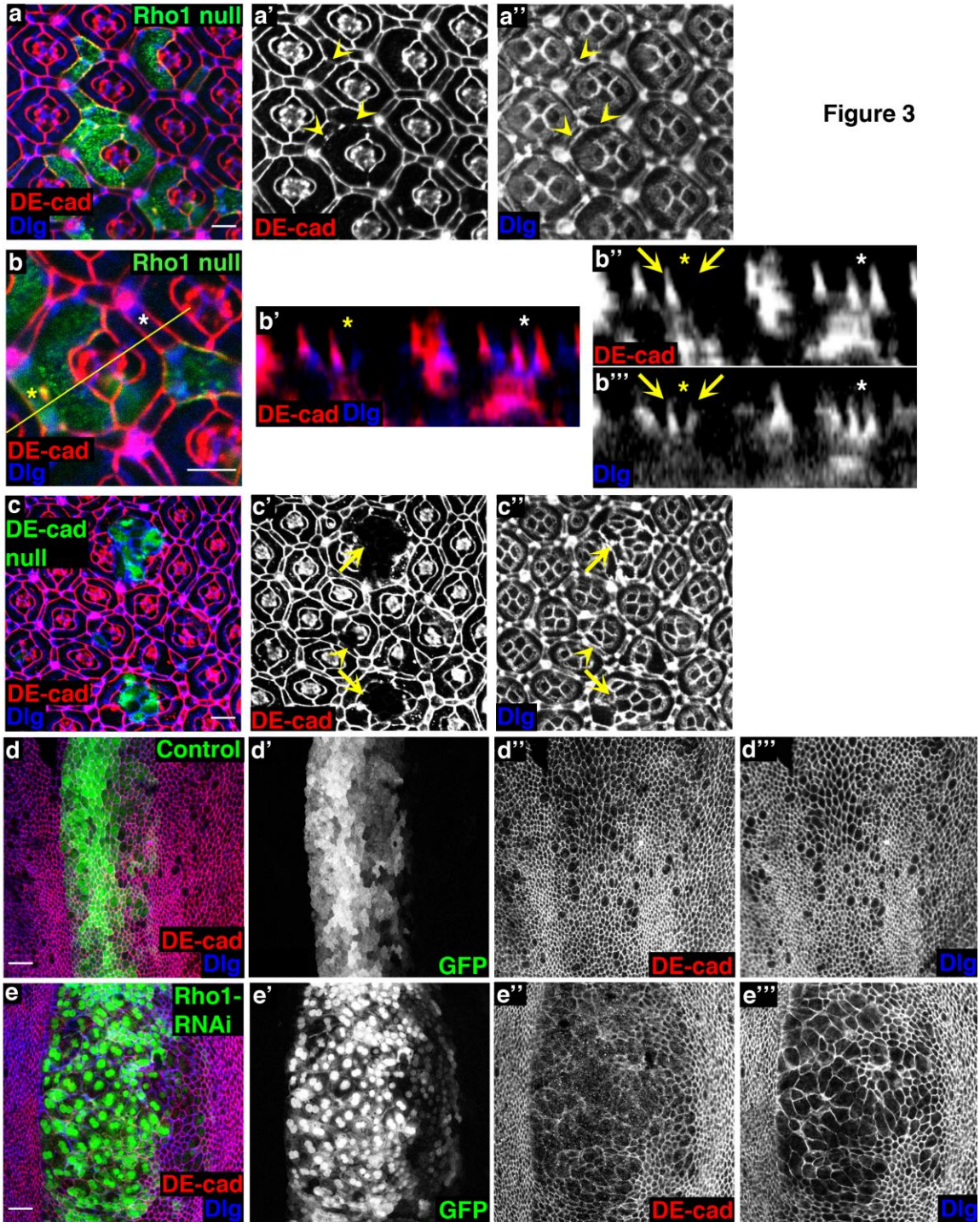
a
Rho1 null
DE-cad
Dlg
a'
DE-cad
a''
Dlg
b
Rho1 null
DE-cad
Dlg
b'
DE-cad Dlg
b''
DE-cad
b'''
Dlg
c
DE-cad
null
DE-cad
Dlg
c'
DE-cad
c''
Dlg
d
Control
DE-cad
Dlg
d'
GFP
d''
DE-cad
d'''
Dlg
e
Rho1-
RNAi
DE-cad
Dlg
e'
GFP
e''
DE-cad
e'''
Dlg

Figure 3

Figure 4. Rok and Myosin are necessary for sustaining apical tension but not maintaining AJs.

Confocal immunofluorescent localization of DE-cadherin in single-cell *rok*^{2} (Rok null) MARCM clones (a). Arrows identify clonal cells. Confocal immunofluorescent localization of DE-cadherin in multiple-cell *rok*^{2} MARCM clone (b). Arrows identify clonal cells, and arrowheads identify AJs between clonal cells. Confocal immunofluorescent localization of DE-cadherin (c and c') and phospho-MLC (c'') in *sqh*^{AX3} (MLC null) MARCM clones. Arrows identify clonal cells, and arrowheads identify AJs between clonal cells. Confocal immunofluorescent localization of DE-cadherin (d and d') and Zip (Myosin heavy chain, MHC) (d'') in *zip*^{1} (MHC null) MARCM clones. Arrows identify clonal cells, and arrowheads identify AJs between clonal cells. Scale bars represent 10 μm.

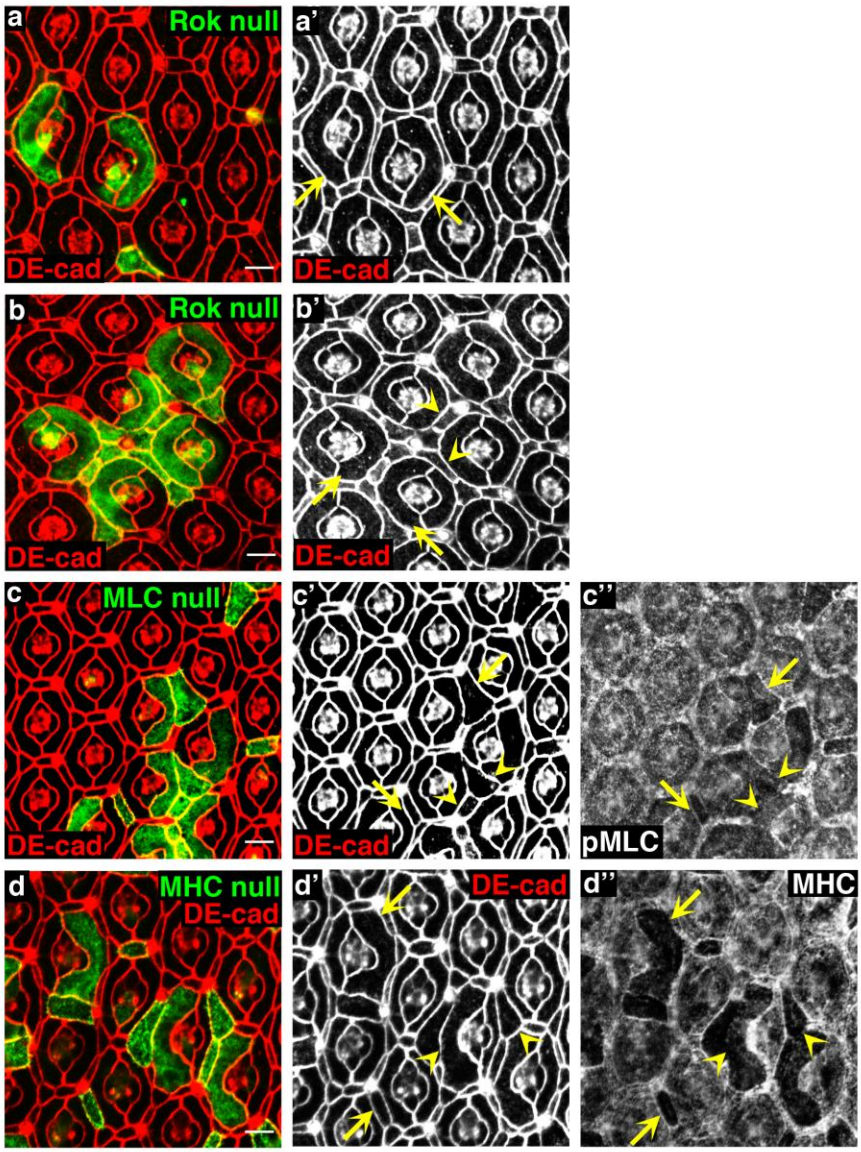
a
Rok null
DE-cad
a'
DE-cad
b
Rok null
DE-cad
b'
DE-cad
c
MLC null
DE-cad
c'
DE-cad
c''
pMLC
d
MHC null
DE-cad
d'
DE-cad
d''
MHC

Figure 4

Figure 5. Dia cooperates with Rok to sustain apical tension but does not maintain formed AJs.

Confocal immunofluorescent localization of DE-cadherin (a and a') and Dia (a'') in *dia*^{5} (Dia hypomorph/loss-of-function (LOF)) MARCM clones. Arrowheads identify AJs between two clonal cells. Confocal immunofluorescent localization of DE-cadherin (b and b') and Dia (b'') in *dia*^{5} MARCM clones expressing Dia-RNAi. Arrowheads identify AJs between two clonal cells. Confocal immunofluorescent localization of DE-cadherin (c, c', d, and d') and phalloidin staining (d'') in clones expressing Dia-CA in 38 hours APF pupal eyes. Yellow arrows identify clonal cells, while blue arrows identify analogous wild type cells. Yellow arrowheads identify AJs between two clonal cells, while blue arrowheads identify AJs between analogous wild type cells. Confocal immunofluorescent localization of DE-cadherin (e and e') and Dia (e'') in *Rho1*^{72} MARCM clones expressing Dia-CA. Arrowheads identify AJs between two clonal cells. Confocal immunofluorescent localization of DE-cadherin (f and f') and Dia (f and f'') in *rok*^{2} MARCM clones expressing Dia-RNAi. Arrowheads identify AJs between two clonal cells. Scale bars represent 10 μm.

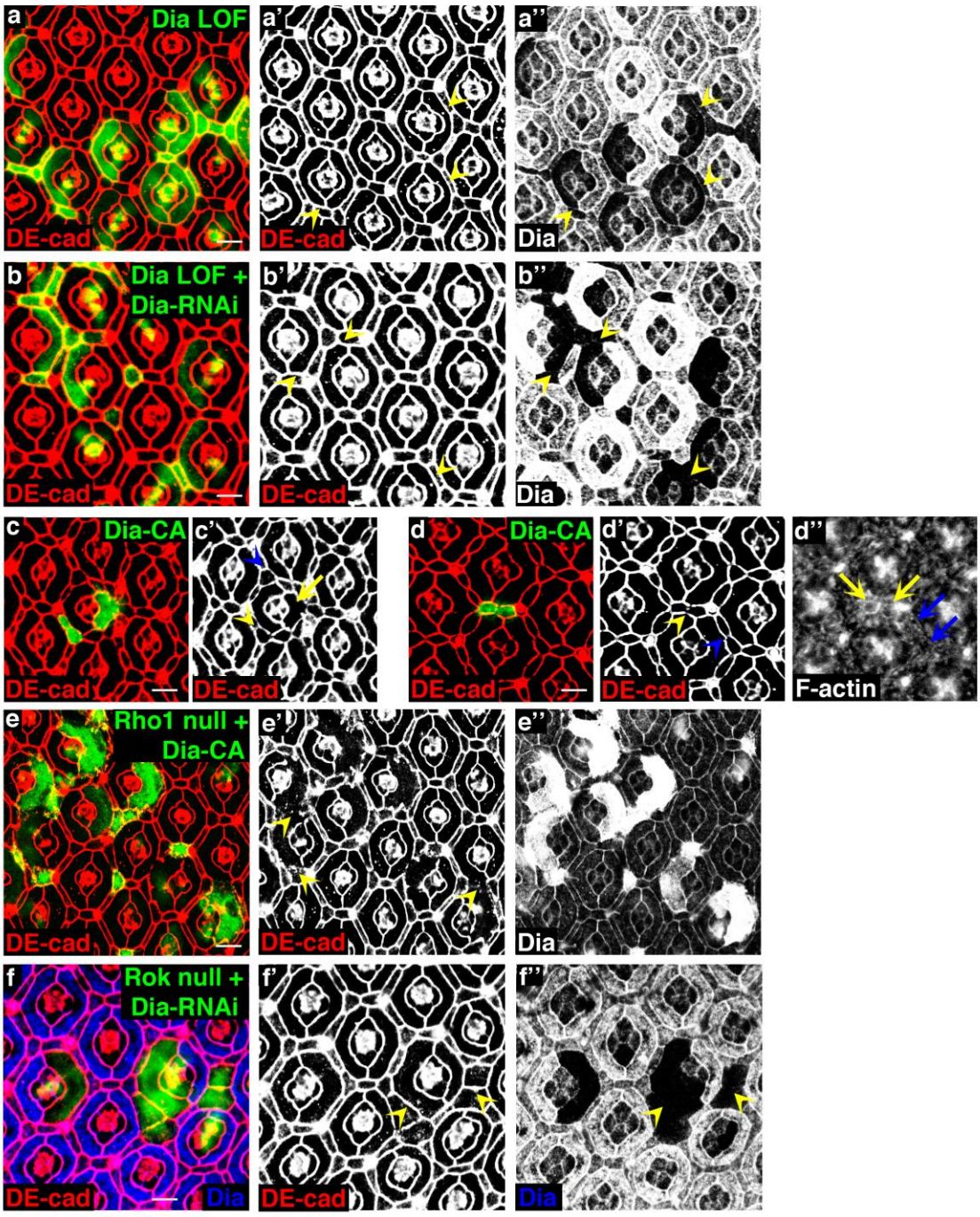
a
Dia LOF
DE-cad
a'
DE-cad
a''
Dia
b
Dia LOF +
Dia-RNAi
DE-cad
b'
DE-cad
b''
Dia
c
Dia-CA
DE-cad
c'
DE-cad
d
Dia-CA
DE-cad
d'
DE-cad
d''
F-actin
e
Rho1 null +
Dia-CA
DE-cad
e'
DE-cad
e''
Dia
f
Rok null +
Dia-RNAi
DE-cad
Dia
f'
DE-cad
f''
Dia

Figure 5

Figure 6. Rho1 does not maintain formed AJs by regulating total cellular DE-cadherin levels.

Western blot analysis of 41 hours APF pupal eyes (a). Quantification of DE-cadherin levels from control and Rho1-RNAi tissue across two independent experiments. Data are represented as mean +/- SD. (b). Confocal immunofluorescent localization of DE-cadherin (c and c') and Armadillo (c and c'') in clones co-expressing Rho1-RNAi and DE-cadherin. Arrowheads identify AJs between two clonal cells. Confocal immunofluorescent localization of DE-cadherin (d and d') and Armadillo (d and d'') in a clone over-expressing DE-cadherin alone. Arrowhead identifies AJ between two clonal cells. Scale bars represent 10 μm.

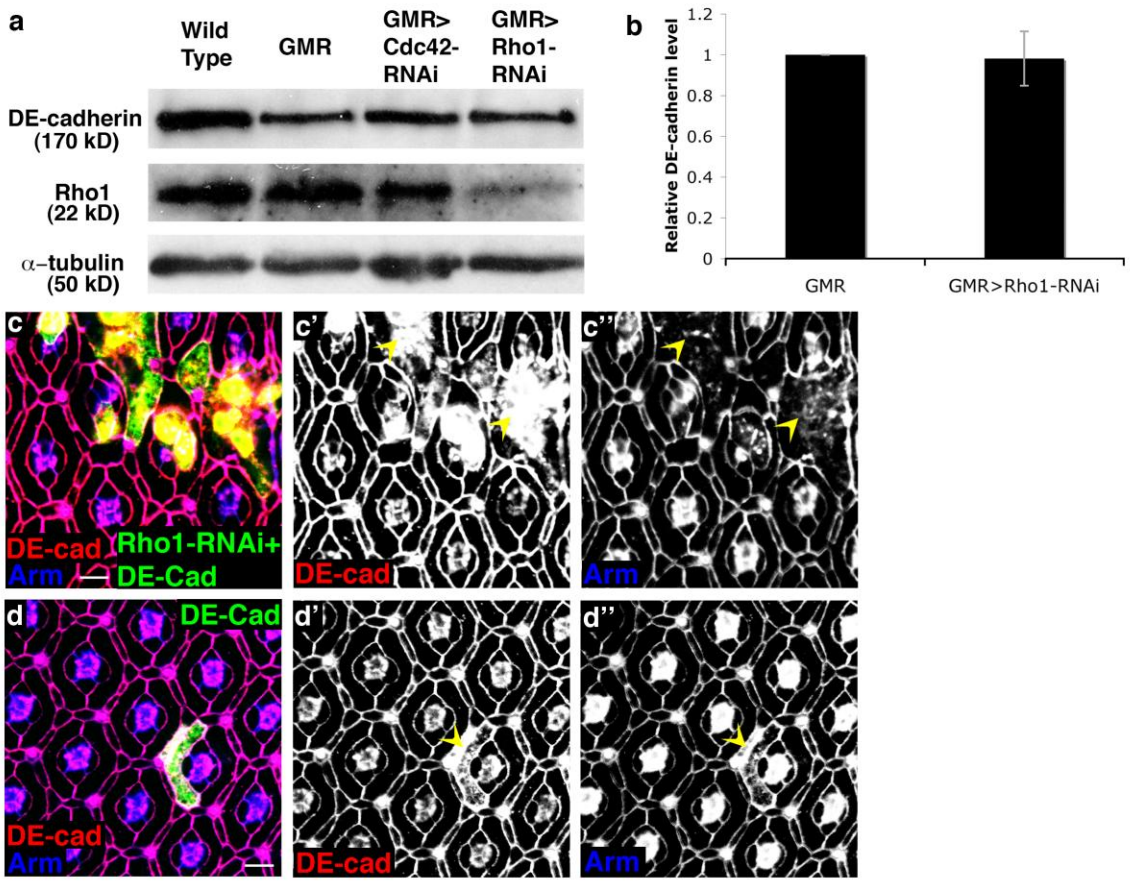
a
Wild Type
GMR
GMR> Cdc42-RNAi
GMR> Rho1-RNAi
DE-cadherin (170 kD)
Rho1 (22 kD)
α–tubulin (50 kD)
b
Relative DE-cadherin level
1.2
1
0.8
0.6
0.4
0.2
0
GMR
GMR>Rho1-RNAi
c
DE-cad
Arm
Rho1-RNAi+ DE-Cad
c'
DE-cad
c''
Arm
d
DE-Cad
DE-cad
Arm
d'
DE-cad
d''
Arm

Figure 6

Figure 7. Rho1 maintains formed AJs by regulating membrane trafficking of DE-cadherin.

Confocal immunofluorescent localization of DE-cadherin in *Rho1*^{72} MARCM clones (a). Confocal immunofluorescent localization of DE-cadherin in *Rho1*^{72} MARCM clones expressing Rab5-DN (b). Arrowheads identify AJs between two clonal cells. Quantification of the ratio of border length positive for DE-cadherin immunofluorescence divided by the total border length between two *Rho1*^{72} clonal cells or two *Rho1*^{72} clonal cells expressing Rab5-DN or Rab5-RNAi (AJ index, see Supplementary Information Table 4) (c). Data are represented as mean +/- SD, p = 0.000066 for Rho1 null + Rab5-DN and p = 0.000351 for Rho1 null + Rab5-RNAi (c). Confocal immunofluorescent localization of DE-cadherin (d and d') and Discs large (d and d'') in *Rho1*^{72} MARCM clones expressing Rab5-CA. Arrowheads identify AJ disruptions between PECs and cone cells. Confocal immunofluorescent localization of DE-cadherin after DE-cadherin endocytosis assay in *Rho1*^{72} MARCM clones (e and e'). Arrowheads identify accumulations of internalized DE-cadherin in Rho1 null clones. Confocal immunofluorescent localization of DE-cadherin (f and f'') and Rho1 (f and f''') in pupal eye expressing Rab5-GFP (f and f'). Arrowheads mark co-localizations between Rab5-GFP, DE-cadherin, and Rho1. This image is 0.75µm basal compared to other pupal eye images. Confocal immunofluorescent localization of DE-cadherin in *Rho1*^{72} MARCM clones expressing Rab11-DN (g). Arrowheads identify AJ disruptions between clonal cells and non-clonal cells. Confocal immunofluorescent localization of DE-cadherin in

Rho1^{72} MARCM clones expressing Rab7-DN (h). Arrowheads identify AJ disruptions between clonal cells. Scale bars represent 10 μm.

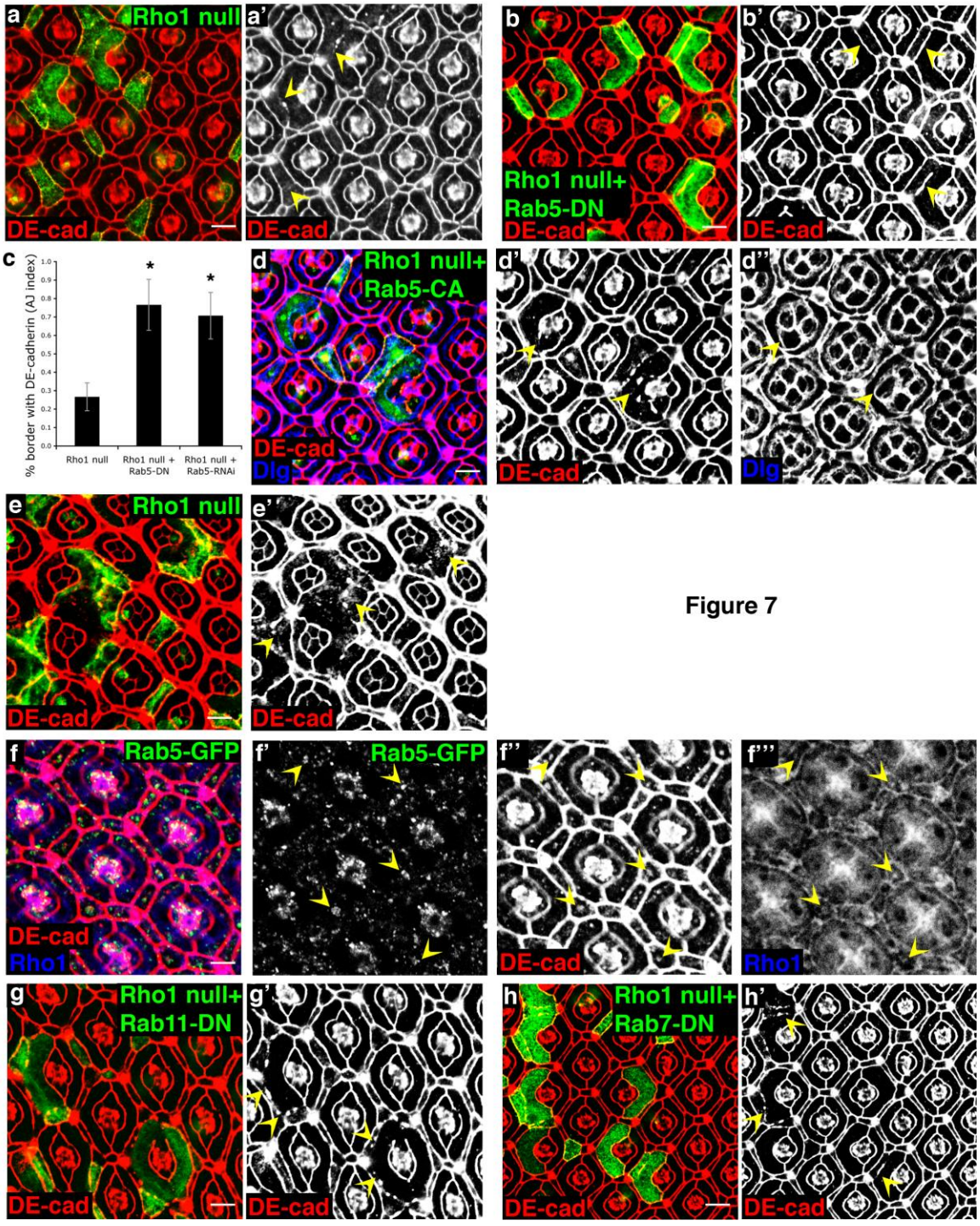
a
Rho1 null
DE-cad
a'
DE-cad
b
Rho1 null+
Rab5-DN
DE-cad
b'
DE-cad
c
% border with DE-cadherin (AJ index)
1.0
0.9
0.8
0.7
0.6
0.5
0.4
0.3
0.2
0.1
0.0
*
*
Rho1 null
Rho1 null + Rab5-DN
Rho1 null + Rab5-RNAi
d
Rho1 null+
Rab5-CA
DE-cad
Dlg
d'
DE-cad
d''
Dlg
e
Rho1 null
DE-cad
e'
DE-cad
f
Rab5-GFP
DE-cad
Rho1
f'
Rab5-GFP
f''
DE-cad
f'''
Rho1
g
Rho1 null+
Rab11-DN
DE-cad
g'
DE-cad
h
Rho1 null+
Rab7-DN
DE-cad
h'
DE-cad

Figure 7

Figure 8. Rho1 regulation of AJs is Cdc42/Par6 dependent.

Confocal immunofluorescent localization of DE-cadherin in *Rho1*^{72} MARCM clones expressing Cdc42-RNAi (a). Confocal immunofluorescent localization of DE-cadherin in *Cdc42*^{4} MARCM clones expressing Rho1-RNAi (b). Confocal immunofluorescent localization of DE-cadherin in *par6*$^{\Delta 226}$ MARCM clones expressing Rho1-RNAi (c). Arrowheads identify AJs between clonal cells. Scale bars represent 10 μm.

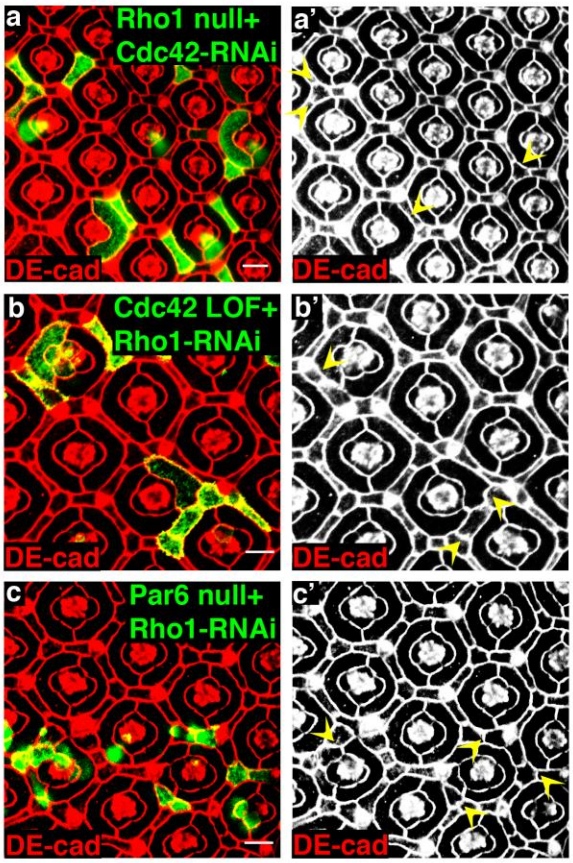
a
Rho1 null+
Cdc42-RNAi
DE-cad
a'
DE-cad
b
Cdc42 LOF+
Rho1-RNAi
DE-cad
b'
DE-cad
c
Par6 null+
Rho1-RNAi
DE-cad
c'
DE-cad

Figure 8

Figure 9. Working model for Rho function in remodeling, formed epithelia.

Rho regulates apical cell tension and AJs independently. Rho sustains apical cell tension mainly through Rok, while Dia can cooperate with Rok for this role. Rho maintains formed AJs by inhibiting DE-cadherin endocytosis, possibly by inhibiting Cdc42/Par6 activity.

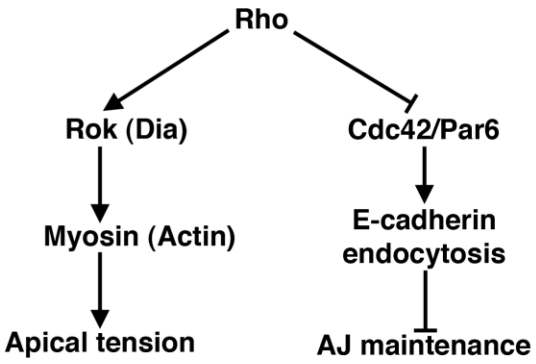
Rho
Rok (Dia)
Cdc42/Par6
Myosin (Actin)
E-cadherin
endocytosis
Apical tension
AJ maintenance

Figure 9

Figure 10. Rho1-RNAi specifically affects Rho1.

Confocal immunofluorescent localization of Rho1 (a and a'') in larval wing disc co-expressing GFP and Rho1-RNAi using *patched-gal4*. Western blot analysis of 41 hours APF pupal eyes (b). Confocal immunofluorescent localization of DE-cadherin in pupal eye co-expressing Rho1-RNAi and Rho1 with *GMR-gal4* (c). Confocal immunofluorescent localization of DE-cadherin (d, d', e, and e') and Rho1 (d, d'', e, and e'') in control or Rho1-RNAi expressing pupal eye 41 hours APF. Confocal immunofluorescent localization of DE-cadherin (f, f', g, and g') and Rho1 (f, f'', g, and g'') in control or Rho1-RNAi expressing pupal eye 21 hours APF. Scale bars represent 10 μm.

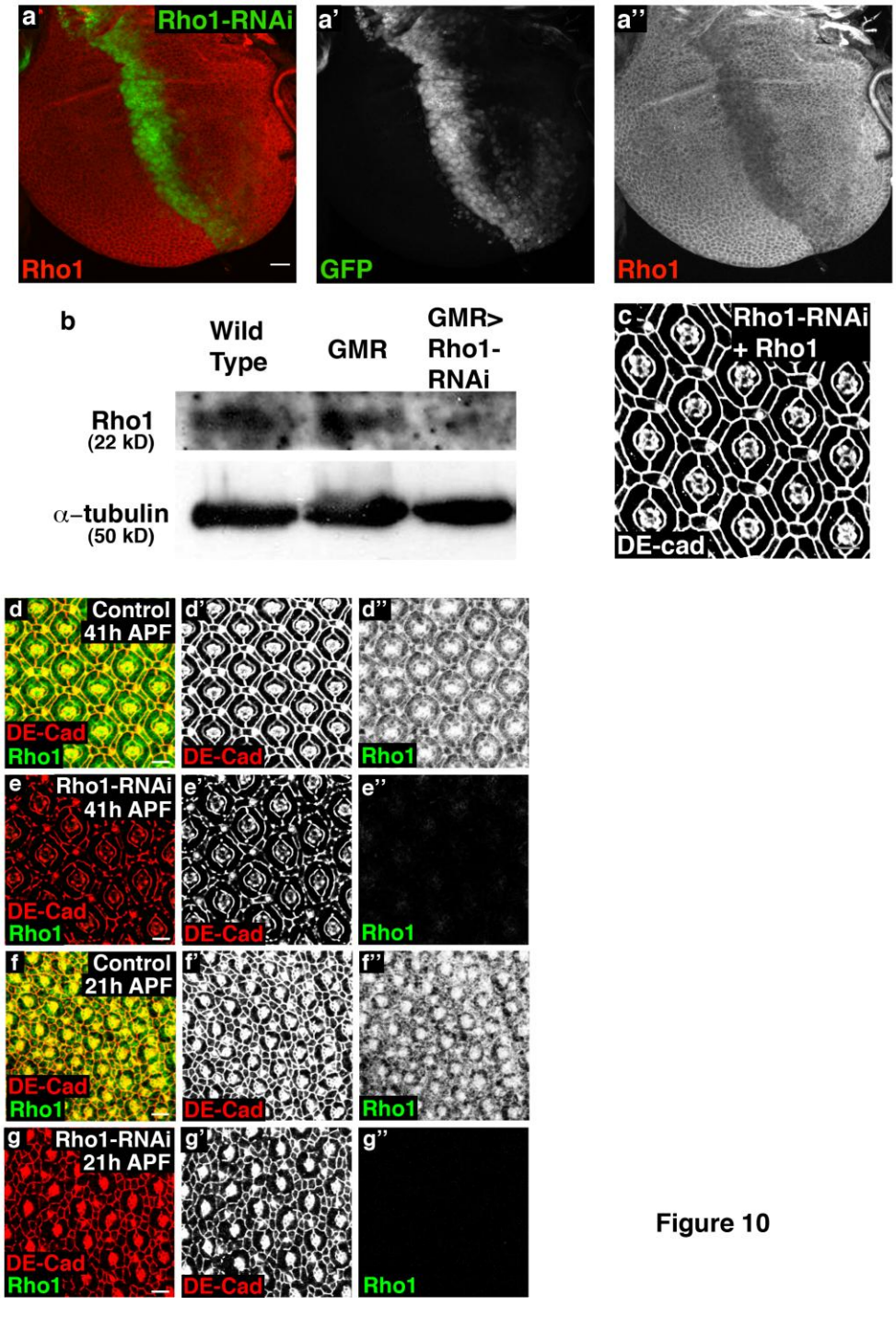
a
Rho1-RNAi
Rho1
a'
GFP
a''
Rho1
b
Wild Type
GMR
GMR> Rho1-RNAi
Rho1 (22 kD)
α–tubulin (50 kD)
c
Rho1-RNAi + Rho1
DE-cad
d
Control 41h APF
DE-Cad
Rho1
d'
DE-Cad
d''
Rho1
e
Rho1-RNAi 41h APF
DE-Cad
Rho1
e'
DE-Cad
e''
Rho1
f
Control 21h APF
DE-Cad
Rho1
f'
DE-Cad
f''
Rho1
g
Rho1-RNAi 21h APF
DE-Cad
Rho1
g'
DE-Cad
g''
Rho1

Figure 10

Figure 11. GMR>Rho1-RNAi phenotypes are enhanced in a Rho1 heterozygous background, Rho1 depletion does not affect localization of the septate junction protein Coracle, Armadillo localization is lost between DE-cadherin null and wild type cells, and Rho1 and Rok depletion decreases phospho-MLC levels.

Adult eyes expressing Rho1-RNAi in a wild type (a) or $Rho1^{72F}$ heterozygous background (b). Adult eye heterozygous for $Rho1^{72F}$ (c). Confocal immunofluorescent localization of DE-cadherin in pupal eye expressing Rho1-RNAi in a wild type (d) or $Rho1^{72F}$ heterozygous background (e). Confocal immunofluorescent localization of DE-cadherin in pupal eye heterozygous for $Rho1^{72F}$ (f). Confocal immunofluorescent localization of DE-cadherin (g and g') and Coracle (g and g'') in $Rho1^{72}$ MARCM clones. Arrowheads identify AJs and SJs between two Rho1 null cells. Confocal immunofluorescent localization of Armadillo in shg^{R69} MARCM clones (h). Arrowheads identify single cell DE-cadherin null clones. Confocal immunofluorescent localization of DE-cadherin (i, i', j, and j') and phospho-MLC (i, i'', j, and j'') in $Rho1^{72}$ and rok^{2} MARCM clones. Arrowheads identify clonal cells. Scale bars represent 10 μm.

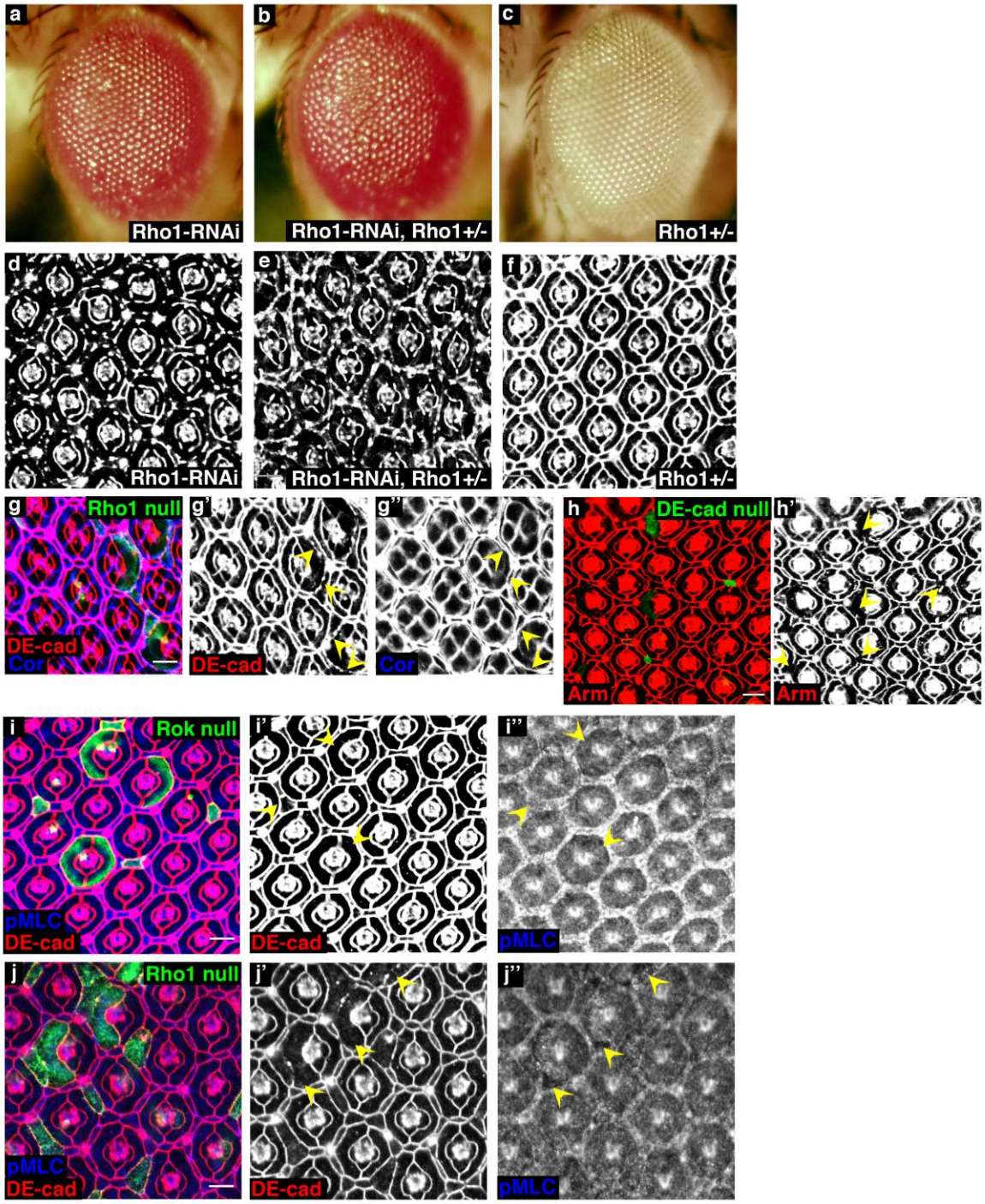
a
Rho1-RNAi
b
Rho1-RNAi, Rho1+/-
c
Rho1+/-
d
Rho1-RNAi
e
Rho1-RNAi, Rho1+/-
f
Rho1+/-
g
Rho1 null
DE-cad
Cor
g'
DE-cad
g''
Cor
h
DE-cad null
Arm
h'
Arm
i
Rok null
pMLC
DE-cad
i'
DE-cad
i''
pMLC
j
Rho1 null
pMLC
DE-cad
j'
DE-cad
j''
pMLC

Figure 11

Figure 12. Dia and Daam do not maintain formed AJs.

Confocal immunofluorescent localization of DE-cadherin (a and a') and Dia (a'') in *dia*^{5} MARCM clones after 30h temperature shift (t.s.) at 29^{o}C. Arrowheads identify AJs between two clonal cells. Confocal immunofluorescent localization of DE-cadherin in Daam^{Ex68} (Daam null) MARCM clones (b). Arrowheads identify AJs between clonal cells. Confocal immunofluorescent localization of DE-cadherin in clones expressing constitutively active Daam (Daam-CA) (c and d). Yellow arrowhead identifies AJ between two clonal cells, while blue arrowhead identifies AJ between two analogous wild type cells (c). Yellow arrows identify clonal cells (d). Scale bars represent 10 μm.

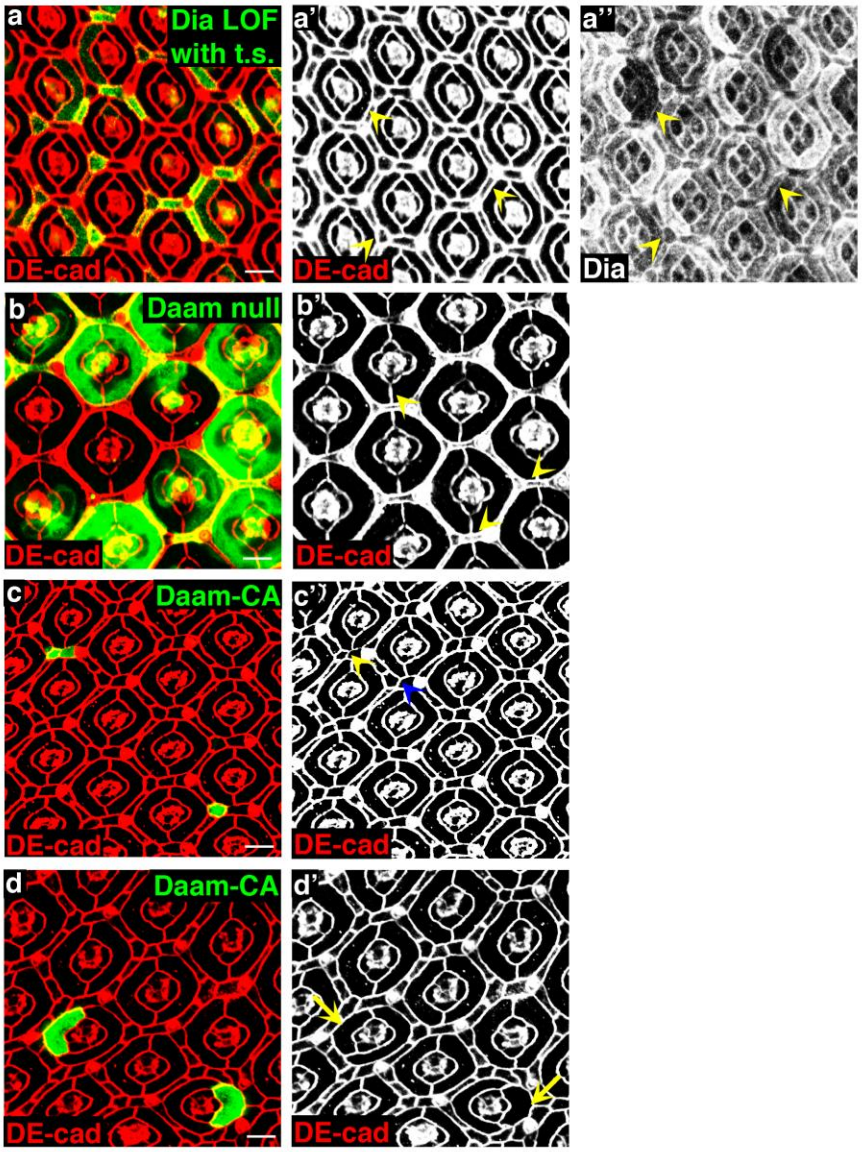
a
Dia LOF
with t.s.
DE-cad
a'
DE-cad
a''
Dia
b
Daam null
DE-cad
b'
DE-cad
c
Daam-CA
DE-cad
c'
DE-cad
d
Daam-CA
DE-cad
d'
DE-cad

Figure 12

Figure 13. Rab5-RNAi expression partially rescues AJ disruptions between Rho1 null cells, Rab5-DN, Rab5-RNAi, or Rab5-CA expression alone does not affect AJs or apical area, and Rho1 depletion increases intracellular DE-cadherin in the endocytic compartment.

Confocal immunofluorescent localization of DE-cadherin in *Rho1*^{72} MARCM clones expressing Rab5-RNAi. Arrowheads identify AJs between clonal cells. Confocal immunofluorescent localization of DE-cadherin in Flp-out clones expressing Rab5-DN (b), Rab5-RNAi (c), or Rab5-CA (d). Arrowheads identify clonal cells. Confocal immunofluorescent localization of DE-cadherin (e, e', f, and f') in pupal eyes expressing either Rab5-GFP alone (e) or Rab5-GFP and Rho1-RNAi (f) with *GMR-gal4*. Arrowheads identify intracellular DE-cadherin that co-localizes with Rab5-GFP. This image is 0.75μm basal compared to other pupal eye images. Scale bars represents 10 μm.

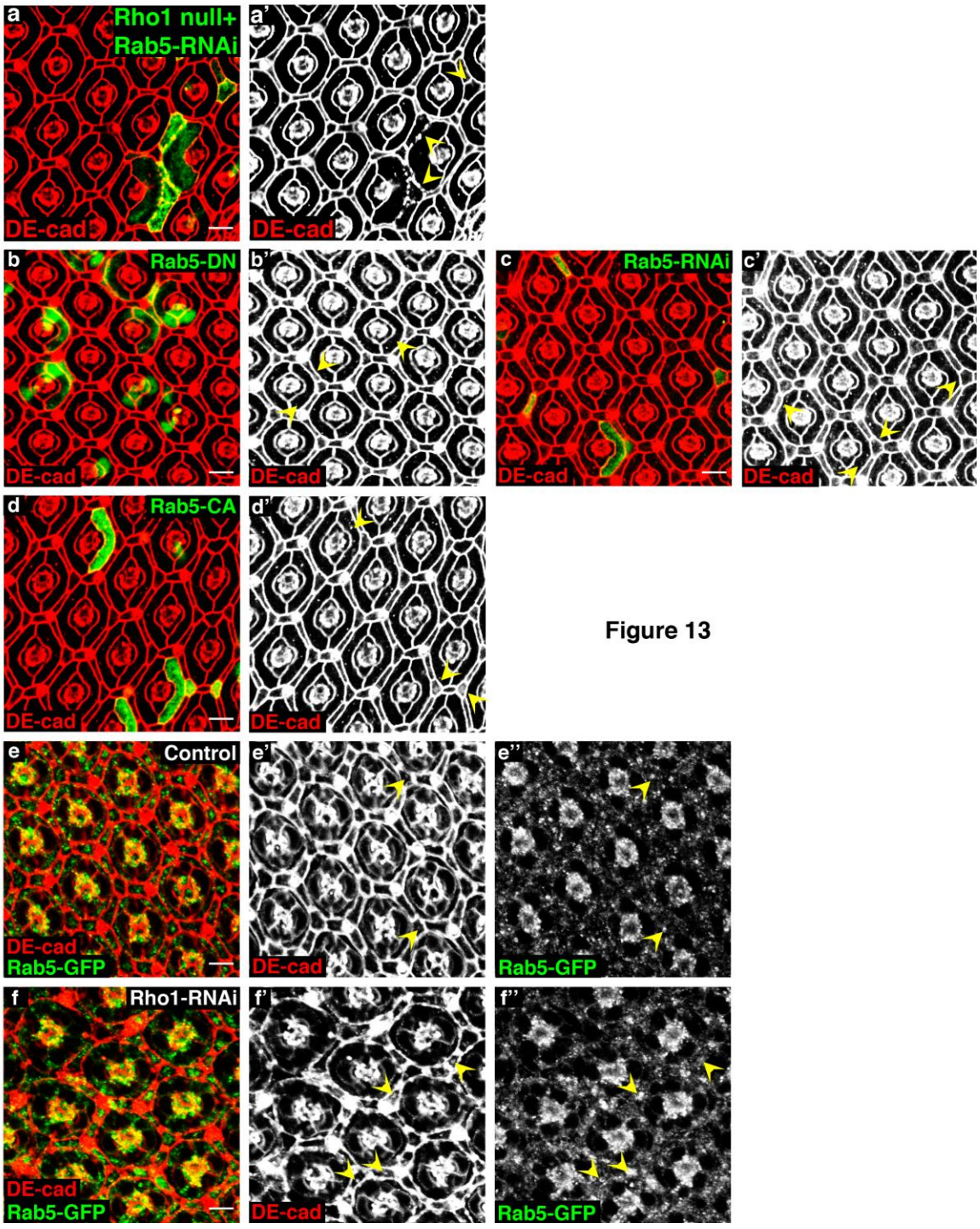
a
Rho1 null+
Rab5-RNAi
DE-cad
a'
DE-cad
b
Rab5-DN
DE-cad
b'
DE-cad
c
Rab5-RNAi
DE-cad
c'
DE-cad
d
Rab5-CA
DE-cad
d'
DE-cad
e
Control
DE-cad
Rab5-GFP
e'
DE-cad
e''
Rab5-GFP
f
Rho1-RNAi
DE-cad
Rab5-GFP
f'
DE-cad
f''
Rab5-GFP

Figure 13

Figure 14. Depletion of Chickadee (Chic) disrupts F-actin but not AJs, expression of Pkn-RNAi disrupts pupal eye patterning but not AJs, Crumbs localization is disrupted by Rho1 depletion or DE-cadherin depletion.

Confocal immunofluorescent localization of DE-cadherin (a and a') and phalloidin staining (a and a'') in *chic*^{221} MARCM clones. Arrowheads identify AJs between clonal cells, and arrows identify clonal cells. Confocal immunofluorescent localization of DE-cadherin in pupal eye expressing Pkn-RNAi (GMR>Pkn-RNAi) (b). Confocal immunofluorescent localization of Armadillo (c, c', d, and d') and Crumbs (c, c'', d, and d'') in *Rho1*^{72} MARCM clones (c) or *shg*^{R69} MARCM clones (d). Arrowheads identify disrupted AJs between Rho1 null cells (c) or around DE-cadherin null cells (d). Scale bars represents 10 μm.

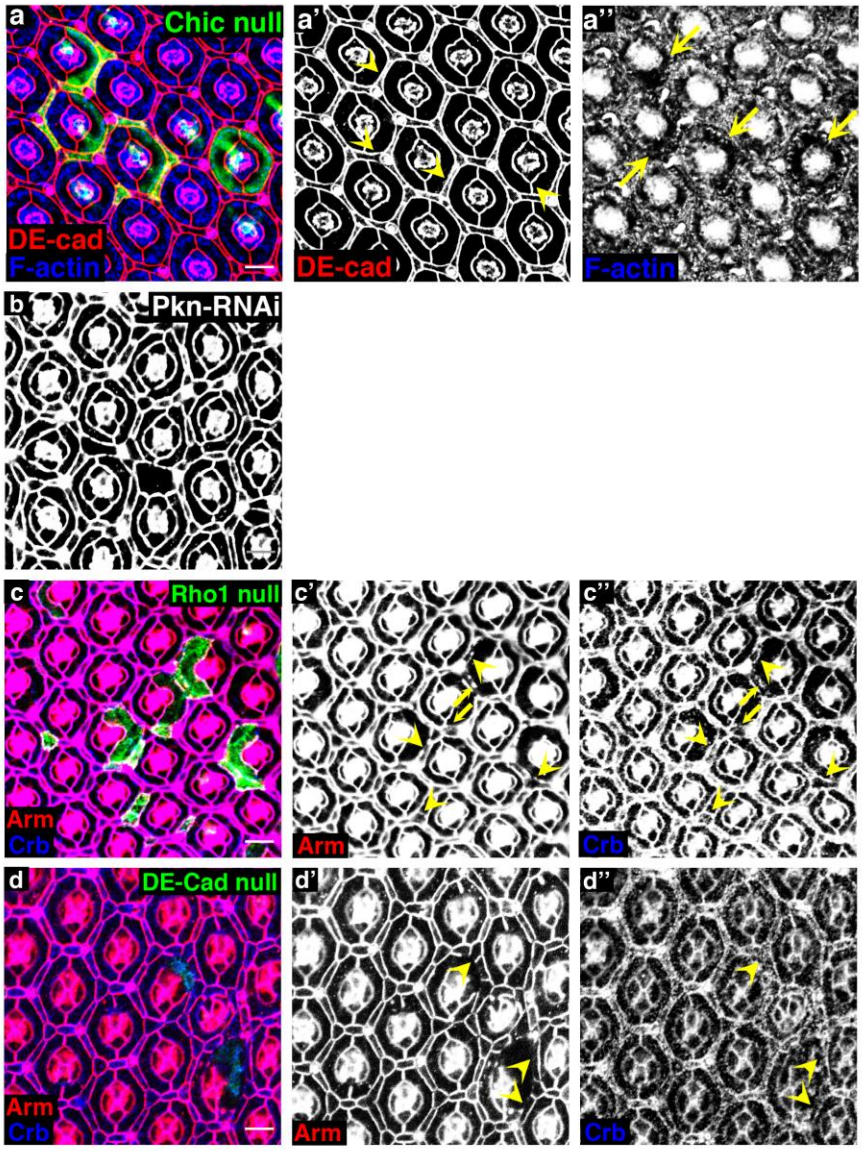
a
Chic null
DE-cad
F-actin
a'
DE-cad
a''
F-actin
b
Pkn-RNAi
c
Rho1 null
Arm
Crb
c'
Arm
c''
Crb
d
DE-Cad null
Arm
Crb
d'
Arm
d''
Crb

Figure 14

Tables

Table 1. Apical area index quantification of *Rho1*^{72}, Rho1-RNAi, *rok*^{2}, and *dia*^{5} clones

Genotype	Apical area index mean	Std dev	N	P
Wild type	0.9975	0.0286	25	
***Rho1*^{72O}**	1.9820	0.1517	40	0.006320
***Rho1*^{72F}**	1.8932	0.1711	23	0.010338
Rho1-RNAi	1.5477	0.0262	67	0.000017
***rok*^{2}**	1.5236	0.0691	35	0.002064
***dia*^{5}**	1.0279	0.0272	76	0.253950
***dia*^{5} + Dia-RNAi**	1.0356	0.0528	43	0.350822
***rok*^{2} + Dia-RNAi**	1.8258	0.1928	38	0.022038*
***Rho1*^{72} + Rho1**	0.8448	0.0792	34	0.065477

Quantification of apical area index. Apical area index is the ratio of a clonal cell apical area divided by an analogous, neighboring non-clonal cell apical area. Quantifications were performed using ImageJ v1.38. P-values were calculated using an unpaired, two-sided Student's t-test against wild type clones, *except for *rok*^{2} + Dia-RNAi which was against *rok*^{2}.

Table 2. F-actin index quantification

Genotype	F-actin index mean	Std dev	N	P
Wild type	1.0125	0.1233	26	
***Rho1*^{72}**	0.7794	0.1829	38	0.018798
***rok*^{2}**	0.9686	0.1084	36	0.620749
***dia*^{5}**	1.0742	0.2761	21	0.131398
***dia*^{5}, Dia-RNAi**	1.0046	0.1396	15	0.857209
***chic*^{221}**	0.6400	0.0279	43	0.000370

Quantification of F-actin index. F-actin index is the ratio of phalloidin staining pixel intensity in a clonal cell divided by an analogous, neighboring non-clonal cell.

Quantifications were performed using ImageJ v1.38. P-values were calculated using an unpaired, two-sided Student's t-test against wild type clones.

Table 3. Phospho-MLC index quantification

Genotype	pMLC index mean	Std dev	N	P (Wild type)	P (*Rho1*^{72})
Wild type	1.0694	0.0396	22		
***Rho1*^{72}**	0.7954	0.0863	40	0.006184	
***rok*^{2}**	0.8234	0.0732	42	0.007296	0.637941

Quantification of phospho-MLC index. Phospho-MLC index is the ratio of phospho-MLC immunofluorescence pixel intensity in a clonal cell divided by an analogous, neighboring non-clonal cell. Quantifications were performed using ImageJ v1.38. P-values were calculated using an unpaired, two-sided Student's t-test against either wild type clones or *Rho1*^{72} clones.

Table 4. Adherens junction index quantification

Genotype	AJ index mean	Std dev	N	P
***Rho1*^{72}**	0.2668	0.0756	41	
***Rho1*^{72} + Rab5-DN**	0.7661	0.1382	54	0.000066
***Rho1*^{72} + Rab5-RNAi**	0.7071	0.1263	36	0.000351
***Rho1*^{72} + Rab11-DN**	0.3487	0.0492	15	0.114392
***Rho1*^{72} + Rab7-DN**	0.3264	0.0646	12	0.394211
***Rho1*^{72} + Rab8-DN**	0.3413	0.0147	12	0.093595
***Rho1*^{72} + Cdc42-RNAi**	0.8946	0.0045	11	0.004461
***Rho1*^{72} + DiaCA**	0.3646	0.0412	37	0.153122
***Rho1*^{72} + Rho1**	1.0000	0.0000	15	0.000027

Quantification of AJ index. AJ index is the ratio of the border length positive for DE-cadherin immunofluorescence divided by the total border length between two clonal

cells. Quantifications were performed using ImageJ v1.38. P-values were calculated using an unpaired, two-sided Student's t-test against *Rho1*^{72} clones.

Table 5. Apical area index quantification in *Rho1*^{72} clones expressing dominant negative Rab transgenes, Rab5-RNAi, or Cdc42-RNAi

Genotype	Apical area index mean	Std dev	N	P
Wild type	0.9975	0.0286	25	
***Rho1*^{72}**	1.9376	0.1526	63	
***Rho1*^{72} + Rho1**	0.8448	0.0792	34	0.000003
***Rho1*^{72} + Rab5DN**	1.9681	0.2906	60	0.839399
***Rho1*^{72} + Rab5-RNAi**	1.8237	0.2366	29	0.435798
***Rho1*^{72} + Rab11DN**	1.9218	0.2022	22	0.912045
***Rho1*^{72} + Rab7DN**	1.9426	0.1964	35	0.971204
***Rho1*^{72} + Rab8DN**	2.0238	0.1738	20	0.610625
***Rho1*^{72} + Cdc42-RNAi**	1.7791	0.3344	35	0.622521

Quantification of apical area index. Apical area index is the ratio of a clonal cell apical area divided by an analogous, neighboring non-clonal cell apical area. Quantifications were performed using ImageJ v1.38. P-values were calculated using an unpaired, two-sided Student's t-test against *Rho1*^{72} clones.

CHAPTER 3

Cdc42 antagonizes Rho1 activity at adherens junctions to limit epithelial cell apical tension

Chapter 3 represents a manuscript currently under revision, entitled “Cdc42 antagonizes Rho1 activity at adherens junctions to limit epithelila tension.”

Cdc42 antagonizes Rho1 activity at adherens junctions to limit epithelial cell apical tension

Stephen J. Warner and Gregory D. Longmore*

Departments of Medicine and Cell Biology

Washington University, St. Louis, MO, 63110

Abstract

In epithelia, cells are arranged in an orderly pattern with a defined orientation and shape. Cadherin containing apical adherens junctions and associated acto-myosin cytoskeleton likely contribute to epithelial cell shape by providing apical tension. The Rho GTPases are well known regulators of both cell junction formation, maintenance, and function and cytoskeletal dynamics. Specifically, Rho promotes acto-myosin activity and cell contractility; however, what controls and localizes this Rho activity as epithelia remodel is unresolved. Using mosaic clonal analysis in the *Drosophila* pupal eye, a post-mitotic epithelium that forms a highly predictable pattern with extreme fidelity, we find that Cdc42 is critical in limiting apical cell tension by antagonizing Rho activity at adherens junctions. It does so by localizing Par6/aPKC to adherens junctions, where this complex limits Rho1 activity, and thus, acto-myosin contractility, independent of its effects upon WASP and Pak. Thus, in addition to its role in the establishment and maintenance of apical-basal polarity in forming epithelia, the Cdc42/Par6/aPKC polarity complex is required to limit Rho activity at AJs and thus modulate apical tension so as to shape the final epithelium.

Introduction

Epithelial cells undergo dynamic changes in cell shape as epithelia undergo morphogenetic changes such as occur during normal development (Montell, 2008), and carcinoma invasion and metastasis where aberrant epithelial cell contractility and morphology are present (Olson and Sahai, 2009). A critical determinant of cell morphology is the acto-myosin cytoskeleton (Montell, 2008), and key regulators of this process are the family of Rho GTPases. Rho, in particular, directly controls acto-myosin contractility by activating two specific effectors: Rho-associated kinase (Rok) to promote phosphorylation and activation of the Myosin Light Chain (MLC), and Diaphanous (Dia) to promote actin filament assembly (Burridge and Wennerberg, 2004). However, how this Rho activity is localized to AJs and regulated during epithelial morphogenesis is not understood. Cdc42, another Rho GTPase, also influences cell morphology. Cdc42-null MEFs have contracted cell bodies (Yang et al., 2006), and Cdc42 regulates *Drosophila* dorsal thorax epithelial cell shape (Georgiou et al., 2008; Leibfried et al., 2008). Moreover, during some tumor cell line invasion in *ex vivo* cultures, Cdc42 cooperates with Rho to activate Myosin and enhance mesenchymal cell motility (Wilkinson et al., 2005). Despite this, precisely how Cdc42 regulates epithelial cell shape during *in vivo* morphogenetic processes is not known.

The *Drosophila* pupal eye is a post-mitotic, non-proliferating remodeling neuroepithelium amenable to *in vivo* clonal genetic loss-of-function analyses. The *Drosophila* eye contains a hexagonal array of repeating functional units called ommatidia. Each ommatidium has a neuronal core of photoreceptors and cone cells

surrounded by light insulating pigment epithelial cells (PECs) (Cagan and Ready, 1989). By 40 hours after puparium formation (APF), the PECs form a highly predictable pattern with extreme fidelity, with each type of PEC (primary, secondary, and tertiary) having a precise morphology repeated across all ommatidia. This, in combination with the use of clonal analysis to genetically modify individual or groups of cells within a tissue of otherwise wild type cells, allows changes in PEC morphology to be easily detected, quantified, and structurally analyzed so as to identify and interrogate molecular pathways that regulate epithelial cell morphology.

The *Drosophila* pupal eye has been used to study other epithelial properties such as cell adhesion (Bao and Cagan, 2005; Hayashi and Carthew, 2004) and cell fate decisions (Nagaraj and Banerjee, 2007). While PECs are all epithelial cells, these studies have revealed important differences between the three types of PECs. For example, two important adhesion molecules in PEC patterning, Roughest and Hibris, are expressed in complementary PECs, with Hibris expressed in primary PECs and Roughest in secondary and tertiary IPCs (Bao and Cagan, 2005).

The pupal eye also serves as a model of a mature epithelium with formed but remodeling intercellular junctions, as opposed to proliferating epithelia (*Drosophila* embryonic or larval, tissue culture) with newly forming junctions between cells. Specifically, differences exist between how adherens junctions (AJs) are maintained and remodeled in the pupal eye epithelium, which is independent of the formin protein Diaphanous (Warner and Longmore, 2009b), compared to the establishment and maintenance of AJs in *Drosophila* embryo and mammalian tissue culture cells, which

requires Diaphanous (Homem and Peifer, 2008; Kobielak et al., 2004; Sahai and Marshall, 2002). Here we used the pupal eye to determine the function of the Rho GTPase Cdc42 in these non-proliferating, remodeling epithelial cells.

Results

Cdc42 regulates septate junction organization but not adherens junctions in non-proliferating, remodeling epithelia

To determine function(s) for Cdc42 in this non-proliferating yet remodeling epithelium, *in vivo*, we performed MARCM clonal analysis (Lee and Luo, 1999) with a strong *Cdc42* loss-of-function (LOF) allele, $Cdc42^{4}$, in *Drosophila* pupal eye PECs (Fig. 1 A and B). Considering Cdc42's well-described role in the establishment and possibly maintenance of epithelial apical-basal polarity and intercellular junctions, we first turned our attention to the possible effects of Cdc42 depletion upon the organization and function of both AJs and septate junctions (SJs, the *Drosophila* functional homolog of vertebrate tight junctions (Furuse and Tsukita, 2006)), and apical-basal polarity. Secondary and tertiary PECs clonal for $Cdc42^{4}$ had unchanged AJs and SJs, as determined by immunofluorescence for DE-cadherin for AJs and Discs large (Dlg), Scribble (Scrib), or Coracle for SJs (Fig. 1 D, E, G). However, in primary PECs, SJ associated proteins, but not AJ proteins, were mislocalized (Fig. 1 C-H). This cell selective effect of Cdc42 depletion on primary PEC SJs was specific as expression of wild type Cdc42 within $Cdc42^{4}$ clonal cells reverted the phenotype (Fig. 1 I, as quantified in Table 1). Although Cdc42 has been shown to be important for proper cell polarity in several mammalian and *Drosophila* cell types (Atwood et al., 2007; Hutterer et al., 2004; Martin-Belmonte et al., 2007; Schwamborn and Puschel, 2004), depletion of Cdc42 in pupal eye epithelia did not disrupt apical-basal polarity, as indicated by the persistent and

appropriate apical localization of DE-cadherin in *Cdc42*^{4} clonal PECs (Fig. 1 F' and H', confocal z-projections). Cdc42 depletion also did not disrupt Crumbs membrane localization (Fig. 13 G-I).

The Dlg/Scrib/Lgl complex is important for apical-basal polarity establishment in mammalian and *Drosophila* epithelia (Bilder, 2004). Surprisingly, although depletion of Cdc42 in PECs disrupted Dlg and Scrib localization (Fig. 1 C, D, G, H), epithelial polarity was unaffected (Fig. 1 F' and H'). To determine directly if Dlg or Scrib was required for maintenance of polarity in pupal eye epithelia, we generated MARCM clones with a *dlg* null allele, *dlg*^{M52}, or a *scrib* null allele, *scrib*^{1}, in pupal eye PECs. As with Cdc42, depletion of Dlg or Scrib did not disrupt epithelial polarity, as determined by apical localization of DE-cadherin (Fig. 10 A-C). To determine whether Dlg and Scrib cooperate to maintain polarity in these epithelial cells, we depleted both Dlg and Scrib by expressing Dlg-RNAi in *Scrib*^{1} MARCM clones. These cells also maintained normal apical-basal polarity (Fig. 10 D). These data indicated that, as opposed to their roles in the establishment and maintenance of polarity in proliferating epithelia (Bilder, 2004; Hutterer et al., 2004; Martin-Belmonte et al., 2007), Cdc42, Dlg, and Scrib were not required for the maintenance of epithelial cell polarity in this non-proliferating epithelium.

Cdc42 inhibits apical cell tension

Cdc42 is also known to regulate cell morphology, but precisely how is not clear. Consistent with previous reports (Georgiou et al., 2008; Leibfried et al., 2008), we found

that all PECs depleted of Cdc42 had decreased apical cell area, as determined by area outlined by DE-cadherin (Fig. 2 A, C, Fig. 3 A, as quantified in Table 2). Analysis of single-cell PEC *Cdc42*^{4} clones indicated the decrease in apical area was cell autonomous and specific to the AJ level (Fig. 3 A and B, as quantified in Table 2). In wild type PECs, the AJs and SJs were aligned along the apical-basal axis (Fig. 3 A and B, white asterisks); however, in *Cdc42*^{4} PEC clones, AJs were spaced within the SJs (Fig. 3 A and B, yellow arrowheads and asterisk). Analysis basal to the SJs revealed no other significant changes in cell shape compared to surrounding cells (data not shown). This decrease in apical cell area in *Cdc42*^{4} clonal cells was rescued by expression of Cdc42 in *Cdc42*^{4} clonal cells (Fig. 2 B and C). We also observed this phenotype in MARCM clones with a weak *Cdc42* LOF allele, *Cdc42*^{2}, and Flp-out clones (Ito et al., 1997) with Cdc42-RNAi (Fig. 2 C, Fig. 11 A, as quantified in Table 2), although these manipulations decreased apical area to a lesser extent compared to the strong LOF allele *Cdc42*^{4} (Fig. 2 C), likely reflecting the amount of residual Cdc42 protein. Moreover, overexpression of Cdc42 in PECs resulted in increased apical area at the AJ level (Fig. 2 C and 3 C, as quantified in Table 2), and PECs overexpressing Cdc42 had AJs that were spaced wider than SJs (Fig. 3 C'', white arrowhead). Depletion of Cdc42 in the pupal wing epithelium, by expressing Cdc42-RNAi in a defined subset of cells, also resulted in decreased epithelial cell apical areas (Fig. 2 D and E). Together, these data indicated that Cdc42 contributes to epithelial cell shape possibly by limiting apical tension of pupal epithelial cells. Unlike Cdc42, MARCM clones null for *rac1* and *rac2* and heterozygous for the *mtl* null allele, *mtl*$^{\Delta}$, did not affect PEC AJs, SJs, or apical area (Fig. 12 G).

Expression of Cdc42 dominant proteins results in non-specific phenotypes

Studies of Rho GTPases function often use dominant negative (DN) proteins to ascertain the effect of inhibiting specific Rho GTPase functions. Whether these manipulations are indeed Rho GTPase type specific has not been directly established (Heasman and Ridley, 2008). Specifically, a recent report observed that inhibiting Cdc42 activity, with Cdc42-DN, disrupted AJs in *Drosophila* embryonic ventral neuroectoderm, which was also observed with genetic mutations of *Cdc42* (Harris and Tepass, 2008). We compared phenotypes from genetic depletion of Cdc42 to Cdc42-DN expression in pupal eye epithelium. When compared to control pupal eye (Fig. 12 A), expression of Cdc42-N17 resulted in severe disruption of AJs mainly between secondary and tertiary PECs while SJs remained intact (Fig. 12 B). Furthermore, in individual and clusters of clones expressing Cdc42-N17, secondary and tertiary PECs exhibited increased apical area (Fig. 12 C). Expression of Cdc42-N17 in primary PECs did not affect their apical area, or AJ and SJ organization (Fig. 12 C). These phenotypes were in stark contrast to Cdc42 LOF clones, which included decreases of all PEC apical areas, no effects on AJs, and mislocalization of primary PEC SJ proteins (Fig. 1 C-H). Even in large $Cdc42^{4}$ clones, with more severe patterning defects, no AJ disruptions were seen (Fig. 12 D), indicating that differences between Cdc42-DN and LOF phenotypes were unlikely the result of Cdc42 protein perdurance in $Cdc42^{4}$ clones. In addition, expression of constitutively active Cdc42, Cdc42-V12, resulted in dramatic apical cell constriction (Fig. 12 E), in contrast to the increase in apical area seen when wild type Cdc42 was

overexpressed (Fig. 2 C and 3 C). These data indicated that phenotypes resulting from expressing Cdc42 dominant proteins did not recapitulate genetic manipulations of Cdc42, at least in the pupal eye epithelium.

Cdc42 inhibits Rho1 activity at AJs

A key determinant of epithelial cell tension and contractility is the activity of the acto-myosin cytoskeleton at AJs. Although Cdc42 activity does influence actin cytoskeletal dynamics, precisely how Cdc42 regulates acto-myosin contractility at AJs is not clear. *Cdc42*^{4} clonal cells had increased staining for F-actin and phospho-MLC (Ser19) at the level of AJs (Fig. 4 A and B, as quantified in Table 3 and 4). Consistent with increased F-actin levels and Myosin activity at AJs being associated with apical constriction, clones with LOF alleles of *twinstar* (*Drosophila cofilin*), which inhibits actin polymerization (Chen et al., 2001), and *slingshot*, which activates Cofilin (Niwa et al., 2002), resulted in increased AJ-associated F-actin, as anticipated, and associated apical cell contraction (Fig. 11 B and C, as quantified in Table 2 and 3). Similarly, expression of an active form of Rho-kinase (Rok-CAT) (Verdier et al., 2006) resulted in increased phospho-MLC at AJs and apical constriction (Fig. 11 D, as quantified in Table 2 and 4). Taken together, one possibility these data suggested was that depletion of Cdc42 led to apical cell constriction through an increase in acto-myosin tension at AJs.

Rho promotes epithelial cell apical tension by increasing acto-myosin activity (Conti and Adelstein, 2008), and *Rho1* null clones exhibit increased apical cell area with decreased F-actin and phospho-MLC staining at AJs (Warner and Longmore, 2009b).

These opposing cellular phenotypes of Cdc42 and Rho1 LOF clones suggested the possibility that the increased apical cell tension apparent following Cdc42 depletion could result from increased Rho1 activity at the AJs due to the absence of Cdc42.

To test this possibility we first determined whether depletion of Cdc42 resulted in increased Rho1 activity. Activation of Rho correlates with its localization to AJs where it can activate specific downstream effectors proteins (Harder and Margolis, 2008). Thus, we determined the localization of Rho1 and the Rho1 effector Dia in *Cdc42*^{4} clonal cells. Both Rho1 and Dia staining were increased at AJs in *Cdc42*^{4} clonal cells (Fig. 4 C-F). In contrast, PEC clones overexpressing Cdc42 had decreased Rho1 and Dia at AJs (Fig. 14 A, 4 G). In a second approach we utilized a GFP-tagged isoform of PKN (another Rho effector), PKNG58AeGFP, which associates with active, Rho-GTP, as a surrogate marker for Rho1 activity (Simoes et al., 2006). The level of PKNG58AeGFP at AJs was increased in PECs depleted of Cdc42 (Fig. 5 A-E, as quantified in Table 5). Together these data indicated that in epithelial cells depleted of Cdc42, Rho1 activity was increased at the level of AJs.

If Cdc42 controls apical cell tension through regulation of Rho1 activity, then depletion of Rho1 in *Cdc42*^{4} clonal cells would be predicted to rescue the decreased apical area seen in *Cdc42*^{4} clonal cells. To test this, we expressed Rho1-RNAi in *Cdc42*^{4} clones or removed a genomic copy of *Rho1* in the background of *Cdc42*^{4} clones. By either approach, depletion of Rho1 in *Cdc42*^{4} clonal cells rescued the decreased apical areas seen in *Cdc42*^{4} clones alone (Fig. 5 F-J, as quantified in Table 2). As controls, heterozygous *Rho1* pupal eyes were indistinguishable from wild type (data not shown).

While depletion of Rho1 in Cdc42 LOF clones rescued the decreased apical area, SJs were still disrupted (Fig. 13 A). In addition, overexpression of Rho1 did not disrupt SJs despite causing apical constriction (Fig. 13 B), indicating that, in contrast to apical cell tension, Cdc42 regulated SJs independent of Rho1. Consistent with Cdc42 regulating apical cell tension through Rho1 (i.e., "upstream"), expression of Cdc42-RNAi, which alone caused decreased apical cell areas (Fig. 2 C, Fig 11 A), had no affect on the increase in apical cell area in *Rho1* null clones (Warner and Longmore, 2009b). These genetic data, coupled with Rho1 activity profiles in Cdc42 depleted cells, indicated that Cdc42 depletion resulted in increased Rho1 activity at AJs, which increased acto-myosin activity, apical cell tension, and thus, decreased apical cell area.

Par6/aPKC mediate Cdc42 functions in remodeling epithelium

Rho GTPases regulate cellular functions by interacting with and activating specific effector proteins, which mediate downstream cellular signaling events. Two major effectors downstream of Cdc42 are p21-activated kinase (Pak), which can phosphorylate and inactive cofilin to promote actin polymerization, and Wiskott-Aldrich-syndrome protein (WASP), which promotes branched actin formation through activation of the Arp2/3 complex (Heasman and Ridley, 2008). Surprisingly, unlike Cdc42 LOF clones, MARCM clones depleted of Pak, using the LOF allele $dPak^{16}$, or WASP, using the LOF allele $wasp^{3}$, exhibited normal apical cell area and SJ organization (Fig. 13 C and D). This indicated that Cdc42 regulated apical cell tension and SJ organization independent of the effectors Pak and WASP, at least individually.

Cdc42 is also present in a complex of highly conserved proteins that includes aPKC, Par3, and Par6. To determine if members of this Par polarity complex (aPKC/Par3/Par6) mediated Cdc42 LOF phenotypes, we generated MARCM clones with LOF alleles of *Drosophila bazooka* (*Drosophila Par3*), *aPKC*, and *par-6*. Bazooka LOF clones did not affect apical area or SJ organization (Fig. 13 E). However, Par6 and aPKC LOF clones both phenocopied Cdc42 LOF clones, with decreased apical area and disrupted primary PEC SJs (Fig. 6 A and B, as quantified in Table 2). These data suggested that Cdc42 required its association with Par6/aPKC to regulate apical cell tension and maintain SJ organization.

To determine if the decreased apical area in cells depleted of Par6 and aPKC also resulted from increased Rho1 activity, we depleted Rho1 in Par6 LOF or aPKC LOF clones. This rescued the decrease in apical area seen in Par6 LOF or aPKC LOF clones (Fig. 6 A-F, as quantified in Table 2). In addition, Par6 and aPKC LOF clones had increased Rho1, F-actin, and phospho-MLC staining at AJs, consistent with increased Rho1 activation (Fig. 14 B and C, 6 C-F, as quantified in Table 3 and 4). These data indicated that, like Cdc42 depletion, depletion of Par6 or aPKC increased Rho1 activity that resulted in increased apical tension.

Cdc42 inhibits Rho1 by localizing Par6/aPKC to the AJs

Cdc42 localizes Par6/aPKC to AJs through an interaction with Par6, which associates with and controls the activity of aPKC (Atwood et al., 2007; Henrique and Schweisguth, 2003). Consistent with this, both Par6 and aPKC were mislocalized from

AJs between *Cdc42*^{4} clonal cells (Fig. 8 A and B), and aPKC was mislocalized between *par-6*$^{\Delta 226}$ clonal cells (Fig. 8 C), as anticipated. Bazooka localization at AJs was not affected by Cdc42 depletion (Fig. 13 F). Therefore we asked whether Par6's interaction with Cdc42 was critical for this complex to function in pupal eye PECs. . Clones expressing the Cdc42-binding mutant Par6 phenocopied Cdc42, Par6, and aPKC LOF clones with decreased apical areas, mislocalized primary PEC SJ proteins (Fig. 9 B), and increased AJ-associated F-actin and phospho-MLC (data not shown). aPKC was also mislocalized from AJs between clonal cells expressing Cdc42-binding mutant Par6 (Fig. 8 E). As controls, clones expressing wild type Par6 exhibited normal apical areas, SJ protein organization (Fig. 9 A), AJ-associated F-actin and phospho-MLC (data not shown), and aPKC localization (Fig. 8 D). In addition,in these clones, wild type Par6 was expressed at equal or higher leves than the Cdc42-binding mutant Par6 (Fig. 15 A-C).

In cells depleted of Cdc42, Par6, or aPKC, or cells expressing a Cdc42-binding mutant Par6, apical area was decreased likely as a result of increased Rho1 activity. A common thread to all these genetic manipulations was mislocalization or absence of aPKC from the AJs, suggesting that the increased Rho1 activity and resultant decreased apical areas in these cells could result from absence of aPKC activity at AJs. To test this possibility we expressed either a membrane-associated, prenylated aPKC isoform, aPKC^{CAAX}, or wild type aPKC, aPKC^{WT}, in Cdc42 LOF clones. aPKC^{WT} overexpression in *Cdc42*^{4} clones did not rescue the decreased apical area; however, expression of aPKC^{CAAX} did (Fig. 9 C-F, as quantified in Table 2). In control clones expressing aPKC^{WT} or aPKC^{CAAX} alone, apical area was not altered, aPKC^{WT} was expressed at equal

or higher levels than aPKC^{CAAX}, and while aPKC^{WT} was diffusely localized within the cell, aPKC^{CAAX} localized to the membrane (Fig. 15 D-E).

Discussion

These data support a model where Cdc42 limits epithelial cell apical tension by localizing Par6/aPKC to AJs, where aPKC inhibits Rho1 activity (Fig. 9 G). aPKC could do this either by directly modulating Rho1 activity or localization, or more likely by either inhibiting a Rho GEF or activating a Rho GAP, that would be predicted to be in the vicinity of the AJ. In this regard a recent report identifying p190 RhoGAP as influencing RhoA activity downstream of Par6 to regulate dendritic spine morphogenesis in hippocampal neurons (Zhang and Macara, 2008) might implicate p190 RhoGAP as also regulating epithelial cell tension downstream of Cdc42. Alternatively, perhaps the E3 ubiquitin ligase Smurf, which has been shown to regulate RhoA degradation downstream of Cdc42/Par6/aPKC in mammalian cells (Wang et al., 2003), functions in this regulation. In addition, as seen in other systems (Georgiou et al., 2008; Leibfried et al., 2008; Nakayama et al., 2008; Zhang and Macara, 2008), Par6/aPKC function independently from Par3 in regulating epithelial cell tension.

Cdc42 depletion was recently demonstrated to decrease apical area of pupal notum epithelial cells (Georgiou et al., 2008; Leibfried et al., 2008), and it was suggested this effect was due to delamination of Cdc42 depleted cells as a result of increased DE-cadherin endocytosis, leading to decreased adhesion with neighboring cells. While we also observed a role for Cdc42 in regulating DE-cadherin endocytosis in pupal eye PECs (Warner and Longmore, 2009b), our data suggests that the decrease in PEC apical area is more likely due to increased Rho1 activity at AJs as opposed to increased DE-cadherin endocytosis. In support of this, directly affecting DE-cadherin endocytosis by inhibiting

Rab5 or Rab11 did not affect PEC apical area (Warner and Longmore, 2009b). Also, overexpression of Cdc42 results in increased apical area, which would not be predicted if the apical area phenotype was due to changes in DE-cadherin endocytosis.

Cdc42 can also influence acto-myosin contractility through another effector, MRCK, which phosphorylates MLC and MLC Phosphatase to effectively increase Myosin activity. Indeed, Cdc42-MRCK was found to positively cooperate with Rho-ROCK signaling in tumor cell line invasion, in *ex vivo* cultures (Wilkinson et al., 2005). In contrast, in the remodeling pupal eye epithelium we found that Cdc42 inhibits acto-myosin activity by antagonizing Rho activity, *in vivo*. The effect of Cdc42-MRCK on carcinoma cell line contractility was cell-type dependent, with some cell types (e.g., A375m2 cells) more dependent on Rho-ROCK than Cdc42-MRCK for maintaining Myosin activity. Therefore, Cdc42 may have different effects on acto-myosin contractility in different epithelial cells. Alternatively, while this study analyzed individual tumor cell lines spread on tissue culture plastic, the regulation of epithelial cell contractility in a polarized epithelial monolayer, *in vivo*, analyzed herein is likely to be distinct.

We also demonstrated that Cdc42 depletion in PECs specifically disrupted SJs and not AJs and only around primary PECs. Several differences exist between primary PECs and secondary and tertiary PECs (Bao and Cagan, 2005; Nagaraj and Banerjee, 2007), and these differences may affect the sensitivity of SJs to Cdc42 depletion. How Cdc42/Par6/aPKC maintain primary PEC SJs is still an unanswered question; perhaps this involves the complex's role in endocytosis. Studies in *Drosophila* notum reported

effects on AJs but not SJs following Cdc42 depletion (Georgiou et al., 2008; Leibfried et al., 2008). However, one important difference between the pupal notum and the pupal eye is the proliferation state, with the notum epithelium undergoing proliferation and the pupal eye PECs being post-mitotic. Perhaps the proliferation state of epithelial cells dictates the junctional phenotypes resulting from Cdc42 depletion. For instance, proliferating epithelial cells are forming new intercellular junctions, while post-mitotic non-proliferating epithelial cells mostly remodel existing junctions.

An important technical consideration resulting from our study was that we observed opposite effects on epithelial junctions and apical tension depending on whether Cdc42 was genetically depleted or inhibited by expressing dominant-inhibitory isoforms of Cdc42. Rac-DN expression also disrupted AJs (Bruinsma et al., 2007) (Fig. 12 F), whereas clones genetically depleted of Rac1, Rac2, and Mtl did not (Fig. 12 G). DN Rho proteins, in general, are thought to function by binding and inhibiting Rho GEFs. Cdc42 and Rac often share upstream GEFs, and Cdc42-DN and Rac-DN expression in pupal eye both disrupted AJs but not SJs. Therefore, one possible explanation for differences between phenotypes resulting from genetic depletion of Cdc42 or Rac compared with inhibition of activation by Cdc42- or Rac-DN expression was that these DN proteins inhibit GEFs common to Cdc42 and Rac, thereby inhibiting both Cdc42 and Rac activities. However, even pupal eyes depleted of Rac1, Rac2, Mtl, and Cdc42 had completely intact AJs (Fig. 12 H). Perhaps Cdc42-DN and Rac-DN expression disrupt AJs by binding GEFs that normally activate Rho1, which when genetically depleted does result in disrupted AJs (Warner and Longmore, 2009b). Regardless, these data

emphasize that caution is needed when interpreting results using Rho GTPase dominant mutant proteins, particularly *in vivo*, and should be corroborated with genetic LOF data at all stages of analysis.

Our results showing that the Cdc42/Par6/aPKC polarity complex negatively regulates Rho1 activity draws parallels to events that occur during epithelial tumor (carcinoma) development and progression. Loss of apical-basal polarity, as a result of mislocalization of Cdc42/Par6/aPKC in proliferating epithelial cells, is considered an early and critical event for carcinoma development (Aranda et al., 2008). In addition, activation of RhoA is often associated with increased cancer cell invasion, migration and metastasis (Heasman and Ridley, 2008). Thus, in addition to its role in the establishment of apical-basal polarity in forming epithelia, the Cdc42/Par6/aPKC polarity complex may also be required to limit Rho activity at AJs and thus modulate apical tension so as to shape the final epithelium.

Materials and methods

Drosophila stocks

All crosses and staging were performed at 25°C unless otherwise noted. w^{1118} was used as wild type. Stocks are described in Flybase (http://flybase.bio.indiana.edu). *GMR-gal4*, *tubulin-gal80*^{ts}, *cdc42*^{4} FRT19A, *cdc42*^{2} FRT19A, UAS-GFP, *pak*^{16} FRT82B, UAS-Cdc42N17, UAS-RacN17, UAS-Cdc42V12, *Rho1*^{72F}, *ssh*$^{1\text{-}11}$ FRT82B, *rac1*^{J11}*rac2*$^{\Delta}$ FRT2A *mtl*$^{\Delta}$ were kindly provided by the Bloomington *Drosophila* Stock Center, *patched-gal4*, *wsp*^{3} FRT82B, and *scrib*^{1} FRT82B by R. Cagan (Mount Sinai, New York, NY), UAS-PKNG58AeGFP by A. Jacinto (Instituto Gulbenkian de Ciência, Oeiras, Portugal), *tsr*^{99E} FRT42D by F. Pichaud (University College London, UK), UAS-Rok-CAT by G-C. Chen (Academia Sinica, Taipei, Taiwan), *par6*$^{\Delta 226}$ FRT19A, *apkc*^{k06403} FRTG13, *baz*^{4} FRT19A, UAS-aPKC^{WT}, UAS-aPKC^{CAAX}, and *dlg*^{m52} by C. Doe (University of Oregon, Eugene, OR), UAS-Dlg-RNAi by the Vienna *Drosophila* RNAi Center. Rho1-RNAi and Cdc42-RNAi were previously described (Warner and Longmore, 2009b).

Clonal analysis and genetics

To generate Flp-out clones overexpressing a transgene, progeny from Act5C>y^{+}>gal4, UAS-GFP; hsFLP crossed to the following genotypes were heat-shocked for 30 minutes at 37°C as 3rd instar larvae or early pupae: (1) UAS-Cdc42-RNAi, (2) UAS-Cdc42, (3) UAS-aPKC^{WT}, (4) UAS-aPKC^{Caax}, (5) UAS-Cdc42-N17, (6), UAS-

Rok-CAT, (7) UAS-Par6^{WT}, (8) UAS-Par6^{ISAA}. Clones were marked by the presence of GFP.

MARCM clones were generated by heat-shocking larvae with the following genotypes for 1 hour at 37^{o}C:

cdc42^{2}, FRT19A/hsFLP, *tub-gal80*, FRT19A; UAS-GFP, UAS-*lacZ*/+; *tub-gal4*/+

cdc42^{4}, FRT19A/hsFLP, *tub-gal80*, FRT19A; UAS-GFP, UAS-*lacZ*/+; *tub-gal4*/+

baz^{4}, FRT19A/hsFLP, *tub-gal80*, FRT19A; UAS-GFP, UAS-*lacZ*/+; *tub-gal4*/+

par-6$^{\Delta 226}$, FRT19A/hsFLP, *tub-gal80*, FRT19A; UAS-GFP, UAS-*lacZ*/+; *tub-gal4*/+

hsFLP, UAS-GFP; *tsr^{99E}*, FRT42D/*tub-gal80*, FRT42D; *tub-gal4*/+

hsFLP, UAS-GFP; *tub-gal4*/+*; pak^{16}*, FRT82D/*tub-gal80*, FRT82D

hsFLP, UAS-GFP; *tub-gal4*/+*; wsp^{3}*, FRT82D/*tub-gal80*, FRT82D

hsFLP, UAS-GFP; *tub-gal4*/+*; ssh$^{1-11}$*, FRT82D/*tub-gal80*, FRT82D

hsFLP, UAS-GFP; *aPKC^{k06403}*, FRTG13/*tub-gal80*, FRTG13; *tub-gal4*/+

hsFLP, UAS-GFP; *GMR-gal4*/+*; rac1^{J11}*, *rac2$^{\Delta}$*, FRT2A, *mtl$^{\Delta}$*/*tub-gal80*, FRT2A

cdc42^{4}, FRT19A/hsFLP, *tub-gal80*, FRT19A; UAS-GFP, UAS-*lacZ*/UAS-Rho1-RNAi; *tub-gal4*/+

cdc42^{4}, FRT19A/hsFLP, *tub-gal80*, FRT19A; UAS-GFP, UAS-*lacZ*/UAS-Cdc42; *tub-gal4*/+

cdc42^{4}, FRT19A/hsFLP, *tub-gal80*, FRT19A; UAS-GFP, UAS-*lacZ*/*Rho1^{72F}*; *tub-gal4*/+

cdc42^{4}, FRT19A/hsFLP, *tub-gal80*, FRT19A; UAS-GFP, UAS-*lacZ*/UAS-aPKC^{WT}; *tub-gal4*/+

cdc42^{4}, FRT19A/hsFLP, *tub-gal80*, FRT19A; UAS-GFP, UAS-*lacZ*/UAS-aPKC^{Caax}; *tub-gal4*/+

par-6$^{\Delta 226}$, FRT19A/hsFLP, *tub-gal80*, FRT19A; UAS-GFP, UAS-*lacZ*/+; *tub-gal4*/UAS-Par6^{WT}

par-6$^{\Delta 226}$, FRT19A/hsFLP, *tub-gal80*, FRT19A; UAS-GFP, UAS-*lacZ*/+; *tub-gal4*/UAS-Par6^{ISAA}

par-6$^{\Delta 226}$, FRT19A/hsFLP, *tub-gal80*, FRT19A; UAS-GFP, UAS-*lacZ*/UAS-Rho1-RNAi; *tub-gal4*/+

par-6$^{\Delta 226}$, FRT19A/hsFLP, *tub-gal80*, FRT19A; UAS-GFP, UAS-*lacZ*/*Rho1*^{72F}; *tub-gal4*/+

hsFLP, UAS-GFP; *aPKC*^{k06403}, FRTG13/*tub-gal80*, FRTG13; *tub-gal4*/UAS-Rho1-RNAi

Clones were marked by the presence of GFP.

Expression of either GFP alone or GFP and Cdc42-RNAi with *patched-gal4* in the pupal wing was performed by crossing *patched-gal4*, UAS-GFP, *tub-gal80*^{ts}/SM6a-TM6b to *w*^{1118} or UAS-Cdc42-RNAi/SM6a-TM6b at 18^{o}C. Progeny were shifted to 29^{o}C 3-4 days after egg laying and dissected at 18 hours APF.

Immunofluorescence

Pupal eyes or wings were dissected in PBS, fixed in 4% paraformaldehyde for 45 minutes, washed once in PBS-T (PBS/0.1% Triton X-100), washed twice in PAXD (PBS containing 1% BSA, 0.3% Triton X-100, 0.3% deoxycholate), and washed once in

PAXDG (PAXD with 5% goat serum), all on ice. The tissue was then incubated overnight at 4°C with primary antibodies diluted in PAXDG, washed three times in PBS-T, and incubated overnight at 4°C with secondary antibodies diluted in PAXDG. After washing twice in PBS-T, the tissue was post-fixed in 4% paraformaldehyde for 25 minutes at room temperature, washed twice in PBS-T, and mounted in Vectashield mounting media (Vector Labs). Antibodies used were rat anti-DE-cadherin (1:20), mouse anti-Armadillo (1:500), mouse anti-Discs large (1:50), mouse anti-Rho1 (1:20), mouse anti-Coracle (1:20), (all from the Developmental Studies Hybridoma Bank at the University of Iowa), rabbit anti-Dia (1:500, from S. Wasserman, UCSD, San Diego, CA), rat anti-Crumbs (1:500, from U. Tepass, University of Toronto, Ontario, CA), rabbit anti-Bazooka (1:500, from A. Wodarz, University of Göttingen, Germany), guinea pig anti-Scrib (1:500, from D. Bilder, University of California, Berkeley, CA), rabbit anti-Par6 (1:500, from J. Knoblich, IMBA, Vienna, Austria), rabbit anti-aPKC (C-20) (1:200, Santa Cruz Biotechnology), and rabbit anti-phospho-Myosin Light Chain 2 (Ser19) (1:20, Cell Signaling). Rhodamine-phalloidin (1:500, Invitrogen) was added in the primary and secondary antibody incubations to visualize F-actin. Secondary antibodies were Alexa 488 and 568 (Invitrogen) and Cy5 (Jackson ImmunoResearch). Immunofluorescence was analyzed on a Zeiss 510 LSM.

Quantification and statistics

Images were analyzed using ImageJ v1.38 (NIH). Apical area indices were calculated as the ratio of a clonal cell apical area divided by an analogous, neighboring non-clonal cell

apical area at AJs. F-actin indices were calculated as the ratio of phalloidin staining pixel intensity in a clonal cell divided by that in an analogous, neighboring non-clonal cell. Phospho-MLC indices were calculated as the ratio of phospho-MLC immunofluorescence pixel intensity in a clonal cell divided by that in an analogous, neighboring non-clonal cell. Pixel intensities for phalloidin staining and phospho-MLC immunofluorescence at AJs were determined by outlining DE-cadherin around a single cell in a confocal image and measuring the average pixel value within that area. PKNG58AeGFP peak pixel intensities were determined from plotting and listing pixel values across a line drawn through PEC AJs (as shown in Fig. 5 A and B). P-values were calculated using unpaired, two-sided Student's t-tests.

Acknowledgements

We thank R. Cagan for support during the initial stages of this work. We thank R. Cagan, A. Jacinto, F. Pichaud, G-C. Chen, C. Doe, S. Wasserman, U. Tepass, A. Wodarz, D. Bilder, J. Knoblich, the Bloomington *Drosophila* Stock Center, the Vienna *Drosophila* RNAi Center, and the Developmental Studies Hybridoma Bank for reagents. This work was supported by grants NIH CA85839 and GM080673 to GDL.

Figures

Figure 1. Cdc42 regulates SJ organization but not AJs or apical-basal polarity

Confocal immunofluorescent localization of DE-cadherin (DE-cad) in wild type pupal eye (A, B). c = cone cell, b = bristle cell, 1^o = primary pigment epithelial cell (PEC), 2^o = secondary PEC, 3^o = tertiary PEC. The photoreceptors are basal to this optical section. Anterior is to the right in all images. This and subsequent pupal eyes are 40 hours APF. Confocal immunofluorescent localization of DE-cadherin (C, C') and Discs large (Dlg) (C, C'', C''') in *Cdc42*^{4} MARCM clones. Arrowheads identify AJs (C') and SJs (C'', C''') around clonal primary PECs. In this and subsequent images of AJs and SJs together, SJs were imaged approximately 1µm basal to the AJs. Confocal immunofluorescent localization of DE-cadherin (D, D') and Scribble (Scrib) (D, D'', D''') in *Cdc42*^{4} MARCM clones. Arrowheads identify AJs (D') and SJs (D'', D''') around *Cdc42*^{4} clonal primary PECs. Confocal immunofluorescent localization of DE-cadherin (E, E', F, F') and Coracle (Cor) (E, E'', E''', F, F'') in apical (E-E''') and lateral (F-F'') optical sections of *Cdc42*^{4} MARCM clones. White line (E) identifies where lateral section (F-F'') was taken. Yellow asterisks identify *Cdc42*^{4} MARCM clones, while white asterisks identify analogous non-clonal, wild type cells. Arrowheads identify AJs (E', F) and SJs (E'', E''', F) around *Cdc42*^{4} clonal primary PECs. Confocal immunofluorescent localization of DE-cadherin (G, G', H, H') and Discs large (G, G'', G''', H, H'') in apical (G-G''') and lateral (H-H'') optical sections of *Cdc42*^{4} MARCM clones. White line (G) identifies where lateral section (H-H'') was taken. Yellow arrowhead identifies AJ (G', H') and SJ (G'', G''', H'') around *Cdc42*^{4} clonal cell, while

red arrowheads identify AJs (G', H') and SJs (G'', H'') around analogous non-clonal, wild type cells. Asterisk identifies photoreceptor axon projecting through ommatidium (H''). Confocal immunofluorescent localization of DE-cadherin (I, I') and Discs large (I, I'', I''') in *Cdc42*^{4} MARCM clones that express wild type Cdc42. Arrowheads identify AJs (I') and SJs (I'', I''') around clonal cells. Scale bars represent 10 μm.

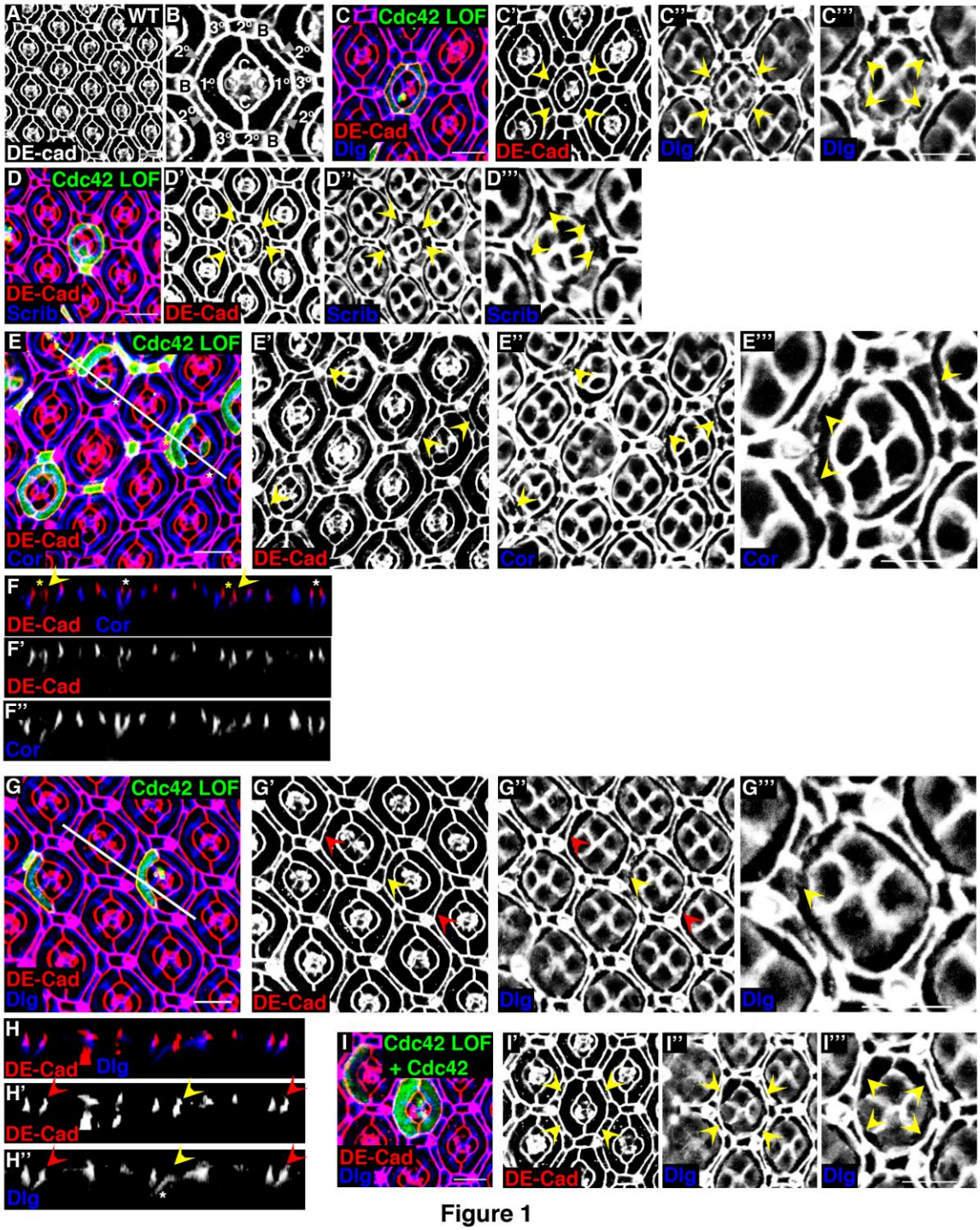
A
WT
DE-cad
B
1°
2°
3°
B
C
Cdc42 LOF
DE-Cad
Dlg
C'
DE-Cad
C''
Dlg
C'''
Dlg
D
Cdc42 LOF
DE-Cad
Scrib
D'
DE-Cad
D''
Scrib
D'''
Scrib
E
Cdc42 LOF
DE-Cad
Cor
E'
DE-Cad
E''
Cor
E'''
Cor
F
DE-Cad
Cor
F'
DE-Cad
F''
Cor
G
Cdc42 LOF
DE-Cad
Dlg
G'
DE-Cad
G''
Dlg
G'''
Dlg
H
DE-Cad
Dlg
H'
DE-Cad
H''
Dlg
I
Cdc42 LOF
+ Cdc42
DE-Cad
Dlg
I'
DE-Cad
I''
Dlg
I'''
Dlg

Figure 1

Figure 2. Cdc42 inhibits apical cell tension

Confocal immunofluorescent localization of DE-cadherin in *Cdc42*^{4} MARCM clones (A-A'''). Arrowheads identify clonal cells. Confocal immunofluorescent localization of DE-cadherin in *Cdc42*^{4} MARCM clones expressing wild type Cdc42 (B-B'''). Arrowheads identify clonal cells. Quantification of apical areas in clonal cells depleted of Cdc42 or overexpressing wild type Cdc42 (apical area index, see Table 2) (C). Data are represented as mean +/- SD. * $P<0.05$, ** $P<0.01$, *** $P<0.001$. Confocal immunofluorescent localization of DE-cadherin (D, D') in pupal wing epithelial cells expressing GFP (D, D'') using *patched-gal4*. Confocal immunofluorescent localization of DE-cadherin (E, E') in pupal wing epithelial cells co-expressing GFP (E, E'') and Cdc42-RNAi using *patched-gal4*. Scale bars represent 10 μm.

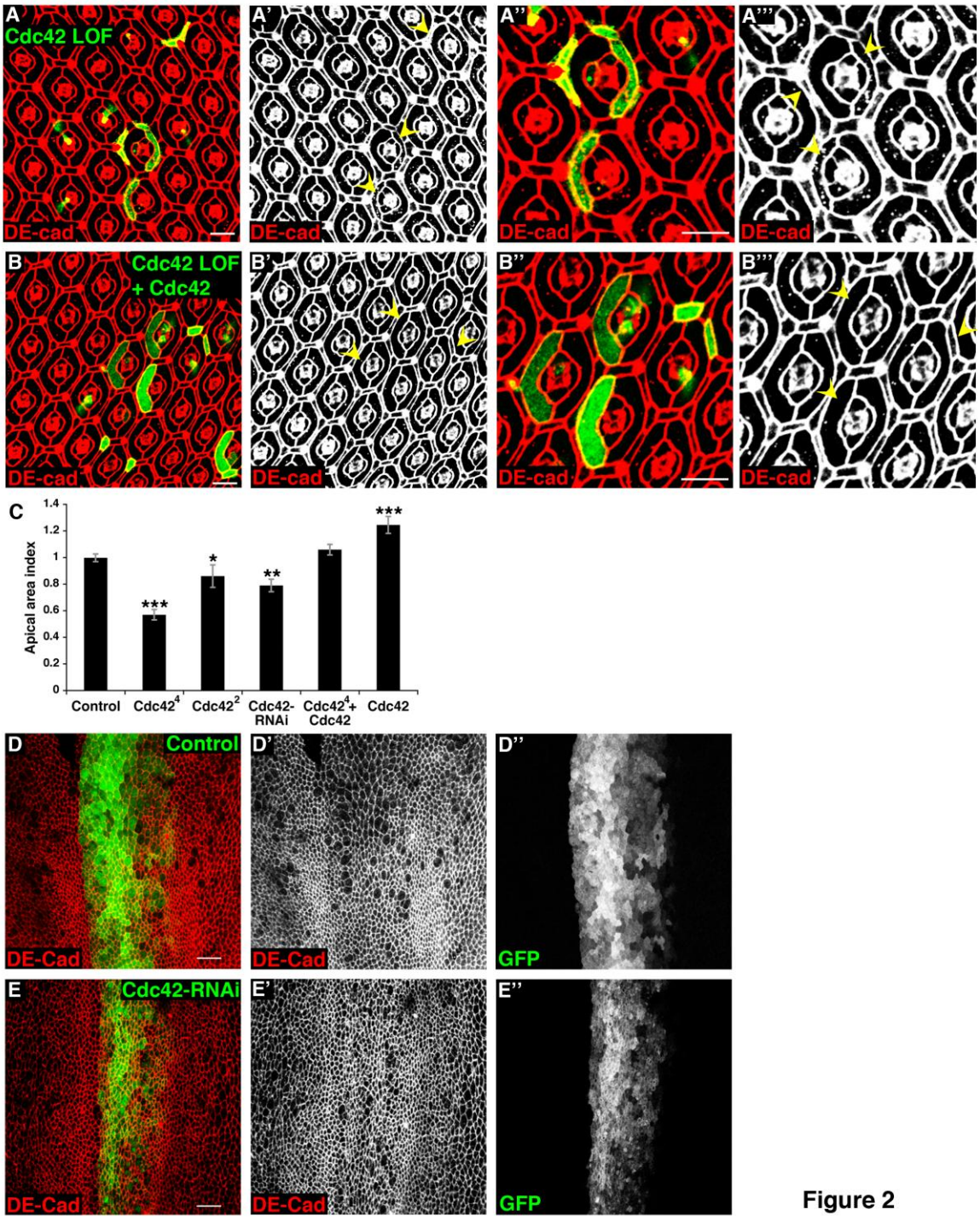
A
Cdc42 LOF
DE-cad
A'
DE-cad
A''
DE-cad
A'''
DE-cad
B
Cdc42 LOF
+ Cdc42
DE-cad
B'
DE-cad
B''
DE-cad
B'''
DE-cad
C
Apical area index
1.4
1.2
1
0.8
0.6
0.4
0.2
0
***
*
**
***
Control
Cdc42^4
Cdc42^2
Cdc42-RNAi
Cdc42^4+ Cdc42
Cdc42
D
Control
DE-Cad
D'
DE-Cad
D''
GFP
E
Cdc42-RNAi
DE-Cad
E'
DE-Cad
E''
GFP

Figure 2

Figure 3. Cdc42 specifically inhibits apical tension at AJs

Confocal immunofluorescent localization of DE-cadherin (A, A', A''', B) and Coracle (Cor) (A, A'', A''', B) in apical (A-A''') and lateral (B) optical sections of *Cdc42*^{4} MARCM clones. White line (A''') identifies where lateral section (B) was taken. Yellow asterisk identifies *Cdc42*^{4} MARCM clone, while white asterisks identify analogous non-clonal, wild type cells. Arrowheads identify AJs (A', A''') and SJs (A'', A''') around clonal cells. Confocal immunofluorescent localization of DE-cadherin (C-C'') and Discs large (C and C'') in Flp-out clones overexpressing wild type Cdc42. Arrowheads identify clonal cells. Scale bars represent 10 μm.

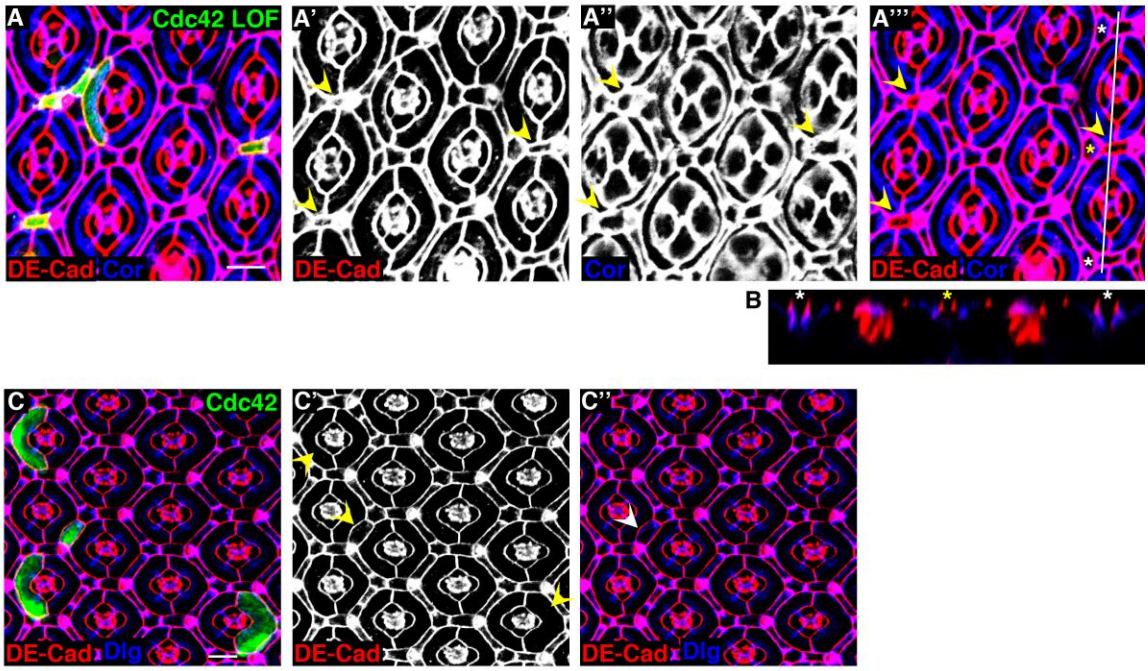
A
Cdc42 LOF
DE-Cad Cor
A'
DE-Cad
A''
Cor
A'''
DE-Cad Cor
B
C
Cdc42
DE-Cad Dlg
C'
DE-Cad
C''
DE-Cad Dlg

Figure 3

Figure 4. Cdc42 inhibits F-actin, pMLC, Dia, and Rho1 localization at AJs

Confocal immunofluorescent localization of DE-cadherin (A, A', B, B'), F-actin (A, A''), and phospho-MLC (B, B'') in *Cdc42*^{4} MARCM clones. Arrowheads identify clonal cells. Yellow asterisks identify bristles around one ommatidum, which have high levels of F-actin (A''). Confocal immunofluorescent localization of DE-cadherin (C, C', E, E'), Dia (C, C''), and Rho1 (E, E'') in *Cdc42*^{4} MARCM clones. Arrowheads identify clonal cells. Pixel intensity profile of DE-cadherin and Dia immunofluorescence along white line in C (D). Asterisks correspond to PECs in C. Pixel intensity profile of DE-cadherin and Rho1 immunofluorescence along white line in E (F). Asterisks correspond to PECs in E. Confocal immunofluorescent localization of DE-cadherin (G, G') and Dia (G, G'') in Flp-out clones overexpressing wild type Cdc42. Arrowheads identify clonal cells. Scale bars represent 10 μm.

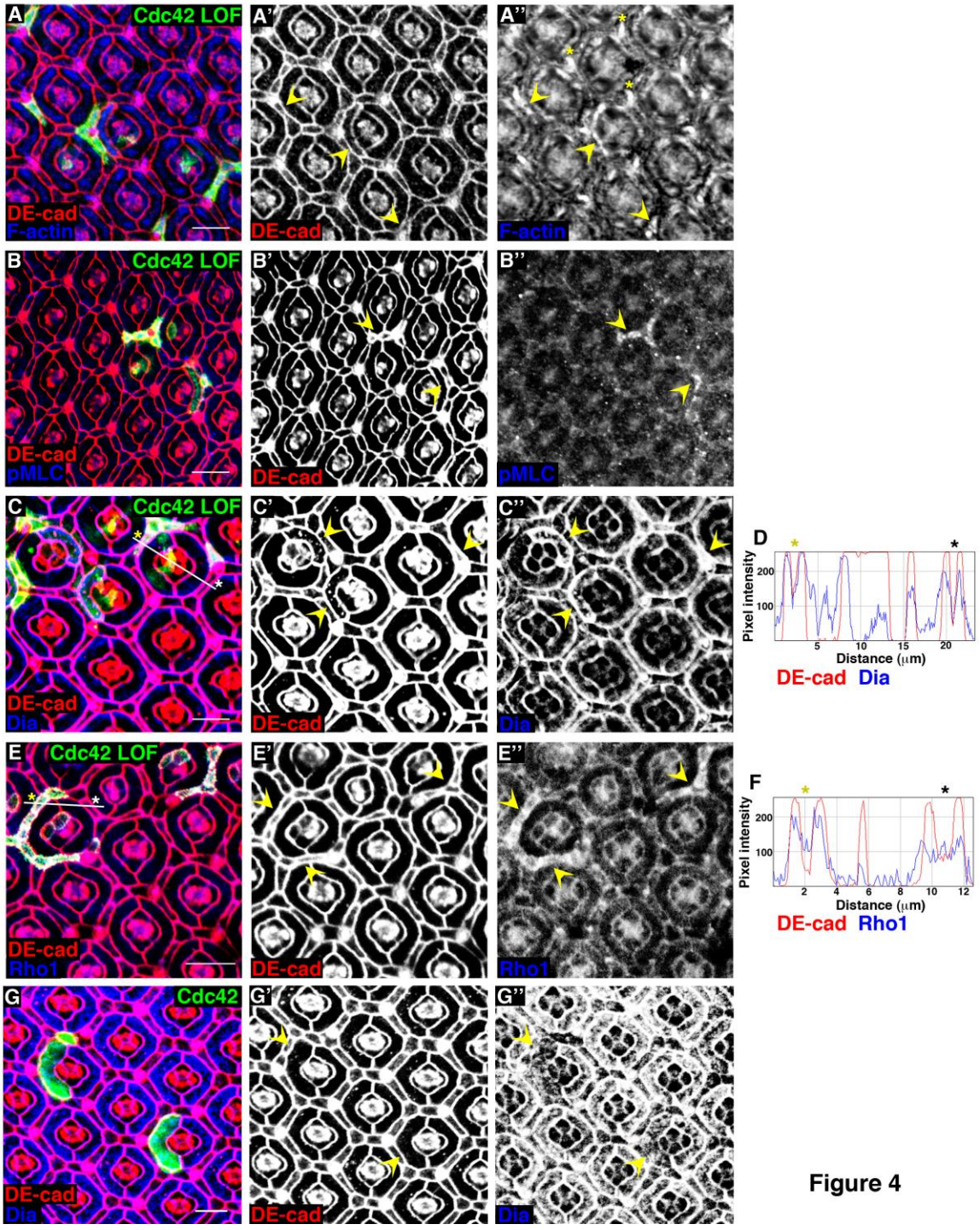
A
Cdc42 LOF
DE-cad
F-actin
A'
DE-cad
A''
F-actin
B
Cdc42 LOF
DE-cad
pMLC
B'
DE-cad
B''
pMLC
C
Cdc42 LOF
DE-cad
Dia
C'
DE-cad
C''
Dia
D
Pixel intensity
200
100
5
10
15
20
Distance (μm)
DE-cad Dia
E
Cdc42 LOF
DE-cad
Rho1
E'
DE-cad
E''
Rho1
F
Pixel intensity
200
100
2
4
6
8
10
12
Distance (μm)
DE-cad Rho1
G
Cdc42
DE-cad
Dia
G'
DE-cad
G''
Dia

Figure 4

Figure 5. Cdc42 inhibits Rho1 activity at AJs to regulate apical cell tension

Confocal immunofluorescent localization of DE-cadherin (A, A') in pupal eye expressing PKNG58AeGFP (A, A'') with *GMR-gal4*. Confocal immunofluorescent localization of DE-cadherin (B, B') in pupal eye expressing PKNG58AeGFP (B, B'') and Cdc42-RNAi with *GMR-gal4*. Pixel intensity profile of DE-cadherin immunofluorescence and PKNG58AeGFP fluorescence in control PECs along white line in H (C). Asterisks correspond to PECs in A. Pixel intensity profile of DE-cadherin immunofluorescence and PKNG58AeGFP fluorescence in PECs expressing Cdc42-RNAi along white line in B (D). Asterisks correspond to PECs in B. Quantification of PKNG58AeGFP peak pixel intensities at AJs in control or Cdc42-RNAi-expressing pupal eyes (see Table 5) (E). Data are represented as mean +/- SD. *** $P<0.0001$. Confocal immunofluorescent localization of DE-cadherin in sibling pupal eyes with $Cdc42^{4}$ MARCM clones (F, F') or $Cdc42^{4}$ MARCM clones in a $Rho1^{72F}$ heterozygous background (G, G'). Arrowheads identify clonal cells. Confocal immunofluorescent localization of DE-cadherin in sibling pupal eyes with $Cdc42^{4}$ MARCM clones (H, H') or $Cdc42^{4}$ MARCM clones that express Rho1-RNAi (I, I'). Arrowheads identify clonal cells. Quantification of apical areas in clonal cells depleted of Cdc42 alone or with Rho1 also depleted (apical area index, see Table 2) (J). Data are represented as mean +/- SD. *** $P<0.001$. Scale bars represent 10 μm.

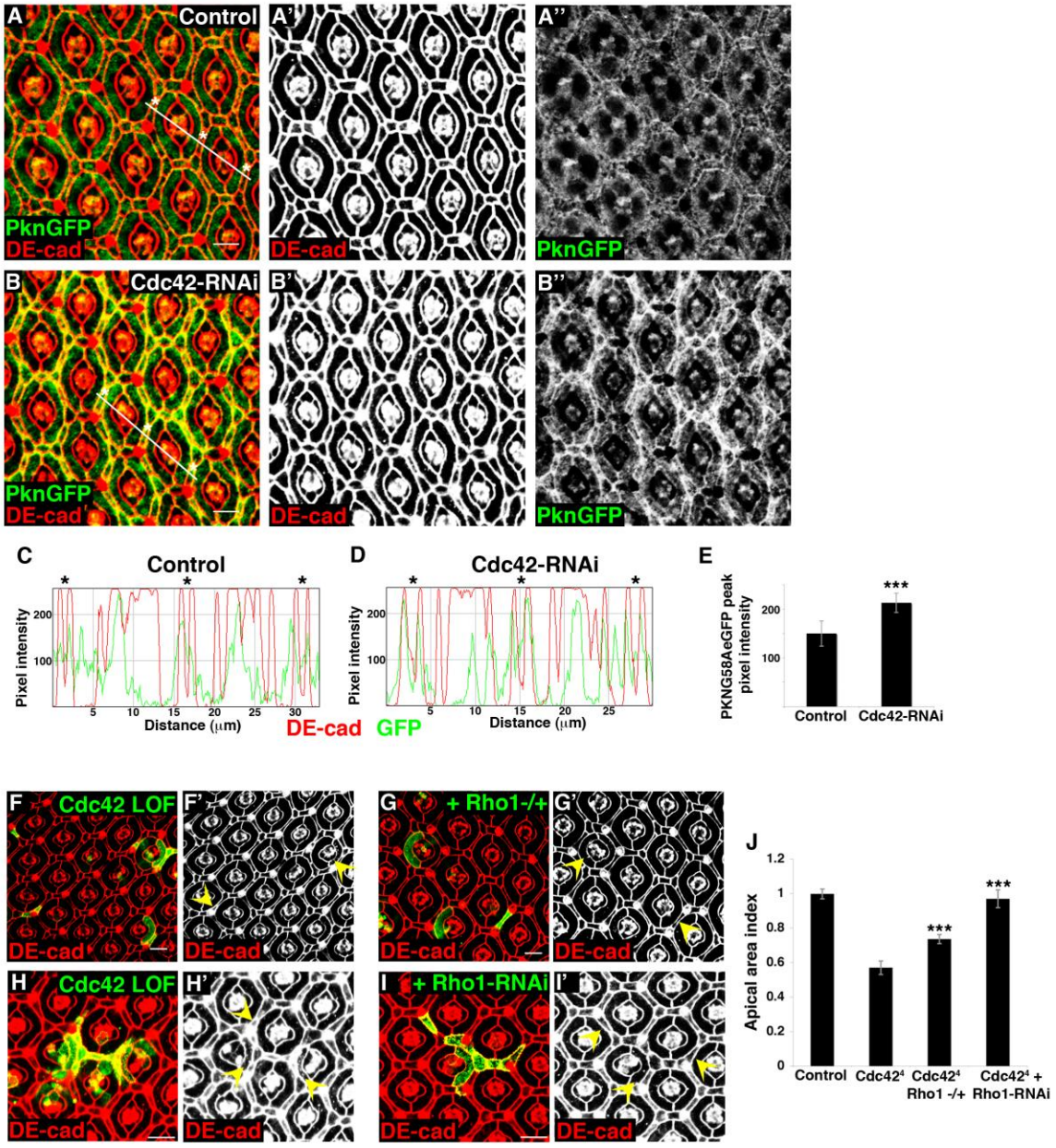
A
Control
PknGFP
DE-cad
A'
DE-cad
A''
PknGFP
B
Cdc42-RNAi
PknGFP
DE-cad
B'
DE-cad
B''
PknGFP
C
Control
Pixel intensity
Distance (μm)
DE-cad
GFP
D
Cdc42-RNAi
Pixel intensity
Distance (μm)
E
PKNG58AeGFP peak pixel intensity
***
Control
Cdc42-RNAi
F
Cdc42 LOF
DE-cad
F'
DE-cad
G
+ Rho1-/+
DE-cad
G'
DE-cad
H
Cdc42 LOF
DE-cad
H'
DE-cad
I
+ Rho1-RNAi
DE-cad
I'
DE-cad
J
Apical area index
***
***
Control
Cdc42⁴
Cdc42⁴ Rho1 -/+
Cdc42⁴ + Rho1-RNAi

Figure 5

Figure 6. Par6 and aPKC depletion phenocopies Cdc42 depletion

Confocal immunofluorescent localization of DE-cadherin (A, A', B, B') and Coracle (A, A'', B, B'') in *par6*$^{\Delta 226}$ MARCM clones (A-A'') and *aPKC*^{k06403} MARCM clones (B-B''). Arrowheads identify AJs (A', B') and SJs (A'', B'') around clonal primary PECs. Confocal immunofluorescent localization of DE-cadherin (C, D, E, F), F-actin (C', E'), and phospho-MLC (D', F') in *par6*$^{\Delta 226}$ (C, C', D, D') and *aPKC*^{k06403} (E, E', F, F') MARCM clones. Arrowheads identify clonal cells. Scale bars represent 10 μm.

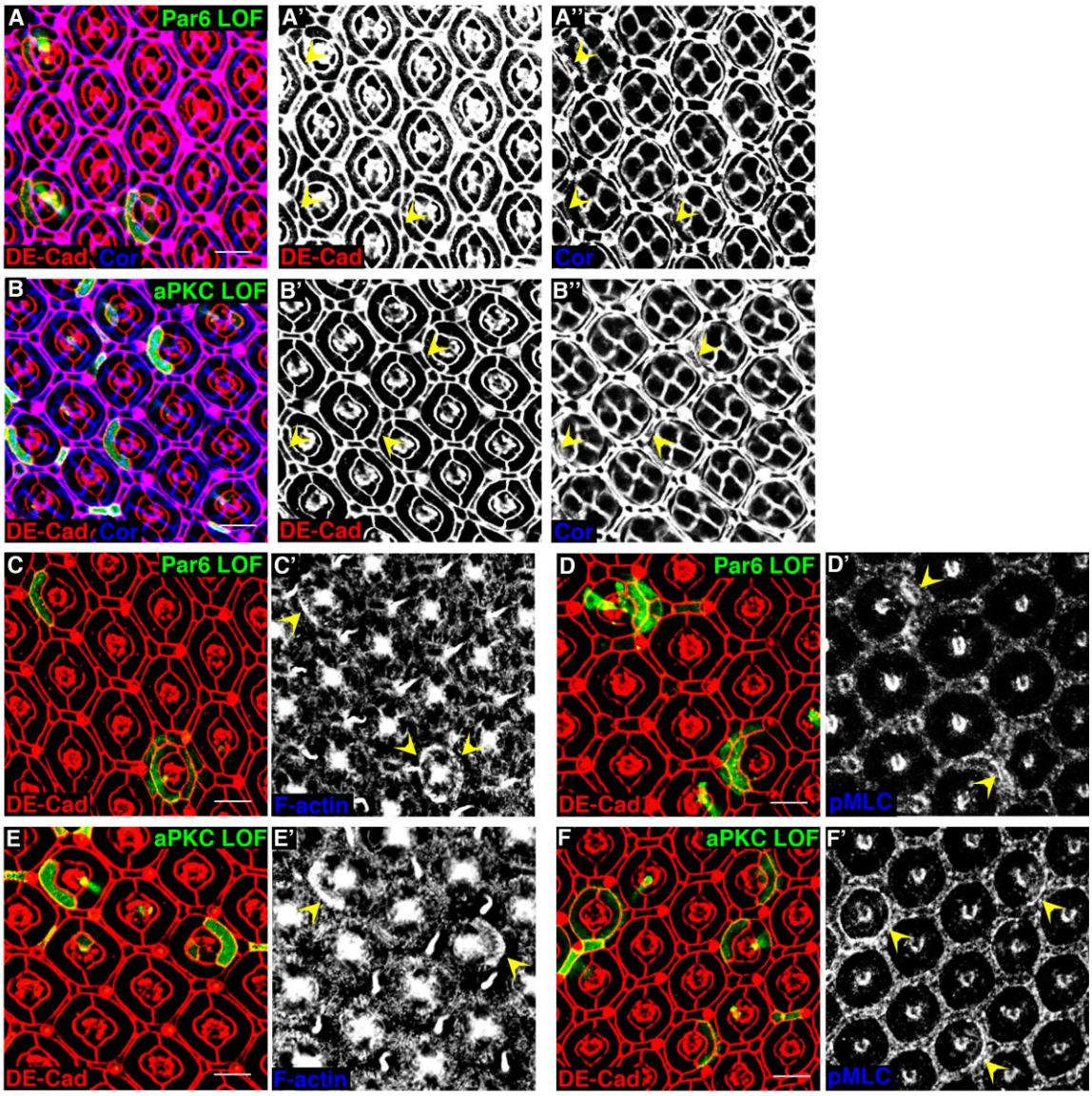
A
Par6 LOF
DE-Cad Cor
A'
DE-Cad
A''
Cor
B
aPKC LOF
DE-Cad Cor
B'
DE-Cad
B''
Cor
C
Par6 LOF
DE-Cad
C'
F-actin
D
Par6 LOF
DE-Cad
D'
pMLC
E
aPKC LOF
DE-Cad
E'
F-actin
F
aPKC LOF
DE-Cad
F'
pMLC

Figure 6

Figure 7. Par6 and aPKC inhibit apical tension in a Rho1-dependent manner

Confocal immunofluorescent localization of DE-cadherin in *par6*$^{\Delta 226}$ MARCM clones alone (A, A'), in a *Rho1*^{72F} heterozygous background (B, B'), or expressing Rho1-RNAi (C, C'). Arrowheads identify clonal cells. Confocal immunofluorescent localization of DE-cadherin in *aPKC*^{k06403} MARCM clones alone (D, D') or *aPKC*^{k06403} MARCM clones expressing Rho1-RNAi (E, E'). Arrowheads identify clonal cells. Quantification of apical areas in clonal cells depleted of Par6 or aPKC alone or with Rho1 also depleted (apical area index, see Table 2) (F). Data are represented as mean +/- SD. *** $P \leq 0.001$. Scale bars represent 10 μm.

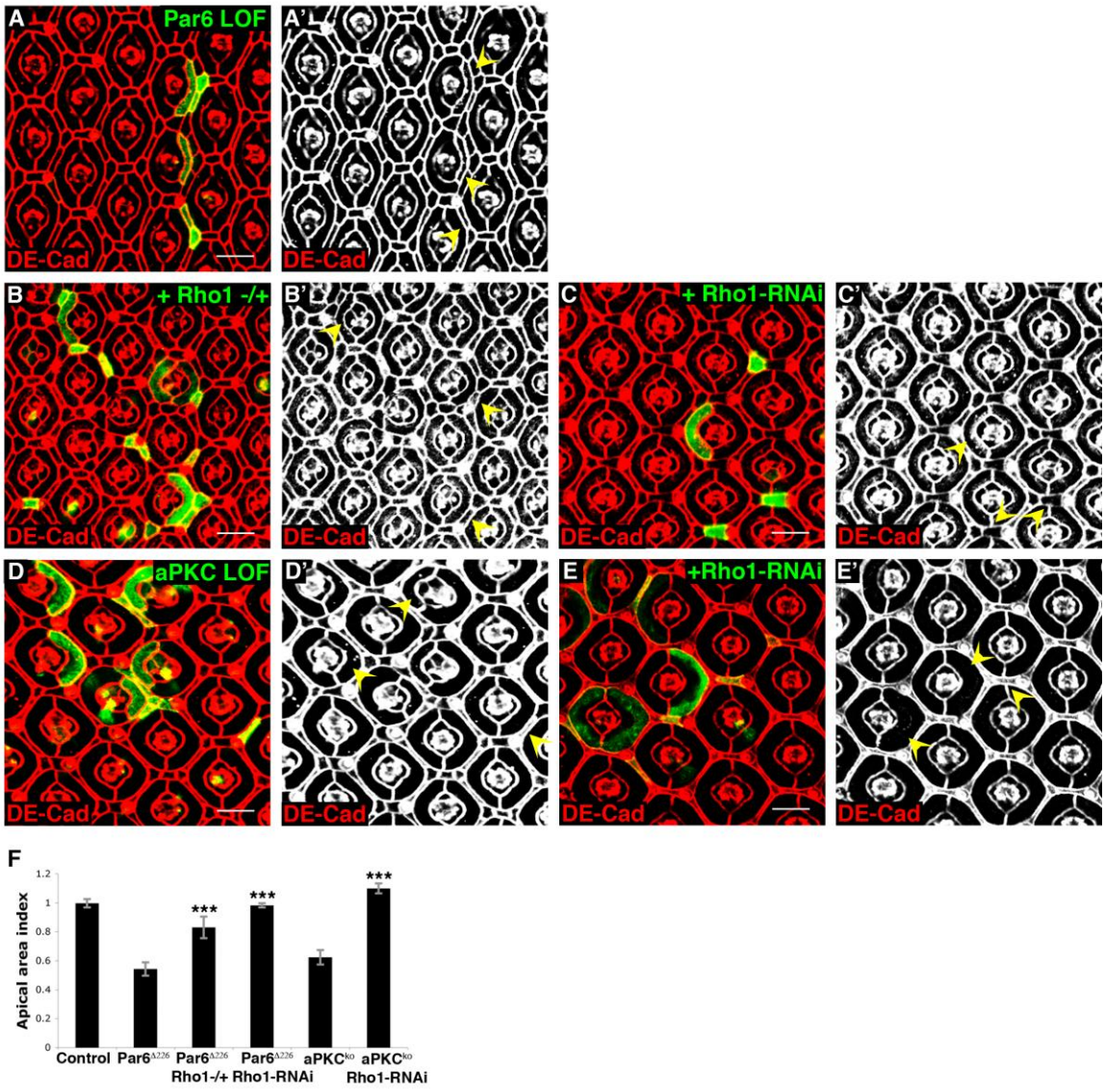
A
Par6 LOF
DE-Cad
A'
DE-Cad
B
+ Rho1 -/+
DE-Cad
B'
DE-Cad
C
+ Rho1-RNAi
DE-Cad
C'
DE-Cad
D
aPKC LOF
DE-Cad
D'
DE-Cad
E
+Rho1-RNAi
DE-Cad
E'
DE-Cad
F
Apical area index
1.2
1
0.8
0.6
0.4
0.2
0
***
***
***
Control
Par6Δ226
Par6Δ226 Rho1-/+
Par6Δ226 Rho1-RNAi
aPKCko
aPKCko Rho1-RNAi

Figure 7

Figure 8. Cdc42 localizes Par6 and aPKC to AJs

Confocal immunofluorescent localization of DE-cadherin (A, A', B, B'), Par6 (A, A''), and aPKC (B, B'') in *Cdc42*^{4} MARCM clones. Arrowheads identify AJs (A', B'), Par6 (A''), and aPKC (B'') between clonal cells. Confocal immunofluorescent localization of DE-cadherin (C, C') and aPKC (C, C'') in *par6*$^{\Delta 226}$ MARCM clones. Arrowheads identify AJs (C') and aPKC (C'') between clonal cells. Confocal immunofluorescent localization of DE-cadherin (D, D', E, E') and aPKC (D, D'', D, D'') in Flp-out clones expressing either wild type Par6 (Par6^{WT}) (D-D'') or Cdc42-binding mutant Par6 (Par6^{ISAA}) (E-E''). Arrowheads identify AJs (D', E') and aPKC (D'', E'') between clonal cells. Scale bars represent 10 μm.

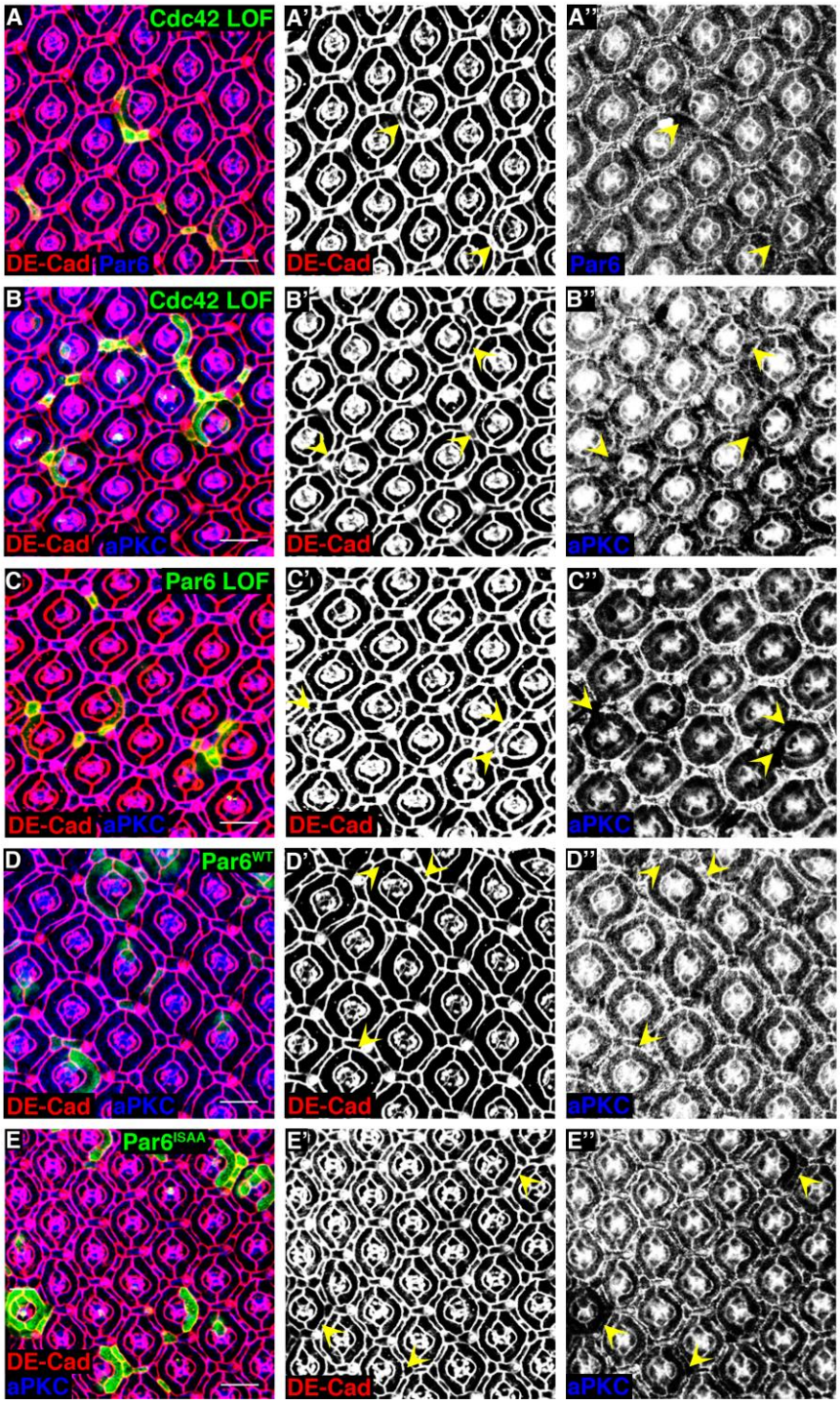
A
Cdc42 LOF
DE-Cad
Par6
A'
DE-Cad
A''
Par6
B
Cdc42 LOF
DE-Cad
aPKC
B'
DE-Cad
B''
aPKC
C
Par6 LOF
DE-Cad
aPKC
C'
DE-Cad
C''
aPKC
D
Par6WT
DE-Cad
aPKC
D'
DE-Cad
D''
aPKC
E
Par6ISAA
DE-Cad
aPKC
E'
DE-Cad
E''
aPKC

Figure 8

Figure 9. Cdc42 inhibits Rho1 activity by localizing Par6/aPKC to AJs

Confocal immunofluorescent localization of DE-cadherin (A, A', B, B') and Coracle (A, A'', B, B'') in Flp-out clones expressing wild type Par6 (A-A'') or Cdc42 binding mutant Par6 (B-B''). Arrowheads identify AJs (A', B') and SJs (A'', B'') around clonal primary PECs. Confocal immunofluorescent localization of DE-cadherin in *Cdc42*^{4} MARCM clones alone (C, C'), expressing wild type aPKC (aPKC^{WT}) (D, D'), or expressing membrane associated aPKC^{CAAX} (E, E'). Arrowheads identify clonal cells. Quantification of apical areas in clonal cells depleted of Cdc42 alone, expressing aPKC^{WT}, or expressing aPKC^{CAAX} (apical area index, see Table 2) (F). Data are represented as mean +/- SD. *** $P<0.001$. Model for Cdc42 function in PECs (G). Cdc42/Par6 localize aPKC to AJs, where aPKC inhibits Rho1 activity and its associated acto-myosin tension. When Cdc42/Par6/aPKC localization to AJs is disrupted, Rho1 activation and acto-myosin tension at AJs increases. Scale bars represent 10 μm.

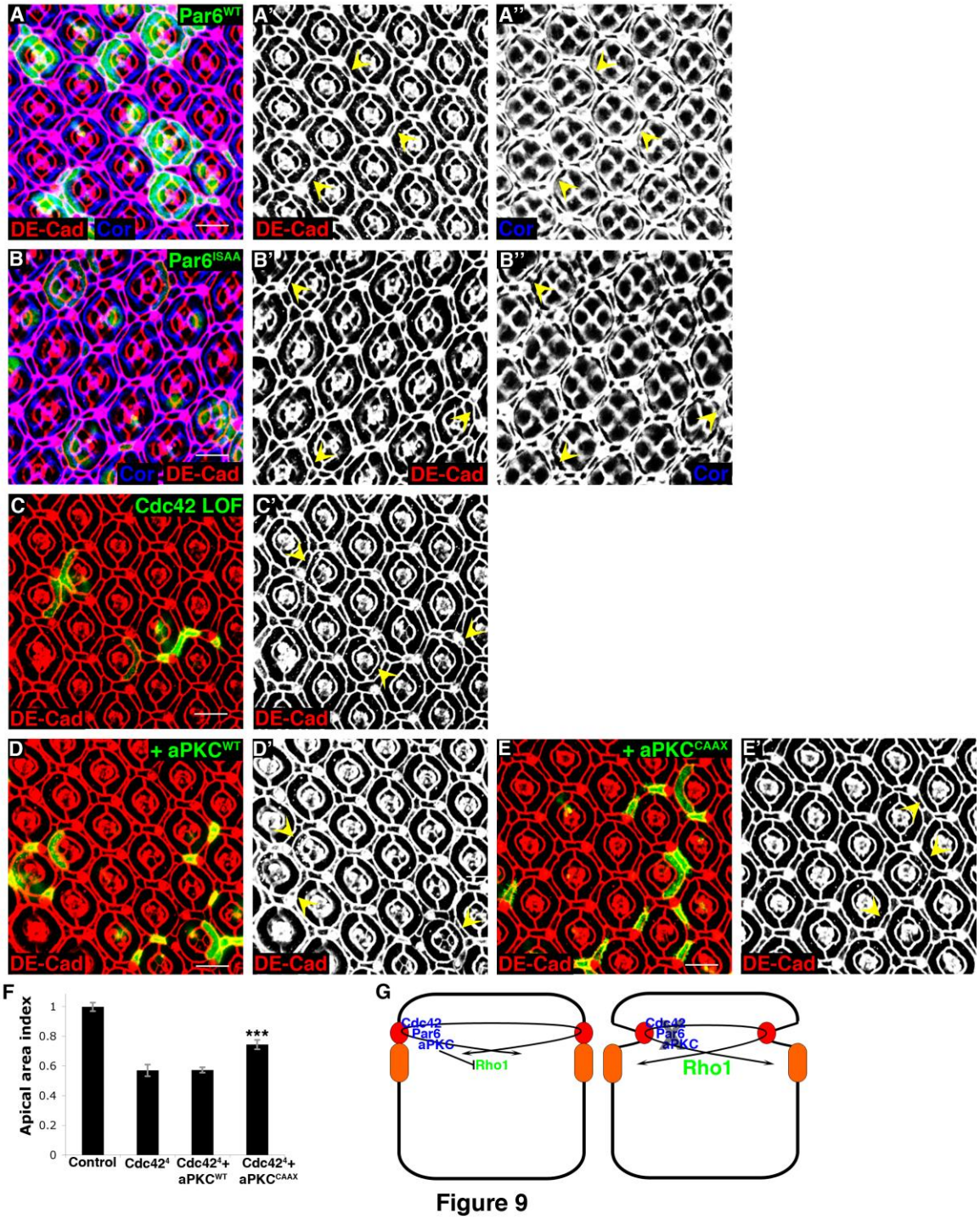
A
Par6WT
DE-Cad
Cor
A'
DE-Cad
A''
Cor
B
Par6ISAA
Cor
DE-Cad
B'
DE-Cad
B''
Cor
C
Cdc42 LOF
DE-Cad
C'
DE-Cad
D
+ aPKCWT
DE-Cad
D'
DE-Cad
E
+ aPKCCAAX
DE-Cad
E'
DE-Cad
F
Apical area index
1
0.8
0.6
0.4
0.2
0
***
Control
Cdc42⁴
Cdc42⁴+ aPKCWT
Cdc42⁴+ aPKCCAAX
G
Cdc42
Par6
aPKC
Rho1
Cdc42
Par6
aPKC
Rho1

Figure 9

Figure 10. Depletion of Dlg/Scrib does not disrupt apical-basal polarity in non-proliferating epithelial cells

Confocal immunofluorescent localization of DE-cadherin (A, A', B, B') and Discs large (A, A'', B, B'') in apical (A-A'') and lateral (B-B'') optical sections of dlg^{M52} MARCM clones. White line (A) identifies where lateral section (B-B'') was taken. Yellow asterisks identify dlg^{M52} MARCM clones, while white asterisks identify analogous non-clonal, wild type cells. Arrowheads identify AJs (A') and SJs (A'') around dlg^{M52} clonal cells. Confocal immunofluorescent localization of DE-cadherin (C, C', D, D') and Discs large (Dlg) (C, C'', D, D'') in $Scrib^{1}$ MARCM clones (C-C'') or $Scrib^{1}$ MARCM clones expressing Dlg-RNAi (D-D''). Arrowheads identify AJs (C', D') and SJs (C'', D'') around clonal cells. Scale bars represent 10 μm.

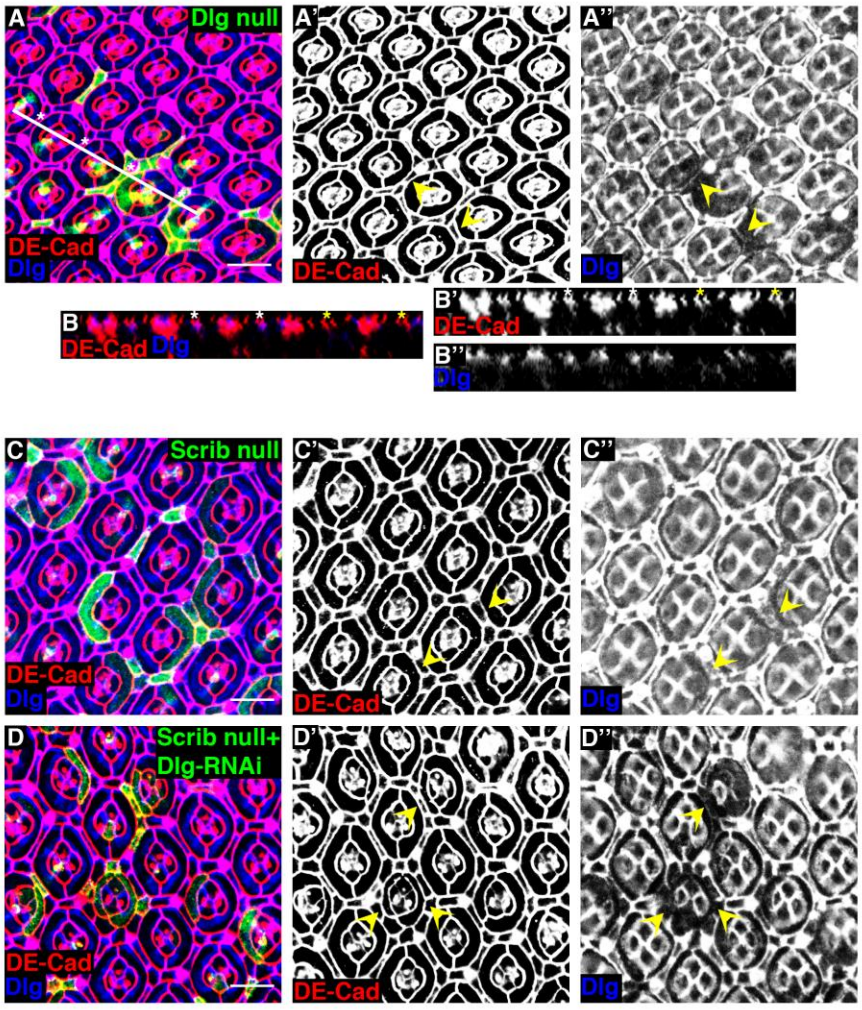
A
Dlg null
DE-Cad
Dlg
A'
DE-Cad
A''
Dlg
B
DE-Cad Dlg
B'
DE-Cad
B''
Dlg
C
Scrib null
DE-Cad
Dlg
C'
DE-Cad
C''
Dlg
D
Scrib null+
Dlg-RNAi
DE-Cad
Dlg
D'
DE-Cad
D''
Dlg

Figure 10

Figure 11. Expression of Cdc42-RNAi decreases PEC apical area, and increases in F-actin or phospho-MLC at AJs is associated with increased apical tension

Immunofluorescent localization of DE-cadherin in Flp-out clones expressing Cdc42-RNAi (A, A'). Arrowheads identify clonal cells (A'). Confocal immunofluorescent localization of DE-cadherin (B, B', C, C') and F-actin (B'', C'') in tsr^{99E} MARCM clones (B-B'') and ssh^{1-11} MARCM clones (C-C''). Arrowheads identify clonal cells. Confocal immunofluorescent localization of DE-cadherin (D, D') and phospho-MLC (D'') in Flp-out clones expressing Rok-CAT. Arrowheads identify clonal cells. Scale bars represent 10 μm.

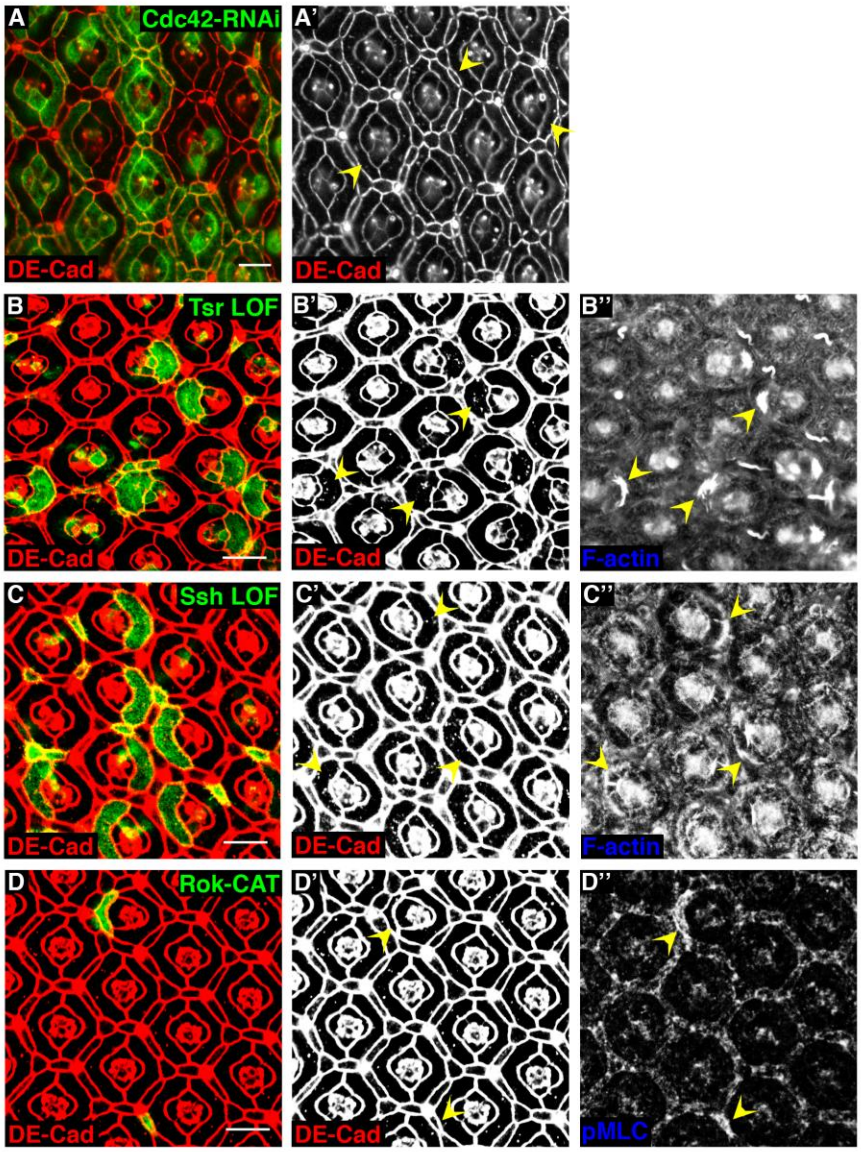
A
Cdc42-RNAi
DE-Cad
A'
DE-Cad
B
Tsr LOF
DE-Cad
B'
DE-Cad
B''
F-actin
C
Ssh LOF
DE-Cad
C'
DE-Cad
C''
F-actin
D
Rok-CAT
DE-Cad
D'
DE-Cad
D''
pMLC

Figure 11

Figure 12. Expression of Cdc42 and Rac dominant proteins results in non-specific phenotypes

Confocal immunofluorescent localization of DE-cadherin (A, B) and Discs large (A', B') in pupal eye expressing either *GMR-gal4* alone (A, A') or Cdc42-N17 with *GMR-gal4* (B, B'). Confocal immunofluorescent localization of DE-cadherin (C, C') and Discs large (C, C'') in Flp-out clones expressing Cdc42-N17. Arrowheads identify AJs (C') and SJs (C'') between clonal cells. Arrows identify clonal cells. Confocal immunofluorescent localization of DE-cadherin in large $Cdc42^{4}$ MARCM clone (D, D'). Confocal immunofluorescent localization of DE-cadherin in Flp-out clone expressing Cdc42-V12 (E, E'). Arrowhead identifies clonal cell. Confocal immunofluorescent localization of DE-cadherin (F) and Discs large (F') in pupal eye expressing Rac-N17 with *GMR-gal4*. Confocal immunofluorescent localization of DE-cadherin (G, G') and Discs large (G, G'') in MARCM clones of $Rac1^{J11}$, $Rac2^{\Delta}$ in Mtl^{Δ} heterozygote. Arrowheads identify AJs (G') and SJs (G'') between clonal cells. Confocal immunofluorescent localization of DE-cadherin in EGUF (*eyeless-gal4*, UAS-Flippase) pupal eye homozygous for $Rac1^{J11}$, $Rac2^{\Delta}$, heterozygous for Mtl^{Δ}, and expressing Cdc42-RNAi (H). Scale bars represent 10 μm.

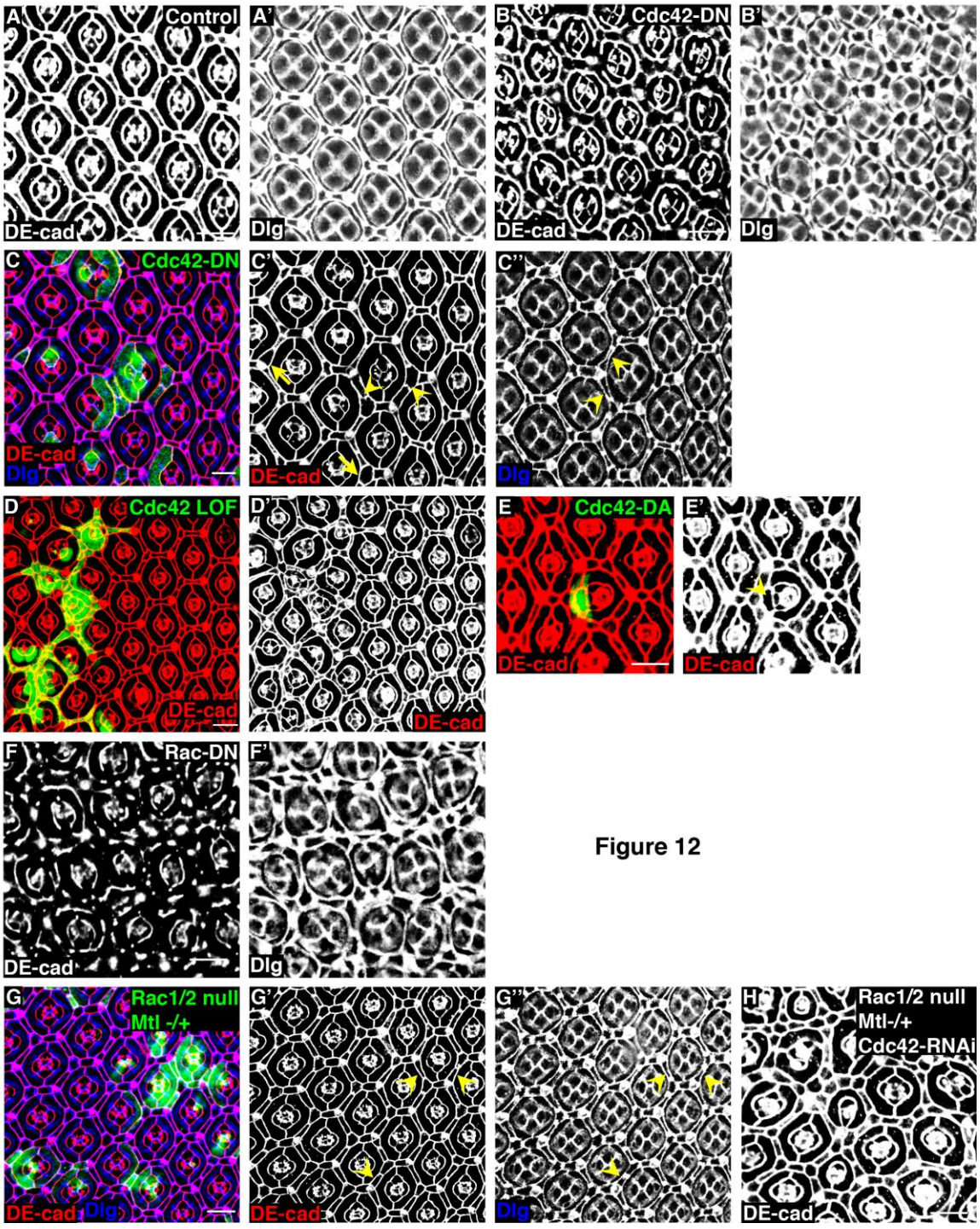
A
Control
DE-cad
A'
Dlg
B
Cdc42-DN
DE-cad
B'
Dlg
C
Cdc42-DN
DE-cad
Dlg
C'
DE-cad
C''
Dlg
D
Cdc42 LOF
DE-cad
D'
DE-cad
E
Cdc42-DA
DE-cad
E'
DE-cad
F
Rac-DN
DE-cad
F'
Dlg
G
Rac1/2 null
Mtl -/+
DE-cad
Dlg
G'
DE-cad
G''
Dlg
H
Rac1/2 null
Mtl-/+
Cdc42-RNAi
DE-cad

Figure 12

Figure 13. Rho1 does not regulate SJs; Pak, WASP, and Baz LOF clones do not phenocopy Cdc42 LOF clones; and Cdc42 depletion does not disrupt Baz or Crbs AJ localization

Confocal immunofluorescent localization of DE-cadherin (A, A', B, B') and Coracle (A, A'', B, B'') in *Cdc42*^{4} MARCM clones in a *Rho1*^{72F} heterozygous background (A-A'') and Flp-out clones overexpressing wild type Rho1 (B-B''). Arrowheads identify AJs (A', B') and SJs (A'', B'') around clonal primary PECs. Confocal immunofluorescent localization of DE-cadherin (C, C', D, D', E, E') and Discs large (C'', D'', E'') in *pak*^{16} MARCM clones (C-C''), *wsp*^{3} MARCM clones (D-D''), and *baz*^{4} MARCM clones (E-E''). Arrows identify clonal cells (C', D', E'), and arrowheads identify SJs around clonal primary PECs (C'', D'', E''). Confocal immunofluorescent localization of DE-cadherin (F, F'), Bazooka (F, F''), Armadillo (G, G', H, H', I, I') and Crumbs (G, G'', H, H'', I, I'') in *Cdc42*^{4} MARCM clones. Arrowheads identify AJs (F', G'), Bazooka (F''), and Crumbs (G'', I'') between or within clonal cells. White line (G) identifies where lateral section (H-H'') was taken. Yellow asterisks identify *Cdc42*^{4} MARCM clones (H''). I is a maximum projection of a z-series stack. Scale bars represent 10 μm.

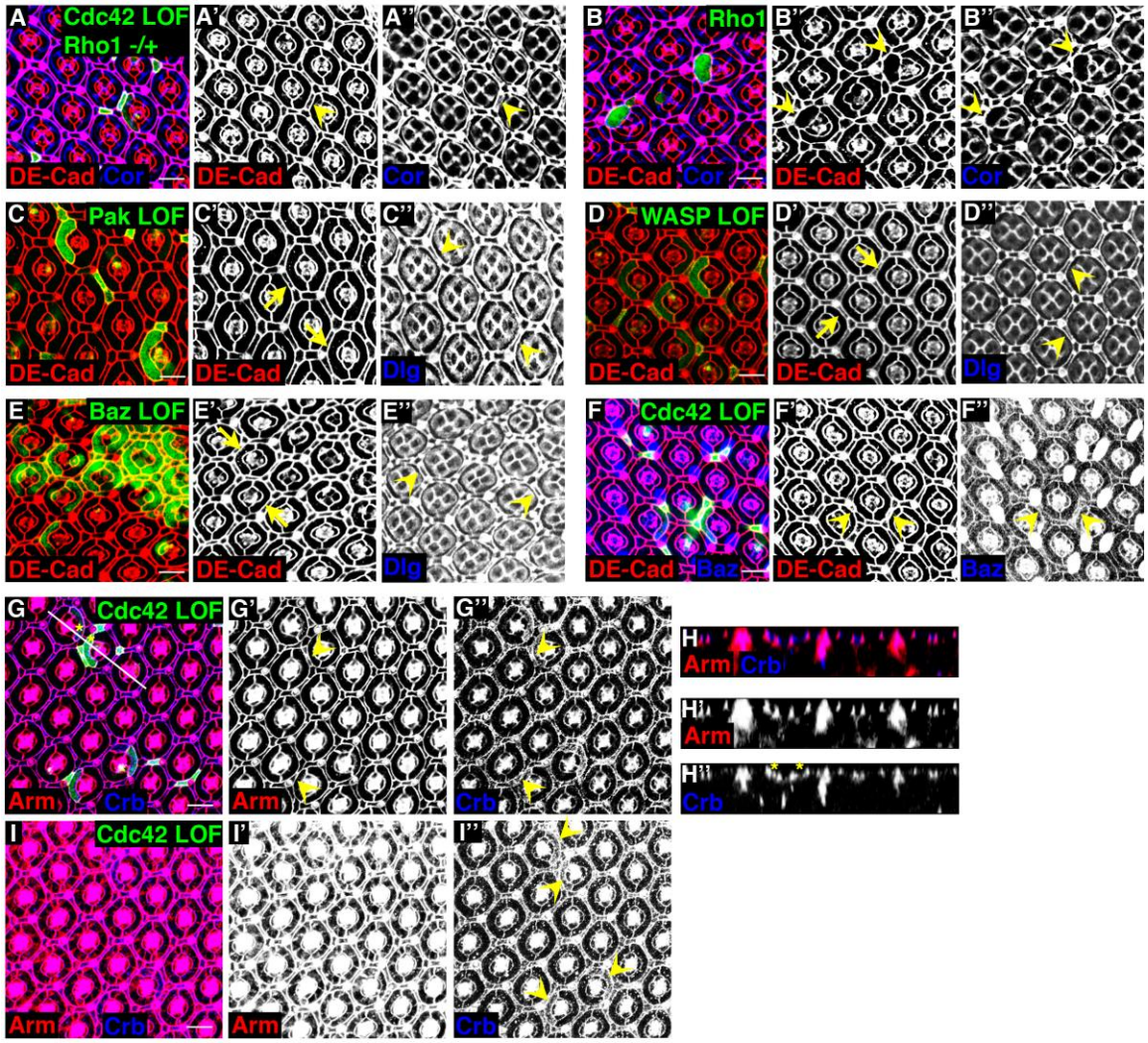
A
Cdc42 LOF
Rho1 -/+
DE-Cad
Cor
A'
DE-Cad
A''
Cor
B
Rho1
DE-Cad
Cor
B'
DE-Cad
B''
Cor
C
Pak LOF
DE-Cad
C'
DE-Cad
C''
Dlg
D
WASP LOF
DE-Cad
D'
DE-Cad
D''
Dlg
E
Baz LOF
DE-Cad
E'
DE-Cad
E''
Dlg
F
Cdc42 LOF
DE-Cad
Baz
F'
DE-Cad
F''
Baz
G
Cdc42 LOF
Arm
Crb
G'
Arm
G''
Crb
H
Arm
Crb
H'
Arm
H''
Crb
I
Cdc42 LOF
Arm
Crb
I'
Arm
I''
Crb

Figure 13

Figure 14. Cdc42 overexpression decreases while Par6 and aPKC depletion increases Rho1 localization at AJs

Confocal immunofluorescent localization of DE-cadherin (A, A') and Rho1 (A, A'') in Flp-out clones overexpressing wild type Cdc42. Confocal immunofluorescent localization of DE-cadherin (B, B', C, C') and Rho1 (B, B'', C, C'') in *par6*$^{\Delta 226}$ MARCM clones (B-B'') and *aPKC*^{k06403} MARCM clones (C-C''). Arrowheads identify clonal cells. Scale bars represent 10 μm.

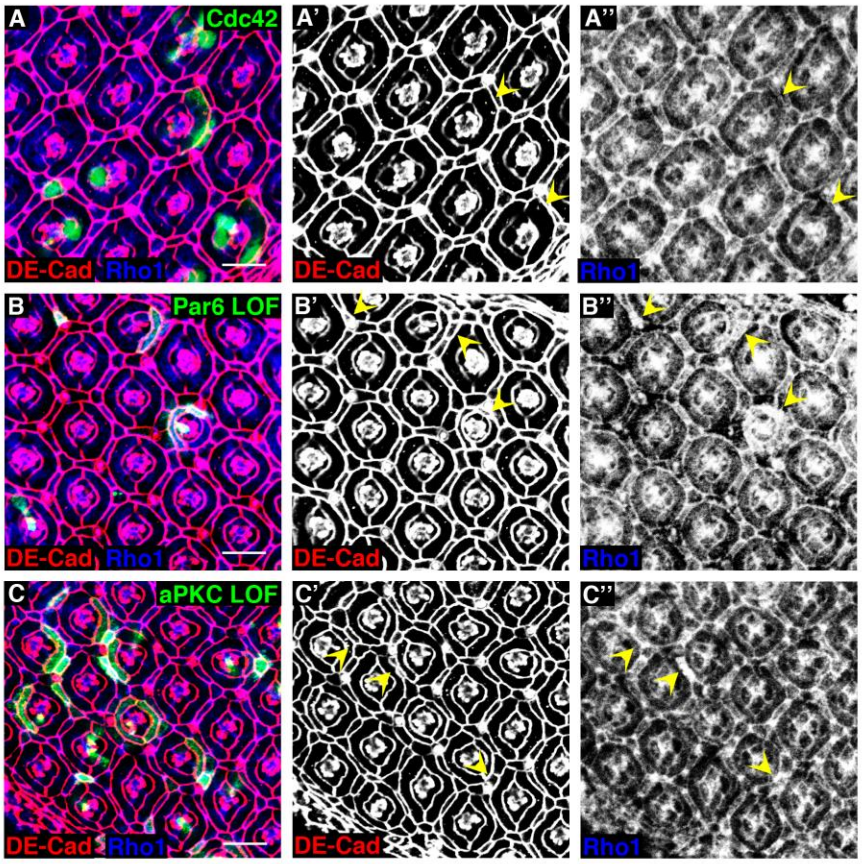
A
Cdc42
DE-Cad
Rho1
A'
DE-Cad
A''
Rho1
B
Par6 LOF
DE-Cad
Rho1
B'
DE-Cad
B''
Rho1
C
aPKC LOF
DE-Cad
Rho1
C'
DE-Cad
C''
Rho1

Figure 14

Figure 15. $Par6^{WT}$ is expressed at equal or higher levels that $Par6^{ISAA}$ and $aPKC^{WT}$ localizes diffusely while $aPKC^{CAAX}$ localizes to the membrane

Confocal immunofluorescent localization of DE-cadherin (A, A', B, B', C, C'), Par6 (A, A'', B, B'') and HA (C, C'') in Flp-out clones expressing wild type Par6 ($Par6^{WT}$) (A-A'') and Cdc42-binding mutant Par6 ($Par6^{ISAA}$), which is tagged with HA (B-B'', C-C''). Confocal immunofluorescent localization of DE-cadherin (D, D', E, E') and aPKC (D, D'', E, E'') in Flp-out clones expressing wild type aPKC ($aPKC^{WT}$) (D-D'') and membrane-targeted aPKC ($aPKC^{CAAX}$) (E-E'').

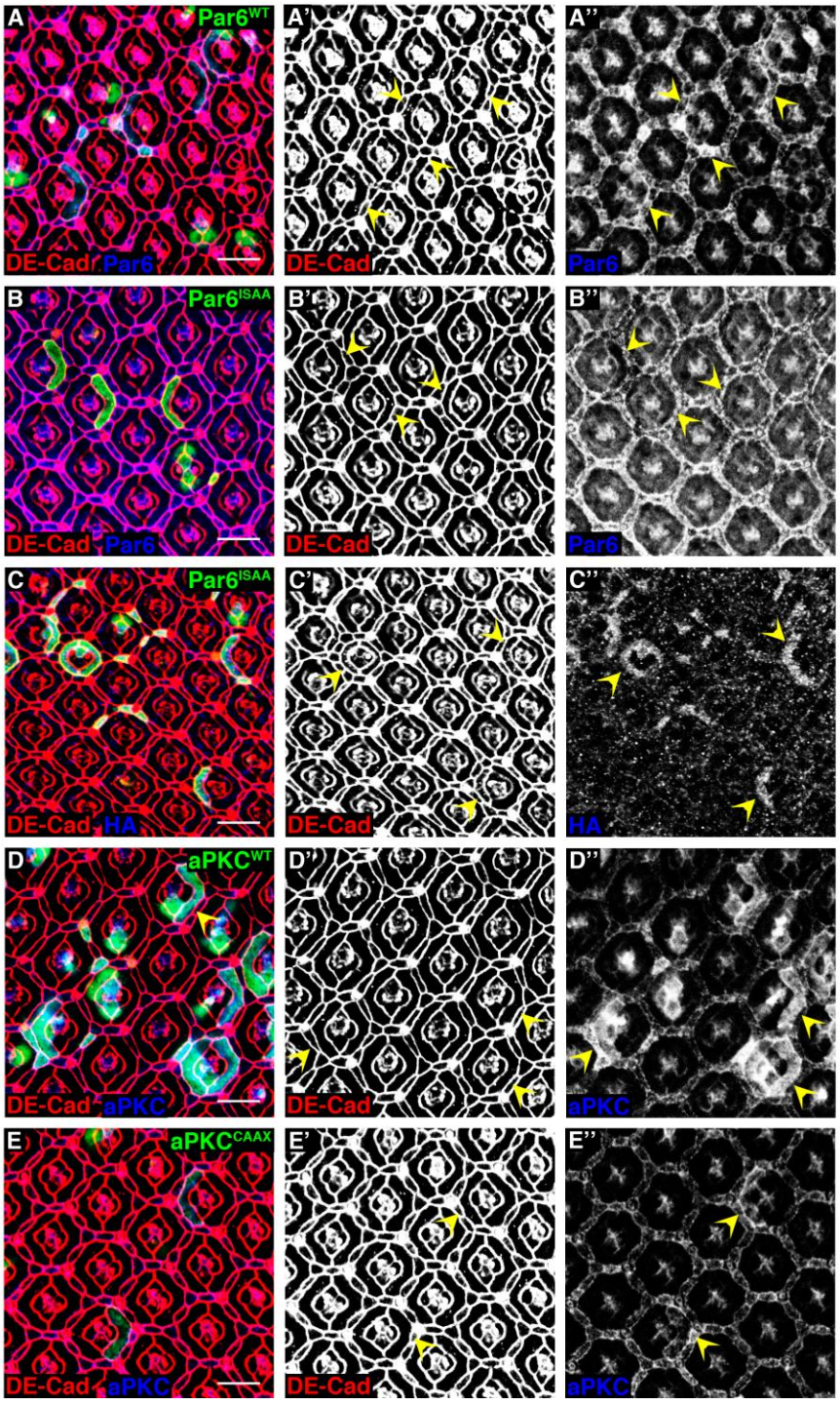
A
Par6WT
DE-Cad Par6
A'
DE-Cad
A''
Par6
B
Par6ISAA
DE-Cad Par6
B'
DE-Cad
B''
Par6
C
Par6ISAA
DE-Cad HA
C'
DE-Cad
C''
HA
D
aPKCWT
DE-Cad aPKC
D'
DE-Cad
D''
aPKC
E
aPKCCAAX
DE-Cad aPKC
E'
DE-Cad
E''
aPKC

Figure 15

Tables

Table 1. SJ mislocalization quantification

Genotype	Percent clonal primary PECs with SJ mislocalizations	N
Cdc42^{4}	86	83
Cdc42^{4} + Cdc42	0	15

Quantification of SJ mislocalization around clonal primary PECs. Clonal primary PECs had mislocalized SJs if one or more of the surrounding SJs were mislocalized compared to SJs surrounding adjacent, non-clonal primary PECs.

Table 2. Apical area index quantification

Genotype	Apical area index mean	Std dev	N	P
Wild type	0.998	0.0286	25	
Cdc42^{4}	0.570	0.0393	105	0.00000033 (Wild type)
Cdc42^{2}	0.860	0.0843	55	0.041 (Wild type)
Cdc42-RNAi	0.790	0.0468	60	0.0053 (Wild type)
***Cdc42^{4}* + Cdc42**	1.059	0.0395	30	0.000015 (*Cdc42^{4}*)
Cdc42	1.245	0.0634	28	0.00032 (Wild type)
***Cdc42^{4}, Rho1^{72F}* +/-**	0.736	0.0264	19	0.00096 (*Cdc42^{4}*)
***Cdc42^{4}* + Rho1-RNAi**	0.969	0.0519	38	0.0000066 (*Cdc42^{4}*)
***Cdc42^{4}* + aPKC^{WT}**	0.572	0.0179	20	0.78 (*Cdc42^{4}*)
***Cdc42^{4}* + aPKC^{CAAX}**	0.744	0.0317	52	0.000028 (*Cdc42^{4}*)
par6$^{\Delta 226}$	0.542	0.0464	32	0.0000011 (Wild type)
***par6$^{\Delta 226}$, Rho1^{72F}* +/-**	0.830	0.0742	31	0.0010 (*par6$^{\Delta 226}$*)
***par6$^{\Delta 226}$* + Rho1-RNAi**	0.977	0.0130	23	0.000015 (*par6$^{\Delta 226}$*)
aPKC^{ko6403}	0.624	0.0498	86	0.0000020 (Wild type)
***aPKC^{ko6403}* + Rho1-RNAi**	1.100	0.0343	30	0.0000037 (*aPKC^{ko6403}*)
Rok-CAT	0.449	0.0655	18	0.0000047 (Wild type)
tsr^{99E}	0.624	0.0590	24	0.00020 (Wild type)
ssh$^{1-11}$	0.808	0.0662	26	0.0060 (Wild type)
***Cdc42^{4}* (SJs)**	1.0311	0.0760	43	0.00038 (*Cdc42^{4}*, AJs)

Quantification of apical area index. Apical area index is the ratio of a clonal cell apical area divided by an analogous, neighboring non-clonal cell apical area at AJs (except for the last row, which was measured at SJs). Quantifications were performed using ImageJ v1.38. P-values were calculated using an unpaired, two-sided Student's t-test against the genotype indicated in parentheses.

Table 3. AJ-associated F-actin index quantification

Genotype	F-actin index mean	Std dev	N	P
Wild type	1.005	0.012	26	
***Cdc42*^{4}**	1.737	0.136	29	0.011
***par6*$^{\Delta 226}$**	1.842	0.228	16	0.023
***aPKC*^{ko6403}**	1.961	0.311	45	0.009
***tsr*^{99E}**	2.001	0.187	19	0.010
***ssh*$^{1-11}$**	1.704	0.329	26	0.024

Quantification of AJ-associated F-actin index. AJ-associated F-actin index is the ratio of phalloidin staining pixel intensity at AJs in a clonal cell divided by an analogous, neighboring non-clonal cell. Quantifications were performed using ImageJ v1.38. P-values were calculated using an unpaired, two-sided Student's t-test against wild type clones.

Table 4. AJ-associated phospho-MLC index quantification

Genotype	pMLC index mean	Std dev	N	P
Wild type	1.0694	0.0396	22	
***Cdc42*^{4}**	1.739	0.134	15	0.0075
***par6*$^{\Delta 226}$**	1.760	0.245	19	0.035
***aPKC*^{k06403}**	1.721	0.236	33	0.0098
Rok-CAT	2.353	0.717	13	0.037

Quantification of AJ-associated phospho-MLC index. AJ-associated phospho-MLC index is the ratio of phospho-MLC immunofluorescence pixel intensity at AJs in a clonal cell divided by an analogous, neighboring non-clonal cell. Quantifications were performed using ImageJ v1.38. P-values were calculated using an unpaired, two-sided Student's t-test against wild type clones.

Table 5. PKNG58AeGFP peak pixel intensity at AJs quantification

Genotype	PKNG58AeGFP peak pixel intensity mean	Std dev	N	P
Control	149.816	25.727	165	
Cdc42-RNAi	212.958	19.723	162	0.0000974

Quantification of PKNG58AeGFP peak pixel intensity at AJs. PKNG58AeGFP peak pixel intensities at AJs were determined from plotting and listing pixel values across a line drawn through PEC AJs (as shown in Fig. 5A, B). Quantifications were performed using ImageJ v1.38. P-value was calculated using an unpaired, two-sided Student's t-test against control.

CHAPTER 4

The Cdc42/Par6/aPKC polarity complex is a negative regulator of apoptosis-induced compensatory proliferation

Chapter 4 represents a manuscript currently under review, entitled “The Cdc42/Par6/aPKC polarity complex is a negative regulator of apoptosis-induced compensatory proliferation.”

The Cdc42/Par6/aPKC polarity complex negatively regulates apoptosis-induced compensatory proliferation

Stephen J. Warner and Gregory D. Longmore*

Departments of Medicine and Cell Biology

Washington University, St. Louis, MO, 63110

Abstract

Disruption of epithelial cell apical-basal polarity is often correlated with increased proliferation, yet how polarity regulates proliferation has not been well characterized. Furthermore, in response to apoptosis from stress or tissue damage, unaffected epithelial cells undergo compensatory proliferation to maintain the epithelium. The signals regulating this compensatory proliferation are not fully appreciated. Here we identify Cdc42 and the Par polarity complex as novel regulators of apoptosis-induced compensatory proliferation. Depletion or disruption of this complex from adherens junctions, but not the Scribble or Crumbs polarity complexes, induces JNK-dependent apoptosis and compensatory proliferation. This is mediated by increased Rho1-Rok activation downstream of Cdc42 depletion, and Rok's regulation of Myosin activity but not F-actin activates JNK. Therefore, disruption of the Cdc42/Par6/aPKC complex by cellular damage provides a signal for epithelial cells to initiate apoptosis-induced compensatory proliferation through activation of Rho1. In cancer states where apoptotic regulation is disrupted, loss of the Cdc42/Par6/aPKC polarity complex organization or localization could contribute to tumor hyperproliferation and explain how polarity regulation contributes to tumor development.

Introduction

Epithelial cells line all surfaces of the body exposed to external environments, which requires unique cellular properties for proper function. For example, epithelial cells have apical-basal polarity. Major insight into proteins involved in epithelial apical-basal polarity establishment and maintenance has been gained from studies of *Drosophila* epithelia during morphogenesis (Bilder, 2004). Three protein complexes have emerged as key regulators in establishing and maintaining epithelial polarity. These include the Par polarity complex composed of Par6/Par3/aPKC, the Scribble polarity complex composed of Scribble (Scrib)/Discs large (Dlg)/Lethal (2) giant larvae (Lgl), and the Crumbs polarity complex composed of Crumbs/Pals/PatJ. While these three complexes all function in epithelial polarity, they do so by different mechanisms (Assemat et al., 2008).

Maintenance of epithelial apical-basal polarity is not only critical for epithelial cell function, but loss of epithelial polarity contributes to epithelial tumor (carcinoma) development (Tanos and Rodriguez-Boulan, 2008). Loss of epithelial polarity markers is associated with early stage tumors before metastasis (Dow and Humbert, 2007; Wodarz and Nathke, 2007). In addition, functional studies in *Drosophila* and mammalian systems have demonstrated that disruption of polarity complexes, either by depletion or mislocalization of protein constituents, often results in increased epithelial proliferation (Bilder, 2004; Zhan et al., 2008). Despite these observations, how epithelial polarity regulation is coupled to proliferation has not been well characterized.

During development and adult homeostasis, epithelia replenish those cells that are damaged and shed during normal physiological conditions. When epithelia are exposed to additional insults, either environmental or genetic, that lead to increased cell death epithelia have a remarkable capacity to compensate for this increased cell loss. For example, *Drosophila* larval imaginal discs, monolayer epithelial tissues, can be subjected to irradiation or tissue ablation causing loss of up to 60% of cells from the tissue, yet compensatory proliferation of surrounding cells results in the development of normal sized adult tissue (Haynie and Bryant, 1977). In the mouse intestine, loss of Mdm2 induces p53-mediated cell death, but compensatory, increased proliferation helps maintain intestinal morphology and function (Valentin-Vega et al., 2008).

The ability of epithelial tissues to compensate for cell loss resulting from physical damage, irradiation, or genetically induced apoptosis has been termed apoptosis-induced compensatory proliferation (Fan and Bergmann, 2008a). In general, this model states that when apoptosis is initiated in epithelial cells, in addition to caspase activation and subsequent apoptosis, these dying cells secrete morphogens to promote proliferation of the surrounding cells, which leads to replacement of the dying cells and maintenance of tissue size. In proliferating epithelial cells, activation of the pro-apoptotic genes Reaper and Hid leads to upregulation and secretion of the morphogens Decapentaplegic (Dpp; *Drosophila* TGF-β) and Wingless (Wg; *Drosophila* Wnt) via increased activity of JNK and, or p53 (Perez-Garijo et al., 2004; Ryoo et al., 2004). In contrast, in response to apoptosis of differentiating, nonproliferating cells, Hedgehog (Hh), not Dpp or Wg, is upregulated and secreted (Fan and Bergmann, 2008b). Recently, the requirement for Dpp

and Wg secreted by apoptotic cells for compensatory proliferation has been questioned (Perez-Garijo et al., 2009). While stress- or injury-induced apoptosis initiates a compensatory proliferation response, programmed apoptosis that occurs during normal development does not. Why this difference exists and how apoptosing epithelial cells signal to initiate compensatory proliferation in response to cellular stress and tissue damage are not clear.

Here we demonstrate that Cdc42, the Rho family GTPase important for polarity responses in forming epithelia and migrating cells, is also a critical and novel negative regulator of apoptosis-induced compensatory proliferation. It does so by properly assembling and localizing the Par polarity complex. When this Cdc42/Par6/aPKC complex is depleted or mislocalized from adherens junctions, dying cells activate Rho1/Rok, which activates Myosin. This Rho/Rok/Myosin cascade is required for JNK activation and resultant Dpp and Wg secretion, leading to compensatory proliferation, independent of Rho/Rok's effects upon actin dynamics. Therefore, loss of epithelial cell polarity, as occurs as a result of cellular damage or during cancer development, provides a signal for cells to undergo compensatory proliferation. In cancer states where apoptotic regulation is disrupted, loss of the Cdc42/Par6/aPKC polarity complex organization or localization could contribute to tumor hyperproliferation and explain how polarity regulation contributes to tumor development.

Results

Cdc42 depletion causes apoptosis in proliferating epithelia, but not in post-mitotic epithelia

In studies designed to determine the role of Cdc42 in *Drosophila* eye epithelia development, depletion of Cdc42 using *eyeless-gal4* (*ey*>Cdc42-RNAi), which is expressed at an early embryonic stage of eye development and persisting throughout development, resulted in early pupal lethality. However, when Cdc42 was depleted selectively at the pupal stage of eye development using *GMR-gal4* (*GMR*>Cdc42-RNAi) there was no change in the number of pupal eye cells (Figures 8C and D) or size of the resulting adult eye (Figures 8A and B). In stark contrast, analysis of *ey*>Cdc42-RNAi larval eye imaginal discs revealed large amounts of ectopic apoptosis, as indicated by immunofluorescence for activated Caspase 3 (Figures 1A and B).

While many differences exist between larval and pupal eye epithelia, one major difference is the proliferation state. Larval eye epithelium undergoes extensive proliferation, primarily anterior to the morphogenetic furrow (MF) (Wolff and Ready, 1991) (Figure 8E), whereas the pupal eye is a post-mitotic, differentiating epithelium (Cagan and Ready, 1989). This raised the possibility that apoptosis from Cdc42 depletion in the larval eye imaginal disc, but not the pupal eye, was related to the proliferation status of epithelia. Consistent with this possibility, *ey*>Cdc42-RNAi caused apoptosis in the larval eye disc primarily in the proliferating compartment anterior to the MF, with the exception of non-epithelial cells near the optic stalk (Figure 1B). This was

not the result of restricted expression of Cdc42-RNAi since in controls, *ey-gal4*-mediated gene expression was uniformly distributed throughout the larval eye disc (Figure 8H). Moreover, GFP-labeled clones with the *Cdc42* LOF allele, $Cdc42^4$, also resulted in apoptosis only anterior to the MF (Figures 1C and D). Posterior to the MF (non-proliferating cells) $Cdc42^4$ clones had little evidence of apoptosis (Figure 1D). Importantly, expression of wild type Cdc42 within $Cdc42^4$ clones rescued the apoptotic clones anterior to the MF (Figure 1E). Finally, if Cdc42 depletion caused epithelial cell apoptosis only in proliferating cells, then depleting Cdc42 in non-proliferating, post-mitotic cells (e.g., pupal eye) should not result in any increase in apoptosis. Indeed, large $Cdc42^4$ clones in the pupal eye were not apoptotic (Figure 1F).

This effect was not restricted to the developing eye epithelium. Depletion of Cdc42 in the developing wing imaginal disc, which has uniform levels of proliferation across the epithelium (Figure 1K'), using *patched-gal4* (*ptc-gal4*) that restricts expression to a band of wing cells along the anterior-posterior axis with a graded anterior border and a sharp posterior border (Figures 1G and 8I), also resulted in ectopic apoptosis (Figure 1H). Apical cell profiles of wild type cells immediately outside the sharp posterior border of the *ptc*>Cdc42-RNAi expression domain were noted to have increased apical areas (Figure 8J), likely due to increased tension on these cells as a result of apical cell contraction of adjacent Cdc42-depleted cells (unpublished data). Expression of Cdc42-RNAi using *engrailed-gal4* (*en-gal4*), which is expressed in the posterior half of the larval wing disc (Figure 1I), also resulted in ectopic apoptosis in the posterior half of the larval wing epithelium (Figure 1J), indicating that depletion of Cdc42 caused apoptosis

independent of its larval wing expression domain. In summary, these data indicated that Cdc42 depletion in proliferating epithelial, but not post-mitotic epithelia, resulted in apoptosis.

Cdc42 negatively regulates apoptosis-induced compensatory proliferation

Induction of apoptosis in developing tissues by irradiation, heat shock, tissue damage, or activation of pro-apoptotic genes can induce compensatory proliferation in the surrounding non-apoptotic cells so as to maintain tissue homeostasis (Fan and Bergmann, 2008a). When apoptosis execution by these signals is concurrently blocked, sustained signals from these "undead" cells exaggerates the compensatory proliferation response and results in hyperproliferation of epithelial tissues. To determine if apoptosis from Cdc42 depletion resulted in compensatory proliferation of neighboring wild type cells, we blocked apoptosis in Cdc42-depleted cells by expressing the baculovirus caspase substrate protein P35, which inhibits effector caspase activity (Hay et al., 1994), using *ptc-gal4* (*ptc*>Cdc42-RNAi, P35). While expression of P35 alone had little effect on larval wing epithelium development (Figure 1K), co-expression of Cdc42-RNAi and P35 resulted in substantial expansion of the *ptc*-expression domain and enlargement of the wing disc as a whole (Figure 1L). Immunofluorescence for phospho-Histone H3, to identify cells undergoing mitosis, revealed that *ptc*>Cdc42-RNAi, P35 wing discs had a uniform increase in cells undergoing mitosis compared to *ptc*>P35 wing discs (Figures 1L' vs 1K'), suggesting that this phenotype was due to non-autonomous overproliferation of the wing disc epithelial cells. We observed the same phenotype using *en-gal4* (Figures

1M and N), indicating that this phenotype was not dependent on promoter or larval wing region depleted of Cdc42. Finally, when P35 and Cdc42-RNAi were co-expressed in the larval eye, using *ey-gal4*, similar results were observed (Figures 8E-G).

This phenotype was also seen using a *Cdc42* LOF allele. GFP-labeled $Cdc42^{4}$ clones that also expressed P35 in larval eye discs were increased in size and resulted in enlargement of the larval eye disc as a whole, compared to clones expressing P35 alone (Figure 1P vs 1O). In addition, the resulting adult eyes with $Cdc42^{4}$ clones expressing P35 displayed a hyperproliferation phenotype with overgrowths of eye tissue (Figures 1Q-T). Taken together, these data identified Cdc42 as a novel regulator of apoptosis-induced compensatory proliferation in developing, proliferating epithelia.

Cdc42 depletion increases JNK activity that promotes both apoptosis and compensatory proliferation

A key component in the apoptosis-induced compensatory proliferation pathway is JNK (Perez-Garijo et al., 2009; Ryoo et al., 2004). Therefore, we asked whether Cdc42 regulated JNK activity. To determine if Cdc42 depletion increased JNK activation, we expressed Cdc42-RNAi in larval wing imaginal discs with *en-gal4* in the background of a *puckered-lacZ* transcriptional reporter (puc^{E69}). Since *puckered* (*puc*) is a transcriptional target regulated by JNK activity, *lacZ* expression was a functional readout of JNK activity (Martin-Blanco et al., 1998). *En*>Cdc42-RNAi increased transcription of *puc* (Figure 2A). $Cdc42^{4}$ clones in the larval eye also resulted in increased *puc-lacZ* expression (Figure 2B).

Next, we determined if increased JNK activation from Cdc42 depletion was responsible for the resulting apoptosis. If so, then increasing JNK activity by decreasing the levels of the JNK phosphatase Puckered should enhance apoptosis resulting from Cdc42 depletion. Removing a genomic copy of *puc* and expressing Cdc42-RNAi with *en-gal4* increased apoptosis compared to *en*>Cdc42-RNAi alone (Figures 2C and D). Conversely, blocking JNK activity by overexpressing Puc should inhibit apoptosis due to Cdc42 depletion. Indeed, co-expressing Cdc42-RNAi with Puc using *en-gal4* substantially rescued the apoptosis seen in *en*>Cdc42-RNAi alone (Figure 2E). Moreover, depletion of JNK itself with JNK-RNAi rescued the apoptosis from *en*>Cdc42-RNAi (Figure 2F). Taken together, these data indicated that Cdc42 depletion resulted in apoptosis through activation of JNK.

Next we asked whether the hyperproliferation that resulted by blocking apoptosis in Cdc42 depleted cells also involved JNK activity. MMP1 is a transcriptional target downstream of active JNK (Uhlirova and Bohmann, 2006). To determine if JNK activity was increased in hyperproliferative cells that co-express Cdc42-RNAi and P35, we determined MMP1 protein levels by immunofluoresence. Whereas P35 expression alone did not affect MMP1 levels (Figure 2G), MMP1 protein levels were increased in cells co-expressing P35 and Cdc42-RNAi (Figure 2H), consistent with increased JNK activity. Increased MMP1 levels were also seen in larval eye $Cdc42^{4}$ clones expressing P35 but not in clones only expressing P35 (Figures 2I and J). Importantly in both the wing and eye imaginal discs, even though the whole imaginal disc was enlarged, increased JNK

activity was detected only in cells where Cdc42 was depleted and P35 expressed (Figures 2H and J).

Having demonstrated an association of increased JNK activity in cells depleted of Cdc42 and expressing P35, we wanted to determine if this increased JNK activity was responsible for the resulting hyperproliferation. To do so, we inhibited JNK activity by overexpressing Puc or depleting JNK in cells expressing Cdc42-RNAi and P35. Compared to *ptc*>Cdc42-RNAi, P35 wing discs, *ptc*>Cdc42-RNAi, P35, Puc and *ptc*>Cdc42-RNAi, P35, JNK-RNAi wing discs were significantly smaller (Figures 2K-M, as quantified in Table 1). As controls, *ptc*>P35, Puc and *ptc*>P35, JNK-RNAi wing discs were similar in size to wild type wing discs (Figure 2N, data not shown). Finally, to determine if JNK was sufficient for driving compensatory proliferation, we overexpressed JNK alone or with P35. Overexpression of JNK alone caused apoptosis (Figure 2O), while co-expressing JNK with P35 resulted in hyperproliferation (Figures 2P and Q), suggesting that JNK alone is sufficient to drive the compensatory proliferation response, as was previously suggested (McEwen and Peifer, 2005; Perez-Garijo et al., 2009; Ryoo et al., 2004).

The secreted morphogens Dpp and Wg, the Drosophila homologues of TGF-β and Wnt, respectively, have been demonstrated to be upregulated downstream of JNK in the apoptosis-induced compensatory proliferation response in proliferating epithelium (Perez-Garijo et al., 2009; Ryoo et al., 2004). We determined Wg protein distribution in *ptc*>Cdc42-RNAi, P35 larval wing discs and larval eye discs with $Cdc42^{4}$ clones expressing P35. In both cases, Wg protein was increased in cells depleted of Cdc42 and

expressing P35 (Figures 9A and B). In addition, cells co-expressing Cdc42-RNAi and P35 had increased *dpp-lacZ* expression (Figure 9C) and phospho-MAD levels (Figures 9D-F), indicative of increased Dpp signaling in these cells. Importantly, phospho-MAD levels were also increased in wild type cells surrounding cells co-expressing Cdc42-RNAi and P35 (Figures 9E and F), consistent with secretion of Dpp from cells expressing Cdc42-RNAi and P35 to cause non-autonomous proliferation.

Cdc42 depletion induces compensatory proliferation through Rho1-Rok activation

Members of the Rho GTPase family can influence JNK activity (Coso et al., 1995; Minden et al., 1995). Specifically RhoA-ROCK has been shown to activate JNK in mammalian cells (Marinissen et al., 2004). Precisely how ROCK activates JNK is not known, but in these cells it appeared to be independent of its effects upon actin dynamics (Marinissen et al., 2004). In addition, other work has identified crosstalk between members of the Rho GTPase family in the regulation of *Drosophila* epithelial morphogenesis (Warner and Longmore, 2009a), but how these different Rho GTPases communicate with one another is not understood. Therefore, one possibility for how depletion of Cdc42, in proliferating epithelial cells, activated JNK and apoptosis-induced compensatory proliferation was through crosstalk with Rho1-Rok signaling.

To test this, we first determined if increased Rho1 could induce apoptosis in proliferating epithelial cells. Similar to what we observed with Cdc42-RNAi expression, *ey*>Rho1 induced ectopic apoptosis specifically in proliferating cells anterior to the MF in eye imaginal discs (Figure 3A). In addition, *ptc*>Rho1 and *en*>Rho1 induced ectopic

apoptosis in larval wing discs (Figures 3B and E). The apoptosis in the larval wing discs from increased Rho1 expression was inhibited by co-expression of Puc (Figure 3C) and enhanced by removing a genomic copy of *puc* (Figure 3F), indicating that it was JNK dependent. Furthermore, in cells overexpressing Rho1, *puc-lacZ* levels (regulated by JNK activity) were increased (Figure 3G). To determine if apoptosis resulting from increased Rho1 expression could activate the compensatory proliferation response, we co-expressed Rho1 with P35 using *ptc-gal4*, and observed hyperproliferation of the wing disc (Figure 3D). In sum, these data indicated that increased Rho1 expression induced a JNK-dependent apoptosis and compensatory proliferation response. Consistent with data from mammalian systems, suggesting that RhoA activates JNK through ROCK, expression of an active form of Rok (Rok-CAT) also induced apoptosis (Figure 3H). When Rok-CAT and P35 were co-expressed, hyperproliferation and upregulation of MMP1 resulted (Figure 3I), indicative of increased JNK activity.

Having demonstrated that increased Rho1-Rok signaling activated JNK leading to apoptosis-induced compensatory proliferation, we asked whether hyperproliferation from *ptc*>Cdc42-RNAi, P35 depended on Rho1-Rok activity. To test this, we depleted Rho1 or Rok from *ptc*>Cdc42-RNAi, P35 cells by either removing a genomic copy of *Rho1* or expressing Rok-RNAi in the context of Cdc42-RNAi and P35 expression. By either approach, the hyperproliferation from expression of Cdc42-RNAi and P35 was attenuated (Figures 3J-L, as quantified in Table 1). As controls, wing discs depleted of Rho1 or Rok and expressing P35 alone were similar in size to wild type wing discs (Figures 3M and N).

Myosin activity but not F-actin assembly downstream of Rok controls compensatory proliferation through JNK

How then does Rok activate JNK in proliferating epithelium? Two main functions downstream of Rok are to promote F-actin assembly by regulating Cofilin activity and to activate Myosin through direct or indirect phosphorylation of the Myosin Light Chain (MLC). Cofilin activity depends on its phosphorylation state, where phosphorylated Cofilin is inactive and unphosphorylated Cofilin is active and severs F-actin. Slingshot (Ssh) is a cofilin phosphatase that promotes Cofilin activity and F-actin severing (Niwa et al., 2002). We used Ssh LOF analysis to inhibit Cofilin and promote F-actin assembly, similar to what can occur downstream of Rok. Larval eye disc clones with ssh^{1-11} resulted in apoptosis anterior to the MF, similar to Cdc42 depletion or Rho1 overexpression (Figure 4A). However, when P35 was expressed in ssh^{1-11} clones to inhibit this apoptosis, no hyperproliferation or upregulation of MMP1 occurred (Figure 4B). As a control, F-actin assembly was clearly increased in these clones (Figure 4C). In addition, overexpression of Serum Response Factor (SRF), a transcription factor regulated by levels of polymerized and monomeric actin downstream of Cofilin activity (Sotiropoulos et al., 1999), also did not cause hyperproliferation with co-expression of P35 in larval wing discs (data not shown). Therefore, these results suggested that Rok did not regulate JNK and compensatory proliferation through F-actin regulation.

When a constitutively active form of Myosin Light Chain Kinase was expressed in larval wing discs, using *ptc-gal4* (*ptc*>MLCK-CA), apoptosis ensued (Figure 4D), like

Cdc42 depletion or Rho1-Rok activation. This apoptosis was attenuated by blocking JNK activity with Puc overexpression (Figure 4E) and enhanced by activating JNK through removing a genomic copy of *puc* (Figure 4F). Surprisingly, and in contrast to actin manipulation, blocking MLCK-CA-induced apoptosis, by co-expressing MLCK-CA with P35, led to hyperproliferation and upregulation of MMP1 (Figure 4G). This indicated that activation of Myosin, a known downstream target of Rok, is sufficient to induce JNK-dependent apoptosis and compensatory proliferation.

To address whether increased Myosin activity was associated with Cdc42 depletion and the compensatory proliferation response, we determined the levels of phospho-MLC in cells co-expressing Cdc42-RNAi and P35. Larval wing disc epithelial cells co-expressing Cdc42-RNAi and P35 had increased levels of phospho-MLC (Figure 4J). To determine if Myosin activity was necessary to induce JNK-dependent apoptosis and the compensatory proliferation response downstream of Cdc42 depletion, we reduced Myosin levels by removing a genomic copy of *Zipper* (*Zip*, *Drosophila* Myosin) in the context of Cdc42 depletion. Reducing *Zip* attenuated both the apoptosis from Cdc42-RNAi expression (Figures 4H and I) and the hyperproliferation from co-expression of Cdc42-RNAi with P35 (Figure 4K, as quantified in Table 1). As a control, wing discs with *Zip* reduction and P35 expression alone were similar in size to wild type wing discs (data not shown). These data indicated that Cdc42 depletion activated JNK in proliferating epithelial cells via increased Myosin activation downstream of Rho1-Rok signaling, independent of Rho1-Rok effects upon actin assembly and SRF.

Cdc42 functions with Par6 and aPKC to regulate compensatory proliferation

We next asked how Cdc42 inhibited Rho1 activity to regulate JNK and compensatory proliferation. Active, GTP-bound, Cdc42 binds to effector proteins, which mediate its downstream cellular functions. Two major Cdc42 effectors are p21-activated kinase (Pak) and Wiscott-Aldrich syndrome protein (WASP). Larval eye imaginal disc clones with Pak and WASP LOF alleles were of normal size and did not have increased apoptosis (Figures 10A and B), and expression of P35 within these clones did not induce hyperproliferation (data not shown).

Another Cdc42 effector is Par6, which is a member of a polarity complex that also includes Par3 and aPKC. Larval eye imaginal disc clones with a Par6 LOF allele, $par6^{\Delta 226}$, were significantly smaller than control clones (Figures 5A and B). We could not detect elevated levels of activated Caspase 3 in these clones (Figures 5A and B), likely due to their extremely small size, but this suggested that Par6-depleted cells had decreased survival capacity compared to wild type cells. To determine if Par6 depletion activated JNK, we generated Par6 LOF clones in the background of *puc-lacZ*. The Par6 LOF clones had increased *lacZ* expression, consistent with increased JNK activation (Figure 5C). Lastly, to determine whether Par6 also negatively regulates compensatory proliferation, we expressed P35 in Par6 LOF clones. This resulted in increased clone size (Figure 5D'), upregulation of MMP1 (Figure 5D''), and hyperproliferation of eye tissue (Figures 5D-H).

Par6 binds to active Cdc42 and recruits Par3 and aPKC to the complex (Henrique and Schweisguth, 2003). Bazooka (*Drosophila* Par3) LOF clones in larval eye imaginal

discs were of normal size, did not have increased apoptosis, and did not increase *puc-lacZ* expression (Figures 10C and D). However, aPKC LOF clones, like Par6 LOF clones, were extremely small (Figures 5I and J), and when P35 was expressed in aPKC LOF clones, clone size increased (Figure 5K'), MMP1 was upregulated (Figure 5K''), and eye tissue overproliferated (Figures 5L-N). Depletion of aPKC through RNAi expression in larval wing discs gave the same phenotypes (Figures 5O-R, 11A and B). These data suggested that Cdc42 negatively regulated compensatory proliferation through its association with the aPKC/Par6 complex.

Having demonstrated that Cdc42, Par6, and aPKC can function individually to negatively regulate compensatory proliferation, we next asked whether assembly of the Cdc42/Par6/aPKC complex was important for this function. First, we observed that Par6 and aPKC, but not Bazooka, were mislocalized from AJs in larval wing disc cells expressing Cdc42-RNAi compared to controls (Figures 6A-D, 10E), indicating that Cdc42 localizes Par6/aPKC to AJs and suggesting that AJ localization of Par6/aPKC may be critical for Cdc42-mediated repression of apoptosis-induced compensatory proliferation. When we overexpressed a Cdc42 binding mutant of Par6 ($Par6^{ISAA}$) in larval wing imaginal discs using *ptc-gal4*, similar to LOF analysis with Cdc42, Par6, and aPKC, apoptosis resulted (Figure 6F), activation of JNK was evident (Figure 6H), and mislocalization of aPKC from AJs was observed (Figure 6L). Furthermore, when $Par6^{ISAA}$ was co-expressed with P35, hyperproliferation and upregulation of MMP1 resulted (Figure 6J). In contrast, overexpression of wild type Par6 did not induce apoptosis (Figure 6E), activate JNK (Figure 6G), mislocalize aPKC from AJs (Figure

6K), or result in hyperproliferation with P35 expression (Figures 6I). These data suggested that the assembly of the Cdc42/Par6/aPKC complex, at AJs, was critical for negatively regulating apoptosis-induced compensatory proliferation.

The Cdc42/Par6/aPKC complex is known for its regulation of epithelial apical-basal polarity (Henrique and Schweisguth, 2003). In addition to this polarity complex there are two others: the Scribble and Crumbs complexes. Therefore to determine if disruption of polarity complexes, in general, resulted in apoptosis-induced compensatory proliferation, we depleted Dlg, Scrib, or Crumbs in larval imaginal disc epithelial cells. While depletion of Dlg and Scrib, either individually or together in the larval eye or wing imaginal discs, induced JNK-dependent apoptosis (Figure 12A-E, data not shown), when P35 was expressed in those cells, compensatory proliferation did not result (Figure 12F, data not shown). Crumbs depletion did not result in apoptosis (Figures 12G and H) or activation of JNK (Figure 12I). These data indicated that the Par polarity complex is unique from other polarity complexes in regulating apoptosis-induced compensatory proliferation.

Cdc42 and aPKC depletion promotes compensatory proliferation following irradiation

Having demonstrated that Cdc42 and the Par polarity complex negatively regulate compensatory proliferation using cells in which apoptosis was inhibited by P35, we next asked if this complex also functions in the well characterized compensatory proliferation response following irradiation (Haynie and Bryant, 1977), independent of P35 expression. Exposure of larvae to irradiation causes imaginal disc cell cycle arrest to

allow for DNA damage repair. Following apoptosis of cells with irreparable DNA damage, the remaining imaginal disc cells undergo proliferation about 8 hours after irradiation exposure (Kondo et al., 2006). If Cdc42 and the Par polarity complex negatively regulate compensatory proliferation, then depletion or disruption of this complex should promote proliferation following irradiation. Consistent with this, 6 hours after larvae were exposed to 40 Gy of irradiation, wing imaginal disc cells depleted of Cdc42 or aPKC had increased proliferation compared with wild type cells present in the same wing disc or wild type wing discs (Figures 7A-C). In controls, depletion of Cdc42 or aPKC in wing discs from unexposed larvae did not significantly alter proliferation levels (Figures 7D-F). Furthermore, in wing imaginal disc cells exposed to irradiation, aPKC was mislocalized from AJs compared to unexposed cells (Figures 7G-K), suggesting that irradiation induces proliferating epithelial cells to initiate compensatory proliferation by mislocalizing the Par polarity complex from AJs.

Discussion

In proliferating epithelia, but not post-mitotic epithelia, disruption of the Cdc42/Par6/aPKC polarity complex leads to increased Rho1-Rok-Myosin activity and a JNK-dependent apoptosis-induced compensatory proliferation response (Figure 7L). This represents a novel upstream regulation of the apoptosis-induced compensatory proliferation response and suggests a mechanism for how an epithelium can maintain tissue homeostasis in response to injury or stress or how disruption of polarity in developing carcinoma contributes to cancer development. Proper localization of Cdc42/Par6/aPKC at epithelial cell AJs may be an indicator of a normal epithelial cell with correct apical-basal polarity; however, stress, tissue damage, or oncologic mutations that cause mislocalization or disruption of this complex may identify abnormal cells that need to be removed by apoptosis. Concurrently, these cells can induce proliferation of surrounding, non-apoptotic cells so they are replaced by normal cells, or in the case of carcinoma where apoptosis regulation is aberrant, apical-basal polarity disruption can lead to hyperproliferation and tumor progression. How irradiation disrupts aPKC localization is unclear; perhaps activation of stress response pathways affects aPKC localization and/or activity, as has been shown previously (Diaz-Meco et al., 1996).

Our data suggested that Cdc42, through a complex with Par6/aPKC localized to the AJ, inhibits Rho1 activity in proliferating epithelial cells. Due to the significant disruption of tissue architecture in hyperproliferative imaginal discs we could not demonstrate direct evidence for activated Rho1 in Cdc42 depleted tissue. However, in a post-mitotic, nonproliferating epithelium (pupal eye), depletion of Cdc42 does not disrupt

tissue architecture and increases levels of the Rho1 effectors PKN and Diaphanous at AJs, indicative of increased Rho1 activation (data not shown). This and genetic data herein indicate that Rho functions downstream of Cdc42/Par6/aPKC polarity complex disruption to regulate apoptosis induced compensatory proliferation. Rho activated JNK and compensatory proliferation through Rok's regulation of Myosin activity but not F-actin assembly. Whether increased acto-myosin tension resulting from Myosin activation or some other function of active Myosin is necessary for JNK activation remains to be determined.

In other examples of crosstalk between Rho family proteins, upstream regulators of GTPase activity have been implicated in mediating these effects. These upstream regulators include Rho guanine nucleotide exchange factors (RhoGEFs), which promote Rho activity, and Rho GTPase-activating proteins (RhoGAPs) and Rho-GDP dissociation inhibitors (RhoGDIs), which inhibit Rho activity. While mammalian RhoGDIs have been shown to mediate crosstalk between Cdc42 and Rac (DerMardirossian et al., 2004) and RhoA and RhoB (Ho et al., 2008), when we deleted the full coding region of the only *Drosophila* RhoGDI, *Drosophila* homozygous for this deletion (i.e., null for RhoGDI) were viable with no gross external defects (unpublished results). Likewise, mammalian p190RhoGAP has been implicated as mediating crosstalk between Rac and Rho (Wildenberg et al., 2006) and Par6/aPKC and Rho (Zhang and Macara, 2008); however, when we deleted the full coding region of the sole *Drosophila* p190RhoGAP, *Drosophila* homozygous the p190RhoGAP deletion were also viable and exhibited no gross external defects (unpublished results). Thus, if Cdc42/Par6/aPKC regulate Rho1 activity through

other RhoGAPs or RhoGEFs, then these remain to be determined. Alternatively, Cdc42 and Rho1 may communicate through other mechanism independent of these upstream Rho GTPase regulators. For example, aPKC may directly or indirectly affect Rho activity.

Like disruption of the Par polarity complex, disruption of the Scribble polarity complex also induced JNK-dependent apoptosis (Figure 12A-E, data not shown) (Igaki et al., 2006; Igaki et al., 2009; Uhlirova et al., 2005). However, in contrast to Par complex disruption, disruption of the Scribble polarity complex did not promote compensatory proliferation (Figure 12F, data not shown) (Igaki et al., 2009). Disruption of these two complexes activates JNK by different upstream signaling events. Disruption of the Par complex activates JNK through a Rho-Rok-Myosin axis while disruption of the Scribble complex activates JNK by increased endocytosis of Eiger (*Drosophila* tumor necrosis factor). Because increased JNK activity alone is sufficient for promoting compensatory proliferation (Figure 2O) (McEwen and Peifer, 2005; Perez-Garijo et al., 2009; Ryoo et al., 2004), this suggests that the mechanism by which JNK is activated may also dictate whether compensatory proliferation occurs, possibly due to differences in localization of active JNK within the cell. Alternatively, increased Eiger signaling following Scribble complex disruption may inhibit JNK-mediated compensatory proliferation.

Expression of P35, to inhibit apoptosis in cells where Cdc42/Par6/aPKC were depleted or mislocalized, exaggerated the compensatory proliferation response leading to epithelial hyperproliferation. Epithelial tumor cells are often resistant to apoptosis (Hajra and Liu, 2004; Hanahan and Weinberg, 2000) and have disrupted epithelial cell polarity

(Tanos and Rodriguez-Boulan, 2008). Therefore, that mislocalization of the Par polarity complex in the presence of inhibited apoptosis results in epithelial hyperproliferation parallels early carcinoma development. This raises the possibility that a significant component of carcinoma development could be misregulation of the apoptosis-induced compensatory proliferation response, which normally is used to remove damaged cells with altered polarity, but when apoptosis is blocked (e.g., cancer) epithelial hyperproliferation results.

Another component of carcinoma cell progression is the acquisition of migration and invasion properties. Interestingly, in addition to hyperproliferation, co-expression of Cdc42-RNAi and P35 in larval wing discs resulted in protrusions of epithelial tissue out of the normal tissue plane in about 25% of wing discs (Figures 13A and B). These protruding cells had high levels of mitotic activity, disorganized AJs, and enrichment of F-actin (Figures 6A and B) and phospho-MLC (data not shown), all phenotypes seen in epithelial cells, including carcinoma cells, with the capacity to migrate and invade. Importantly we have not observed similar protrusions with any other manipulation that caused hyperproliferation of imaginal discs, either from the compensatory proliferation response (e.g., co-expression of P35 with JNK, Rho1, Rok-CAT, MLCK-CA, aPKC-RNAi, or $Par6^{ISAA}$) or from an independent mechanism of inducing proliferation (e.g., overexpression of the Hippo pathway transcriptional activator Yorkie). This suggests that this effect was not strictly dependent or associated with hyperproliferation, was specific to depletion of Cdc42, and interestingly, was not seen with Par6 or aPKC depletion. In addition, in instances where hyperproliferation from Cdc42 depletion and

P35 expression was attenuated (depletion JNK or Zip), we still observed tissue protrusions (Figures 13C-F). These data indicated that Cdc42 depletion, in addition to activating the compensatory proliferation response, also caused epithelial tissue remodeling. Whether this phenotype represents an invasive process (as seen in cancer metastasis) or tissue/organ protrusions remains to be determined. While Cdc42 depletion activates Rho1 to regulate compensatory proliferation, perhaps Cdc42 depletion also activates Rac to induce epithelial tissue remodeling.

Acknowledgements

We thank R. Cagan for support during the initial stages of this work. This work was supported by grants NIH CA85839 and GM080673 to GDL.

Methods

Drosophila stocks and genetics

All crosses and staging were performed at 25°C unless otherwise noted. w^{1118} was used as wild type. Stocks are described in Flybase (http://flybase.bio.indiana.edu). *GMR-gal4*, *ey-gal4*, tubulin-$gal80^{ts}$, $cdc42^{4}$ FRT19A, UAS-GFP, pak^{16} FRT82B, ssh^{1-11} FRT82B, puc^{E69}, UAS-P35, UAS-JNK, UAS-Rho1, *dpp-lacZ*, and UAS-aPKC-RNAi were kindly provided by the Bloomington *Drosophila* Stock Center, *patched-gal4*, wsp^{3} FRT82B, UAS-Puc, and $scrib^{1}$ FRT82B by R. Cagan (Mount Sinai, New York, NY), Zip^{1} by T. Wolff (Washington University, St. Louis, MO), *en-gal4* (J. Skeath, Washington University, St. Louis, MO), baz^{4} FRT19A, $par6^{\Delta 226}$ FRT19A, $apkc^{k06403}$ FRTG13, UAS-$aPKC^{WT}$, and UAS-$aPKC^{Caax}$ by C. Doe (University of Oregon, Eugene, OR), UAS-$MLCK^{CA}$ by M. VanBerkum (Wayne State University, Detroit, MI), UAS-Dlg-RNAi and UAS-Crb-RNAi by the Vienna *Drosophila* RNAi Center (Vienna, Austria), UAS-Scrib-RNAi and UAS-JNK-RNAi by the National Institute of Genetics (Shizuoka, Japan). Rho1-RNAi and Cdc42-RNAi were previously described (Warner and Longmore, 2009a). GFP-labeled clones in larval eye discs were generated using the following stocks: *tub-gal80*, FRT19A; *ey*-FLP, *act*>y^{+}>*gal4*, UAS-GFP (19A Tester); *yw*, *ey*-FLP; *act*>y^{+}>*gal4*, UAS-GFP; *tub-gal80*, FRT82B (82B Tester) (both provided by T. Xu, Yale Univeristy, New Haven, CT); and *yw*, *ey*-FLP; *tub-gal80*, FRTG13; *act*>y^{+}>*gal4*, UAS-GFP. Expression of UAS-$MLCK^{CA}$ using *patched-gal4* was early larval lethal, so these crosses were performed using *patched-gal4*, $tub\text{-}gal80^{ts}$ and progeny were shifted from 18°C to 29°C five days after egg laying.

Irradiation treatment

Wandering third-instar larvae were exposed to 40 Gy of irradiation and dissected either 20 minutes or 6 hours after exposure.

Immunofluorescence

Wing or eye imaginal discs from wandering third-instar larvae were dissected and processed as previously described (Warner and Longmore, 2009a). Antibodies used were rat anti-DE-cadherin (1:20), mouse anti-Discs large (1:50), mouse anti-Wg (1:10), mouse anti-MMP1 (all from the Developmental Studies Hybridoma Bank at the University of Iowa), rabbit anti-β-galactosidase (1:2000, ICN/Cappel), rabbit anti-phospho-Mad (1:100, R. Cagan, Mount Sinai, New York, NY), rabbit anti-cleaved Caspase 3 (1:100, Cell Signaling), rabbit anti-phospho-Histine H3 (1:1000, Upstate Laboratories, Syracuse, NY), rabbit anti-Bazooka (1:500, from A. Wodarz, University of Göttingen, Germany), guinea pig anti-Scrib (1:500, from D. Bilder, University of California, Berkeley, CA), rabbit anti-Par6 (1:500, from J. Knoblich, IMBA, Vienna, Austria), rabbit anti-aPKC (C-20) (1:200, Santa Cruz Biotechnology), and rabbit anti-phospho-Myosin Light Chain 2 (Ser19) (1:20, Cell Signaling). Rhodamine-phalloidin (1:500, Invitrogen) was added in the primary and secondary antibody incubations to visualize F-actin. Secondary antibodies were Alexa 488 and 568 (Invitrogen) and Cy5 (Jackson ImmunoResearch). Immunofluorescence was analyzed on a Zeiss 510 LSM.

Quantification and statistics

Larval wing disc areas were measured by outlining wing discs and determining the number of pixels within the outline. Quantifications were performed using ImageJ v1.38. P-values were calculated using an unpaired, two-sided Student's t-test.

Figures

Figure 1. Depletion of Cdc42 causes apoptosis in proliferating epithelia, and inhibiting apoptosis in Cdc42-depleted cells results in hyperproliferation

Confocal immunofluorescent localization of DE-cadherin (DE-cad) (A, A', B, B') and activated Caspase 3 (AC3) (A, A'', B, B'') in control (*ey*>GFP) (A) and *ey*>Cdc42-RNAi (B) larval eye discs. Arrowheads identify morphogenetic furrow. Confocal immunofluorescent localization of DE-cadherin (C, D, E,) and activated Caspase 3 (C'', D'', E'') in GFP-labeled control clones (C), $Cdc42^4$ clones (D), and $Cdc42^4$ clones expressing wild type Cdc42 (E) in larval eye discs. Arrowheads identify morphogenetic furrow. Confocal immunofluorescent localization of DE-cadherin (F) and activated Caspase 3 (F'') in GFP-labeled $Cdc42^4$ clones in pupal eye 40 hours after puparium formation. Arrowheads identify developmentally normal apoptosis in periphery of pupal eye. Confocal immunofluorescent localization of DE-cadherin (G, H, I, J) and activated Caspase 3 (G', H', I', J') in control (G, I), *ptc*>Cdc42-RNAi (H), and *en*>Cdc42-RNAi (J) larval wing discs. Confocal immunofluorescent localization of DE-cadherin (K-N) and phospho-Histone H3 (phospho-H3) (K', L') in larval wing discs expressing P35 (K, M) and P35 with Cdc42-RNAi (L, N) with *ptc-gal4* (K, L) or *en-gal4* (M, N). Confocal immunofluorescent localization of DE-cadherin (O, P) in GFP-labeled clones expressing P35 (O) or $Cdc42^4$ clones expressing P35 (P). Adult eyes resulting from generation of control clones (Q), clones expressing P35 (R), $Cdc42^4$ clones (S), and $Cdc42^4$ clones expressing P35 (T). Scale bars represent 100 μm (A-E, G-T) and 20 μm (F).

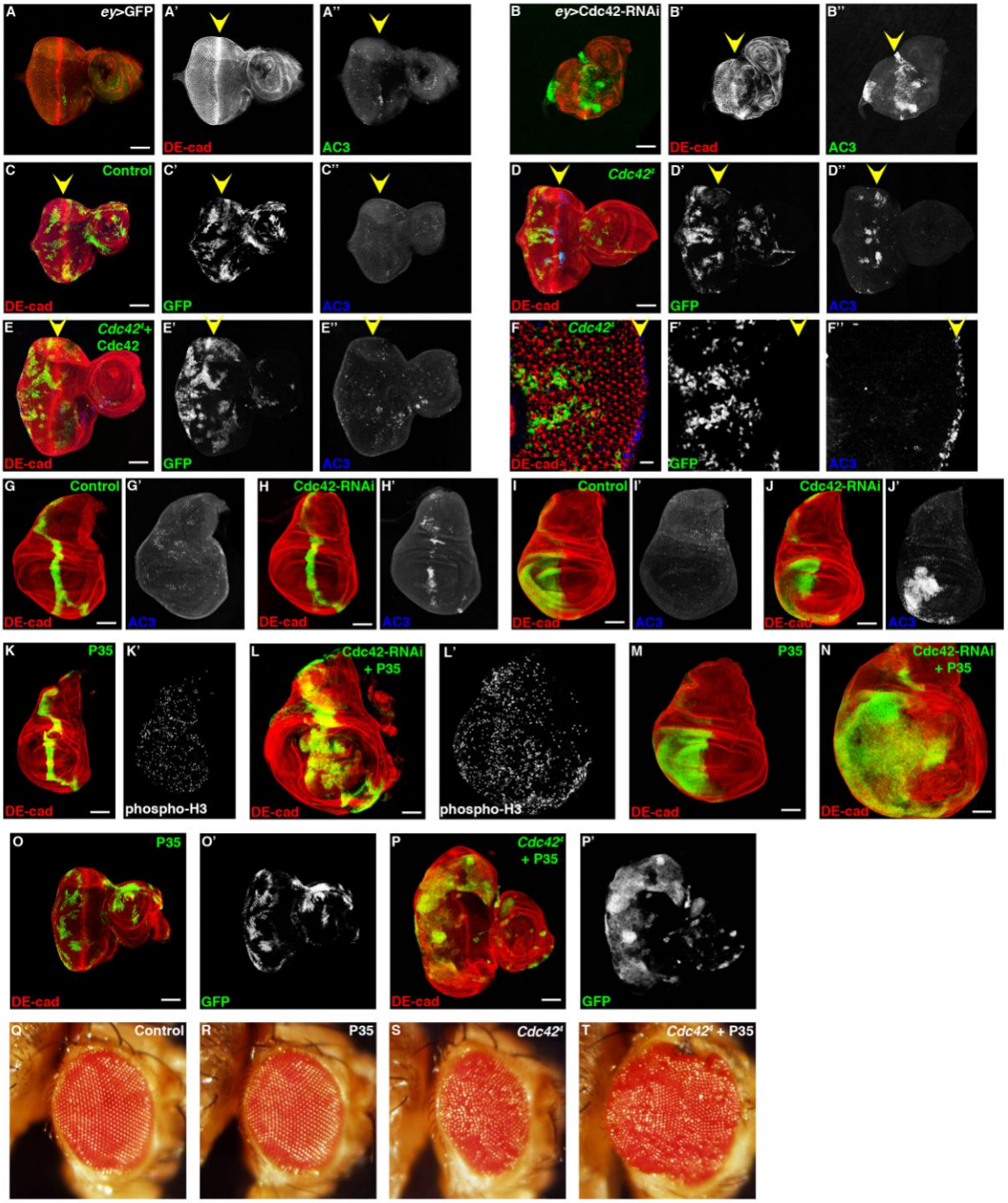
A ey>GFP
A' DE-cad
A'' AC3
B ey>Cdc42-RNAi
B' DE-cad
B'' AC3
C Control
C' GFP
C'' AC3
DE-cad
D Cdc42i
D' GFP
D'' AC3
DE-cad
E Cdc42i+ Cdc42
E' GFP
E'' AC3
DE-cad
F Cdc42i
F' GFP
F'' AC3
DE-cad
G Control
G' AC3
DE-cad
H Cdc42-RNAi
H' AC3
DE-cad
I Control
I' AC3
DE-cad
J Cdc42-RNAi
J' AC3
DE-cad
K P35
K' phospho-H3
DE-cad
L Cdc42-RNAi + P35
L' phospho-H3
DE-cad
M P35
DE-cad
N Cdc42-RNAi + P35
DE-cad
O P35
O' GFP
DE-cad
P Cdc42i + P35
P' GFP
DE-cad
Q Control
R P35
S Cdc42i
T Cdc42i + P35

Figure 1

Figure 2. Cdc42 negatively regulates JNK activity

Confocal immunofluorescent localization of DE-cadherin (A, B) and β-galactosidase (A', B'') in larval wing disc expressing Cdc42-RNAi with *en-gal4* (A) and eye disc with GFP-labeled $Cdc42^{4}$ clones (B), both in a heterozygous background of puc^{E69} (*puc-lacZ*). Confocal immunofluorescent localization of DE-cadherin (C-F) and activated Caspase 3 (C'-F') in larval wing discs expressing Cdc42-RNAi alone (C), in a puc^{E69} heterzygous background (D), with Puc overexpression (E), and with JNK-RNAi expression (F). Confocal immunofluorescent localization of DE-cadherin (G-J) and MMP1 (G''-J'') in larval wing discs expressing P35 alone (G) and Cdc42-RNAi with P35 (H) using *ptc-gal4* and eye discs with GFP-labeled clones expressing P35 alone (I) and $Cdc42^{4}$ clones expressing P35 (J). Confocal immunofluorescent localization of DE-cadherin (K-N) in larval wing discs expressing Cdc42-RNAi with P35 (K), Cdc42-RNAi with P35 and Puc (L), Cdc42-RNAi with P35 and JNK-RNAi (M), and P35 with Puc (N) using *ptc-gal4*. Confocal immunofluorescent localization of DE-cadherin (O-Q) and activated Caspase 3 (O') in larval wing discs overexpressing JNK alone (O), expressing P35 (P), and co-expressing JNK with P35 (Q) using *ptc-gal4*. Scale bars represent 100 μm.

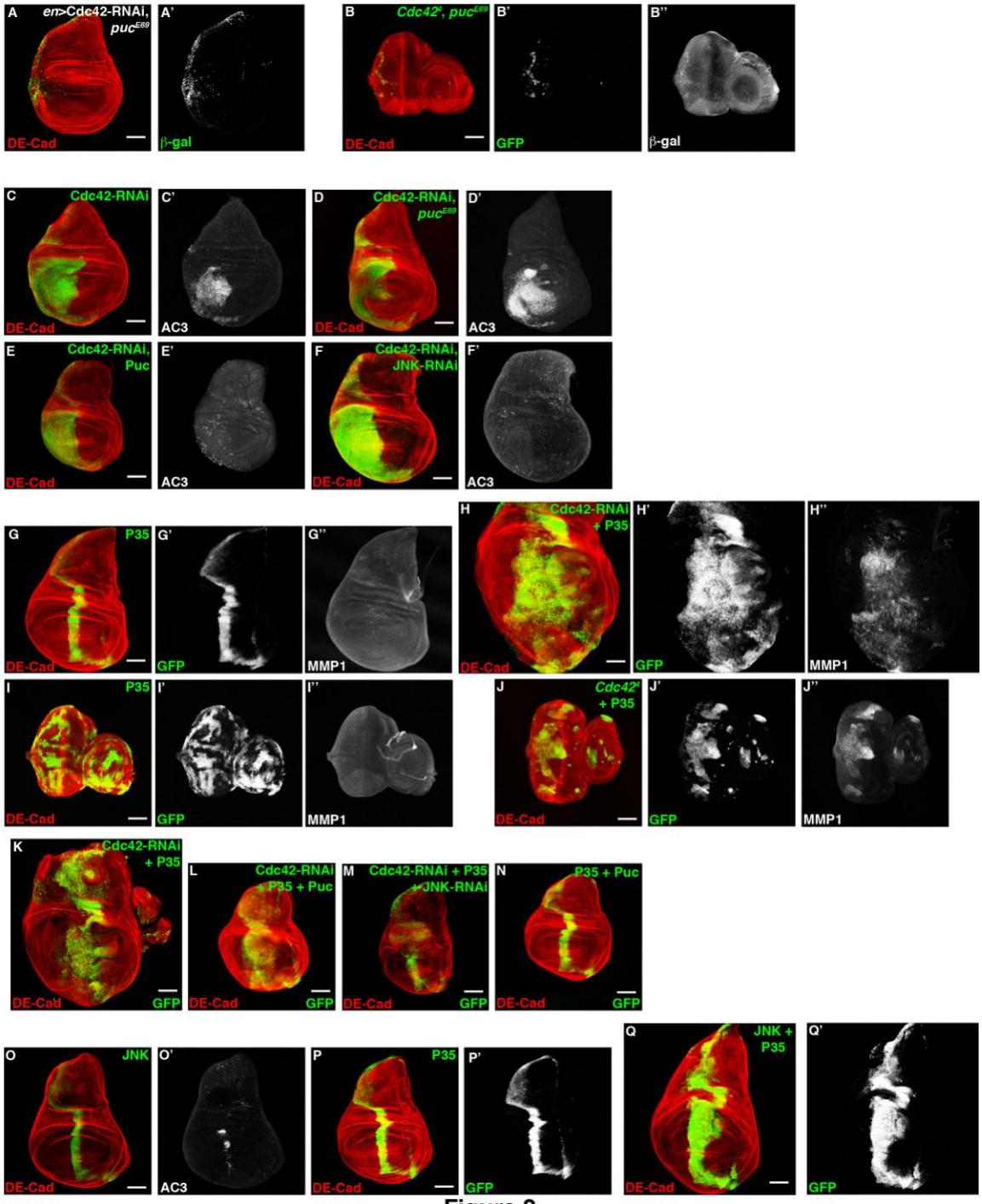
A
en>Cdc42-RNAi, pucE69
DE-Cad
A'
β-gal
B
Cdc42¹, pucE69
DE-Cad
B'
GFP
B''
β-gal
C
Cdc42-RNAi
DE-Cad
C'
AC3
D
Cdc42-RNAi, pucE69
DE-Cad
D'
AC3
E
Cdc42-RNAi, Puc
DE-Cad
E'
AC3
F
Cdc42-RNAi, JNK-RNAi
DE-Cad
F'
AC3
G
P35
DE-Cad
G'
GFP
G''
MMP1
H
Cdc42-RNAi + P35
DE-Cad
H'
GFP
H''
MMP1
I
P35
DE-Cad
I'
GFP
I''
MMP1
J
Cdc42¹ + P35
DE-Cad
J'
GFP
J''
MMP1
K
Cdc42-RNAi + P35
DE-Cad
GFP
L
Cdc42-RNAi + P35 + Puc
DE-Cad
GFP
M
Cdc42-RNAi + P35 + JNK-RNAi
DE-Cad
GFP
N
P35 + Puc
DE-Cad
GFP
O
JNK
DE-Cad
O'
AC3
P
P35
DE-Cad
P'
GFP
Q
JNK + P35
DE-Cad
Q'
GFP

Figure 2

Figure 3. Rho1 and Rok promote compensatory proliferation downstream of Cdc42 depletion

Confocal immunofluorescent localization of DE-cadherin (A, A') and activated Caspase 3 (A, A'') in larval eye disc overexpressing Rho1 using *ey-gal4*. Confocal immunofluorescent localization of DE-cadherin (B-D) and activated Caspase 3 (B', C') in larval wing discs overexpressing Rho1 (B), Rho1 and Puc (C), and Rho1 and P35 (D) using *ptc-gal4*. Confocal immunofluorescent localization of DE-cadherin (E-G), activated Caspase 3 (E', F'), and β-galactosidase (G') in larval wing discs overexpressing Rho1 (E) and overexpressing Rho1 in a puc^{E69} heterzygous background (F, G) using *en-gal4*. Confocal immunofluorescent localization of DE-cadherin (H, I) and activated Caspase 3 (H') in larval wing discs expressing Rok-catalytic domain (Rok-CAT) alone (H) and with P35 (I) using *ptc-gal4*. Confocal immunofluorescent localization of DE-cadherin in larval wing discs expressing Cdc42-RNAi with P35 (J), Cdc42-RNAi with P35 in a $Rho1^{72F}$ heterozygous background (K), Cdc42-RNAi with P35 and Rok-RNAi (L), Rok-RNAi with P35 (M), and P35 in a $Rho1^{72F}$ heterozygous background (N) using *ptc-gal4*. Scale bars represent 100 μm.

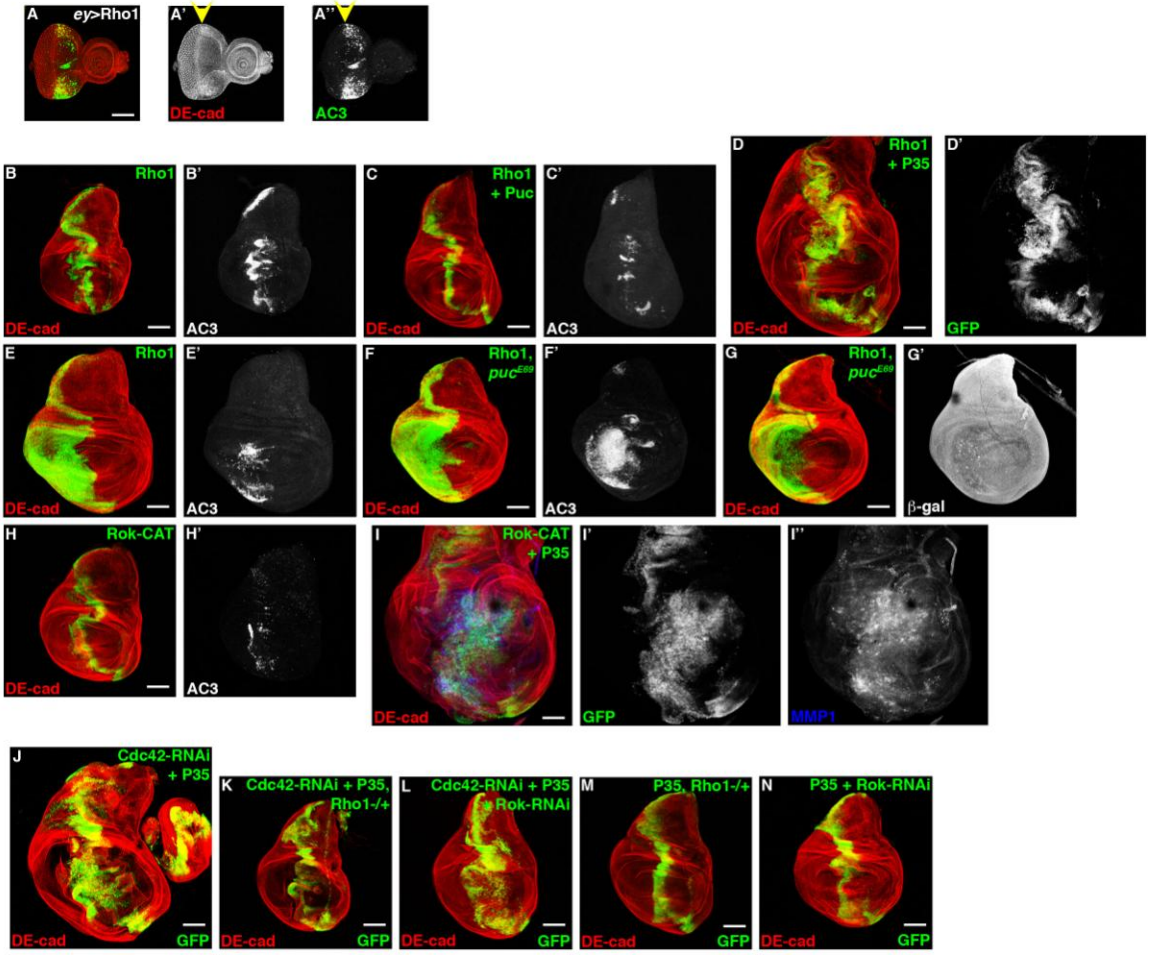
A ey>Rho1
A'
DE-cad
A''
AC3
B Rho1
DE-cad
B'
AC3
C Rho1 + Puc
DE-cad
C'
AC3
D Rho1 + P35
DE-cad
D'
GFP
E Rho1
DE-cad
E'
AC3
F Rho1, puc^E69
DE-cad
F'
AC3
G Rho1, puc^E69
DE-cad
G'
β-gal
H Rok-CAT
DE-cad
H'
AC3
I Rok-CAT + P35
DE-cad
I'
GFP
I''
MMP1
J Cdc42-RNAi + P35
DE-cad
GFP
K Cdc42-RNAi + P35, Rho1-/+
DE-cad
GFP
L Cdc42-RNAi + P35 + Rok-RNAi
DE-cad
GFP
M P35, Rho1-/+
DE-cad
GFP
N P35 + Rok-RNAi
DE-cad
GFP

Figure 3

Figure 4. Activation of Myosin, but not increased F-actin, induces compensatory proliferation downstream of Cdc42 depletion

Confocal immunofluorescent localization of DE-cadherin (A-C), activated Caspase 3 (A'') and MMP1 (B''), and phalloidin staining (C'') in GFP-labeled ssh^{1-11} clones alone (A) and ssh^{1-11} clones expressing P35 (B, C). Confocal immunofluorescent localization of DE-cadherin (D-G), activated Caspase 3 (D''-F''), and MMP1 (G'') in larval wing discs expressing constitutively active MLCK ($MLCK^{CA}$) alone (D), $MLCK^{CA}$ with Puc (E), $MLCK^{CA}$ in a heterozygous puc^{E69} background (F), and $MLCK^{CA}$ with P35 (G) using *ptc-gal4*. Confocal immunofluorescent localization of DE-cadherin (H, I) and activated Caspase 3 (H', I') in larval wing discs expressing Cdc42-RNAi alone (H) and Cdc42-RNAi in a Zip^{1} heterozygous background (I) using *en-gal4*. Confocal immunofluorescent localization of DE-cadherin (J, K) and phospho-MLC (J'') in larval wing discs expressing Cdc42-RNAi with P35 (J) and Cdc42-RNAi with P35 in a Zip^{1} heterozygous background (K) using *ptc-gal4*. Scale bars represent 100 μm.

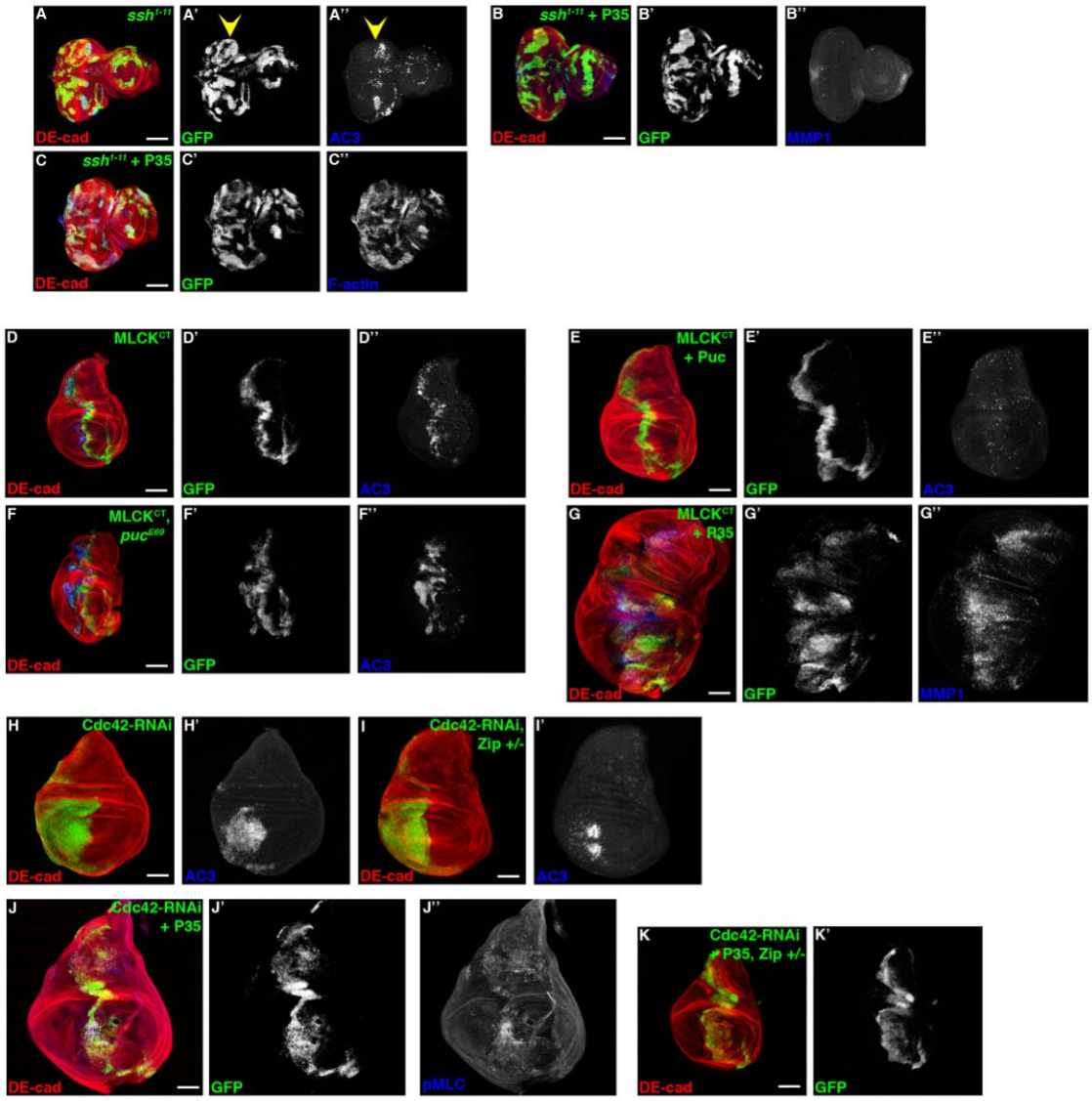
A
ssh^ts1
DE-cad
A'
GFP
A''
AC3
B
ssh^ts1 + P35
DE-cad
B'
GFP
B''
MMP1
C
ssh^ts1 + P35
DE-cad
C'
GFP
C''
F-actin
D
MLCK^CT
DE-cad
D'
GFP
D''
AC3
E
MLCK^CT + Puc
DE-cad
E'
GFP
E''
AC3
F
MLCK^CT, puc^E69
DE-cad
F'
GFP
F''
AC3
G
MLCK^CT + R35
DE-cad
G'
GFP
G''
MMP1
H
Cdc42-RNAi
DE-cad
H'
AC3
I
Cdc42-RNAi, Zip +/-
DE-cad
I'
AC3
J
Cdc42-RNAi + P35
DE-cad
J'
GFP
J''
pMLC
K
Cdc42-RNAi + P35, Zip +/-
DE-cad
K'
GFP

Figure 4

Figure 5. Par6 and aPKC negatively regulate apoptosis-induced compensatory proliferation

Confocal immunofluorescent localization of DE-cadherin (A-D), activated Caspase 3 (A'', B''), β-galactosidase (C''), and MMP1 (D'') in GFP-labeled control clones (A), $par6^{\Delta 226}$ clones alone (B), $par6^{\Delta 226}$ clones in a puc^{E69} heterozygous background (C), and $par6^{\Delta 226}$ clones expressing P35 (D). Adult eyes resulting from generation of control clones (E), clones expressing P35 (F), $par6^{\Delta 226}$ clones (G), and $par6^{\Delta 226}$ clones expressing P35 (H). Confocal immunofluorescent localization of DE-cadherin (I-K), activated Caspase 3 (I'', J''), and MMP1 (K'') in GFP-labeled control clones (I), $aPKC^{K06430}$ clones alone (J), and $aPKC^{K06430}$ clones expressing P35 (K). Adult eyes resulting from generation of control clones (L), $aPKC^{K06430}$ clones (M), and $aPKC^{K06430}$ clones expressing P35 (N). Confocal immunofluorescent localization of DE-cadherin (O-R, R'), activated Caspase 3 (O'-Q'), and MMP1 (R''') in larval wing discs expressing aPKC-RNAi alone (O, P), in a puc^{E69} heterozygous background (Q), and with P35 (R) using *ptc-gal4* (O, R) and *en-gal4* (P, Q). Scale bars represent 100 μm.

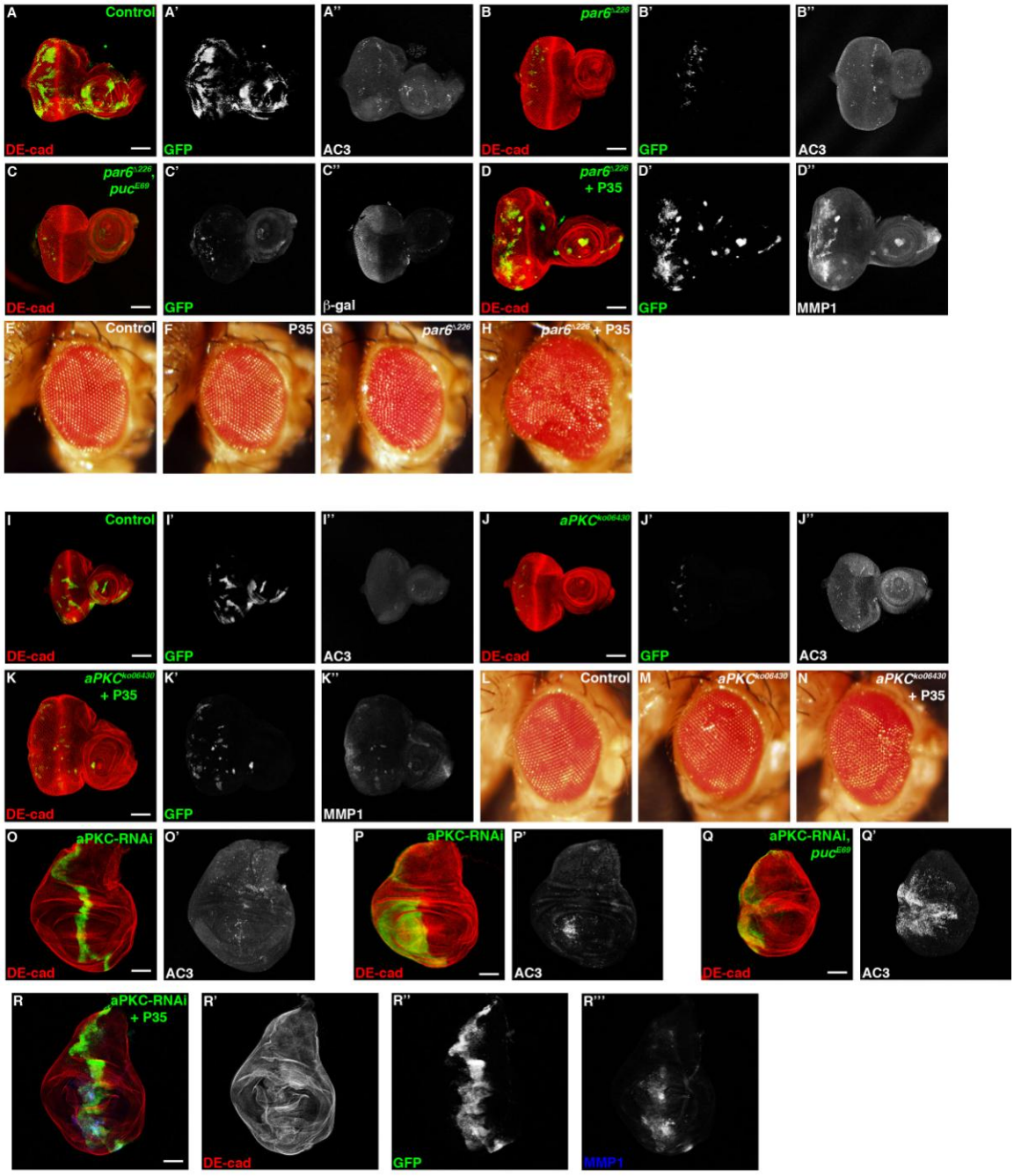
A Control
DE-cad
A'
GFP
A''
AC3
B par6Δ226
DE-cad
B'
GFP
B''
AC3
C par6Δ226, pucE69
DE-cad
C'
GFP
C''
β-gal
D par6Δ226 + P35
DE-cad
D'
GFP
D''
MMP1
E Control
F P35
G par6Δ226
H par6Δ226 + P35
I Control
DE-cad
I'
GFP
I''
AC3
J aPKCko06430
DE-cad
J'
GFP
J''
AC3
K aPKCko06430 + P35
DE-cad
K'
GFP
K''
MMP1
L Control
M aPKCko06430
N aPKCko06430 + P35
O aPKC-RNAi
DE-cad
O'
AC3
P aPKC-RNAi
DE-cad
P'
AC3
Q aPKC-RNAi, pucE69
DE-cad
Q'
AC3
R aPKC-RNAi + P35
R'
DE-cad
R''
GFP
R'''
MMP1

Figure 5

Figure 6. Cdc42 functions with Par6/aPKC to negatively regulate apoptosis-induced compensatory proliferation

Confocal immunofluorescent localization of DE-cadherin (A-D, A'-D'), Par6 (A, A'', B, B'') and aPKC (C, C'', D, D'') in control larval wing discs (A, C) and larval wing discs expressing Cdc42-RNAi (B, D) with *ptc-gal4*. Confocal immunofluorescent localization of DE-cadherin (E-J), activated Caspase 3 (E', F'), β-galactosidase (G'', H''), and MMP1 (I'', J'') in larval wing discs expressing either wild type Par6 ($Par6^{WT}$) (E, G, I) or Cdc42 binding mutant Par6 ($Par6^{ISAA}$) (F, H, J) alone (E, F), in a puc^{E69} heterozygous background (G, H), and with P35 (I, J) using *ptc-gal4* (E, F, I, J) and *en-gal4* (G, H). Confocal immunofluorescent localization of DE-cadherin (K, K', L, L'), and aPKC (K, K'', L, L'') in larval wing disc expressing wild type Par6 (K) and Cdc42 binding mutant Par6 (L) with *ptc-gal4*. Scale bars represent 10 μm (A-D, K, L) and 100 μm (E-J).

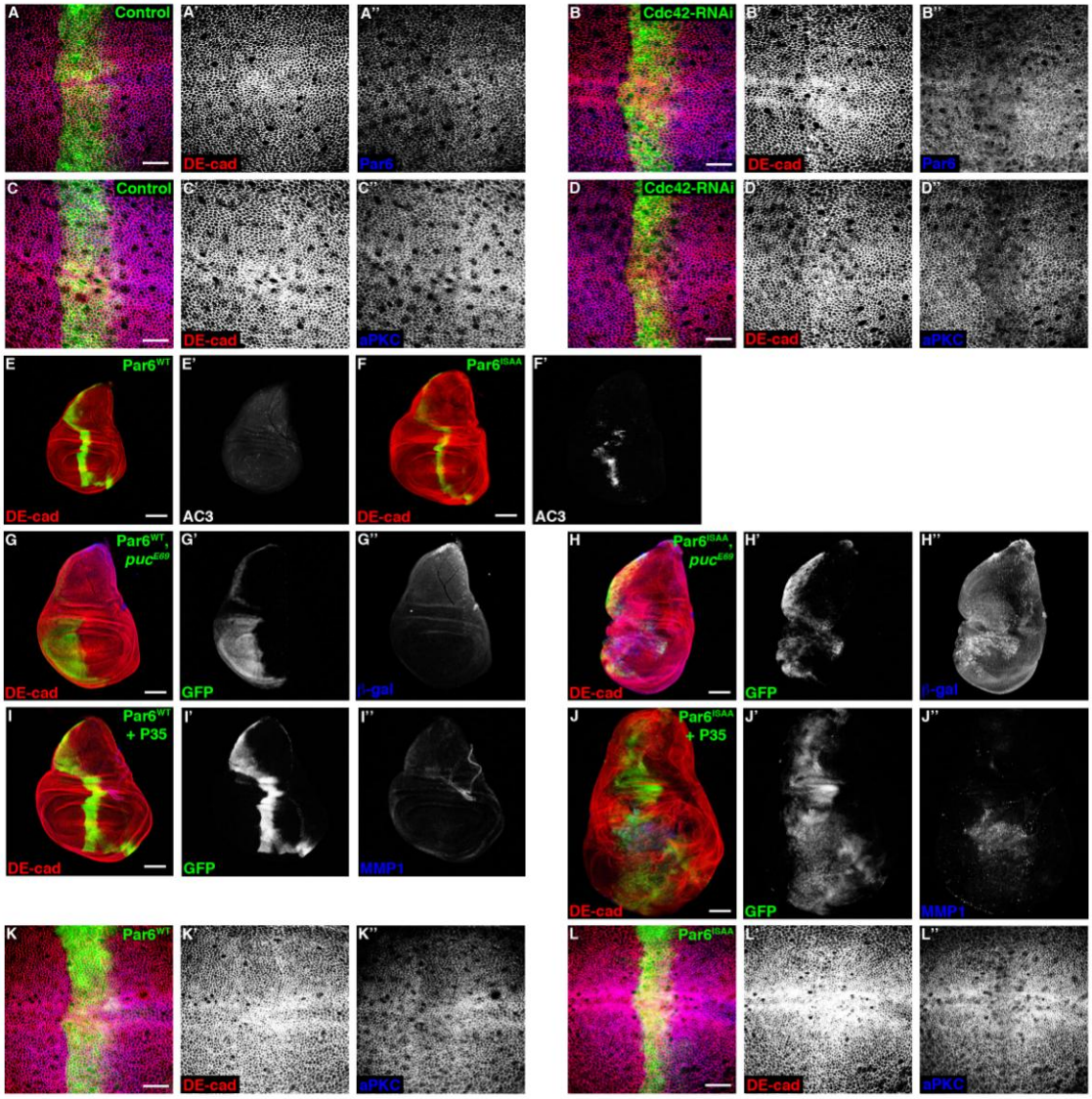
A Control
A'
A''
DE-cad
Par6
B Cdc42-RNAi
B'
B''
DE-cad
Par6
C Control
C'
C''
DE-cad
aPKC
D Cdc42-RNAi
D'
D''
DE-cad
aPKC
E Par6WT
E'
DE-cad
AC3
F Par6ISAA
F'
DE-cad
AC3
G Par6WT, pucE69
G'
G''
DE-cad
GFP
β-gal
H Par6ISAA, pucE69
H'
H''
DE-cad
GFP
β-gal
I Par6WT + P35
I'
I''
DE-cad
GFP
MMP1
J Par6ISAA + P35
J'
J''
DE-cad
GFP
MMP1
K Par6WT
K'
K''
DE-cad
aPKC
L Par6ISAA
L'
L''
DE-cad
aPKC

Figure 6

Figure 7. Cdc42 and aPKC depletion promotes compensatory proliferation following irradiation treatment

Confocal immunofluorescent localization of DE-cadherin (A-F) and phospho-Histone H3 (A'-F') in control larval wing discs (A, D), larval wing discs expressing Cdc42-RNAi (B, E), and larval wing discs expressing aPKC-RNAi (C, F) using *en-gal4* from larvae either 6 hours after 40 Gy of irradiation exposure (A-C) or unexposed (D-F). Confocal immunofluorescent localization of DE-cadherin (G-K) and aPKC (G'-K') in larval wing discs from larvae unexposed to irradition (G, I) or 20 minutes after exposure to 40 Gy of irradiation (H, J, K). Boxes (G', H') represent where images were expanded in I, J, K. Model for regulation of apoptosis-induced compensatory proliferation (L). Tissue damage or oncogenic mutations disrupting epithelial polarity or irradiation leads to mislocalization of Cdc42/Par6/aPKC from adherens junctions (green oval). This activates a Rho1/Rok/Myosin/JNK cascade, resulting in apoptosis and proliferation. Scale bars represent 100 μm (A-F) and 10 μm (G-K).

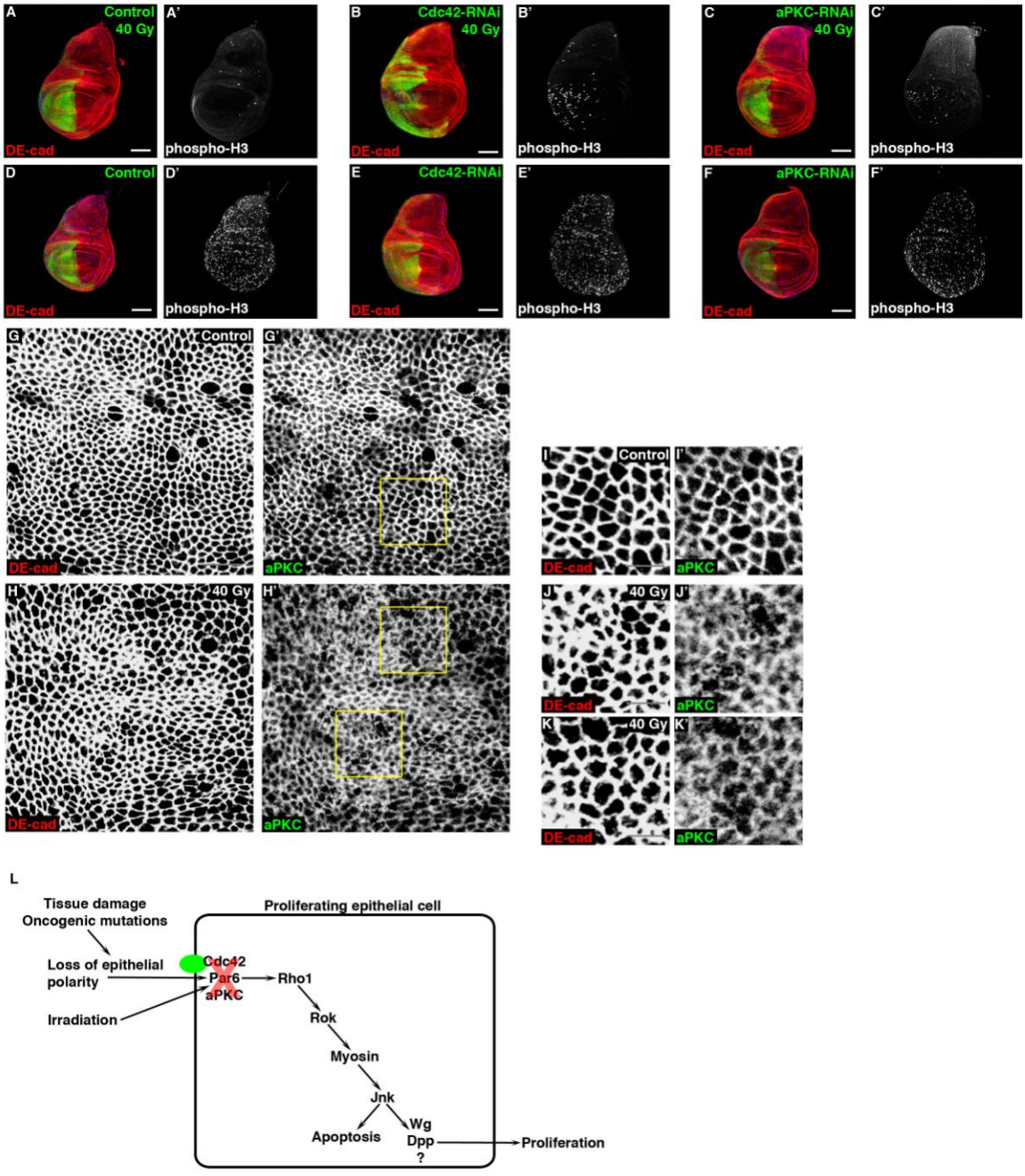
A
Control
40 Gy
DE-cad
A'
phospho-H3
B
Cdc42-RNAi
40 Gy
DE-cad
B'
phospho-H3
C
aPKC-RNAi
40 Gy
DE-cad
C'
phospho-H3
D
Control
DE-cad
D'
phospho-H3
E
Cdc42-RNAi
DE-cad
E'
phospho-H3
F
aPKC-RNAi
DE-cad
F'
phospho-H3
G
Control
DE-cad
G'
aPKC
H
40 Gy
DE-cad
H'
aPKC
I
Control
DE-cad
I'
aPKC
J
40 Gy
DE-cad
J'
aPKC
K
40 Gy
DE-cad
K'
aPKC
L
Tissue damage
Oncogenic mutations
Loss of epithelial
polarity
Irradiation
Proliferating epithelial cell
Cdc42
Par6
aPKC
Rho1
Rok
Myosin
Jnk
Apoptosis
Wg
Dpp
?
Proliferation

Figure 7

Figure 8. *GMR*>Cdc42-RNAi does not decrease the adult eye size or number of pupal eye epithelial cells, *ey*>Cdc42-RNAi, P35 promotes hyperproliferation of larval eye discs, *ey-gal4* is expressed throughout the larval eye disc, and Cdc42 depletion alters apical area of adjacent cells

Scanning electron micrograph of wild type adult eye (A) and adult eye resulting from *GMR*>Cdc42-RNAi (B). Confocal immunofluorescent localization of DE-cadherin in wild type pupal eye (C) and *GMR*>Cdc42-RNAi pupal eye (D) at 40 hours after puparium formation. Confocal immunofluorescent localization of DE-cadherin and phospho-Histone H3 in wild type larval eye disc (E), larval eye disc expressing P35 alone (F), and larval eye disc co-expressing Cdc42-RNAi and P35 (G) with *ey-gal4*. Confocal immunofluorescent localization of DE-cadherin (H) in larval eye disc expressing GFP (H, H') with *ey-gal4*. Confocal immunofluorescent localization of DE-cadherin in control larval wing disc (I) and larval wing disc expressing Cdc42-RNAi with *ptc-gal4* (J). Arrowhead identifies sharp posterior border of *ptc* expression domain. Scale bars represent 10 μm.

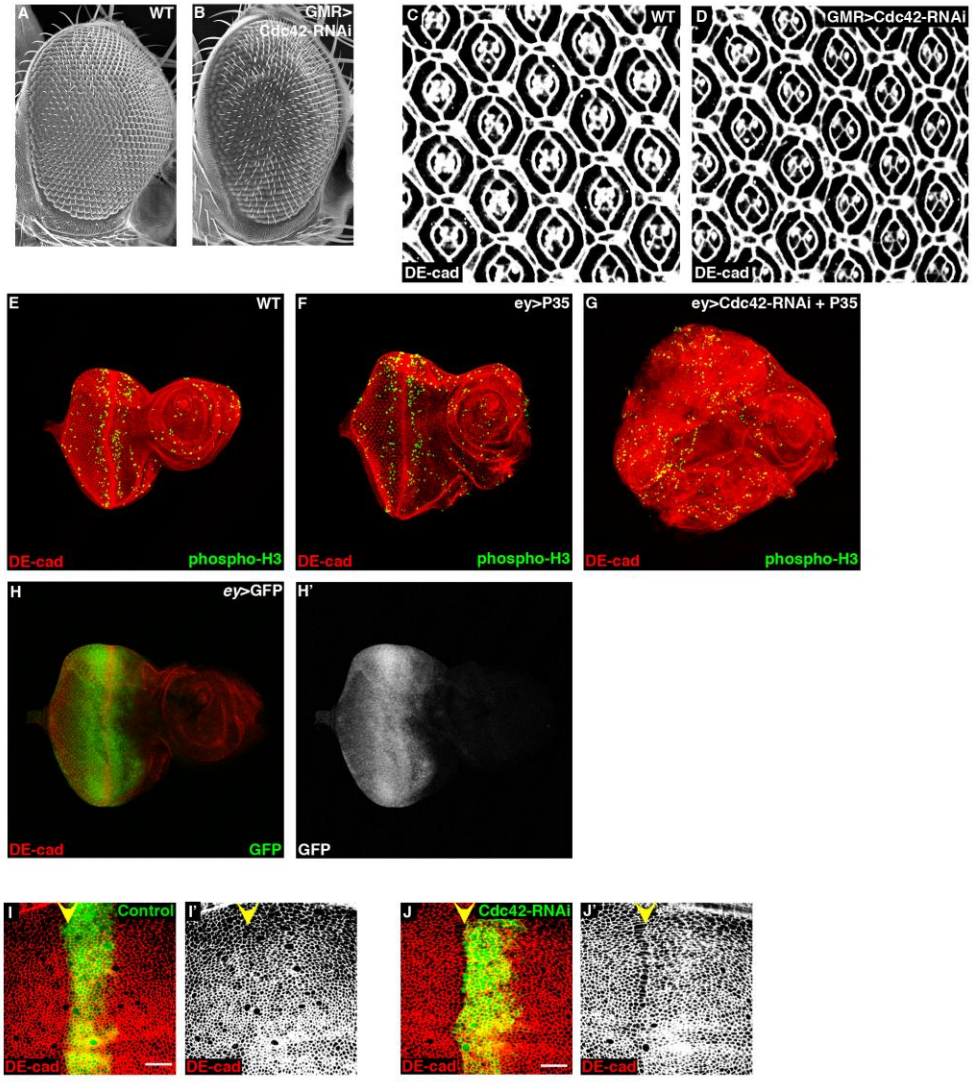
A
WT
B
GMR>
Cdc42-RNAi
C
WT
DE-cad
D
GMR>Cdc42-RNAi
DE-cad
E
WT
DE-cad
phospho-H3
F
ey>P35
DE-cad
phospho-H3
G
ey>Cdc42-RNAi + P35
DE-cad
phospho-H3
H
ey>GFP
DE-cad
GFP
H'
GFP
I
Control
DE-cad
I'
DE-cad
J
Cdc42-RNAi
DE-cad
J'
DE-cad

Figure 8

Figure 9. Blocking apoptosis in Cdc42 depleted cells induces Wg and Dpp expression

Confocal immunofluorescent localization of DE-cadherin (A, B) and Wingless (Wg) (A, A'', B, B'') in larval eye disc with *Cdc42*^{4} GFP-labeled clones expressing P35 (A) and larval wing disc co-expressing Cdc42-RNAi and P35 with *en-gal4* (B). Confocal immunofluorescent localization of DE-cadherin (C) and β-galactosidase (C, C'') in larval wing disc co-expressing Cdc42-RNAi and P35 with *ptc-gal4*. Confocal immunofluorescent localization of DE-cadherin (D-F) and phospho-MAD (pMAD) (D-F, D''-F'', D'''-F''') in larval wing discs expressing P35 alone (D) and P35 and Cdc42-RNAi (E, F) with *ptc-gal4* (D, E) and *en-gal4* (F). Scale bars represent 100 μm.

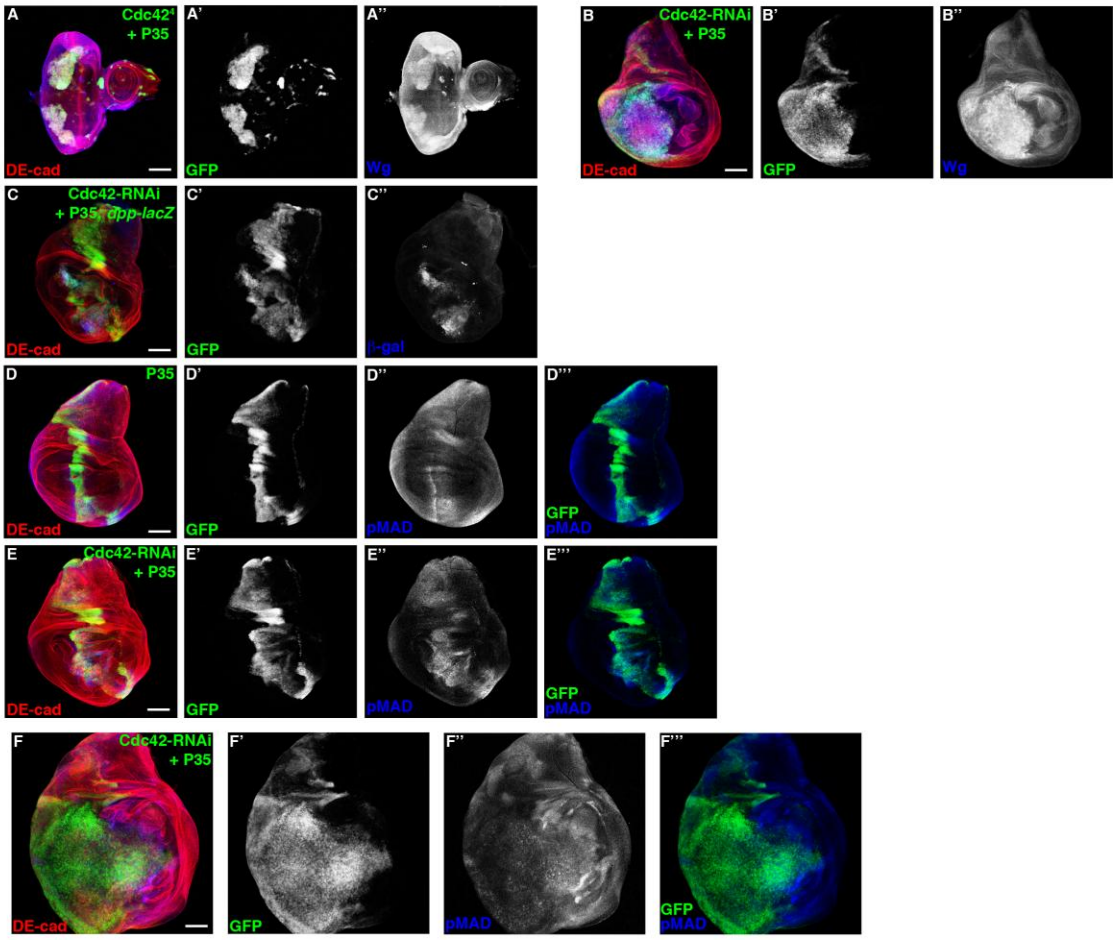
A
Cdc42[4]
+ P35
DE-cad
A'
GFP
A''
Wg
B
Cdc42-RNAi
+ P35
DE-cad
B'
GFP
B''
Wg
C
Cdc42-RNAi
+ P35 dpp-lacZ
DE-cad
C'
GFP
C''
β-gal
D
P35
DE-cad
D'
GFP
D''
pMAD
D'''
GFP
pMAD
E
Cdc42-RNAi
+ P35
DE-cad
E'
GFP
E''
pMAD
E'''
GFP
pMAD
F
Cdc42-RNAi
+ P35
DE-cad
F'
GFP
F''
pMAD
F'''
GFP
pMAD

Figure 9

Figure 10. Pak, WASP, and Bazooka do not regulate apoptosis-induced compensatory proliferation, and Cdc42 depletion does not affect Bazooka localization

Confocal immunofluorescent localization of DE-cadherin (A-C, A'-C') and activated Caspase 3 (A-C, A'''-C''') in larval eye discs with GFP-labeled clones of pak^{16} (A), wsp^{3} (B), and baz^{4} (C). Yellow arrowheads indentify morphogenetic furrow. Confocal immunofluorescent localization of DE-cadherin (D, D') and β-galactosidase (D, D''') in larval eye disc with GFP-labeled baz^{4} clones in a puc^{E69} heterozygous background (D). Confocal immunofluorescent localization of DE-cadherin (E, E') and Bazooka (E, E'') in larval wing disc expressing Cdc42-RNAi with *ptc-gal4* (E). Scale bars represent 100 μm (A-D) and 10 μm (E).

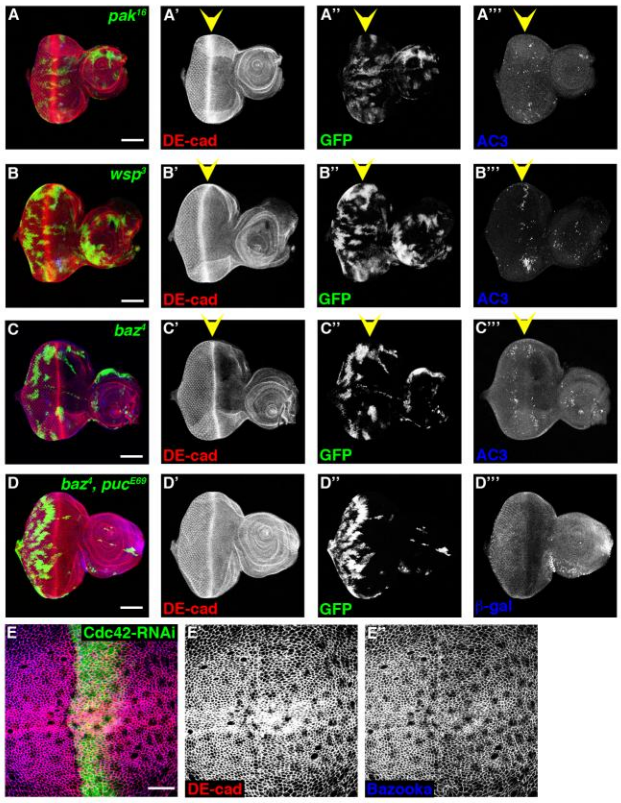
A
pak10
A'
DE-cad
A''
GFP
A'''
AC3
B
wsp3
B'
DE-cad
B''
GFP
B'''
AC3
C
baz1
C'
DE-cad
C''
GFP
C'''
AC3
D
baz1, pucE69
D'
DE-cad
D''
GFP
D'''
β-gal
E
Cdc42-RNAi
E'
DE-cad
E''
Bazooka

Figure 10

Figure 11. aPKC-RNAi effectively depletes aPKC protein levels

Confocal immunofluorescent localization of DE-cadherin (A, A', B, B') and aPKC (A, A''', B, B''') in larval wing discs expressing aPKC-RNAi with *ptc-gal4* (A, B). Scale bars represent 100 μm (A) and 20 μm (B).

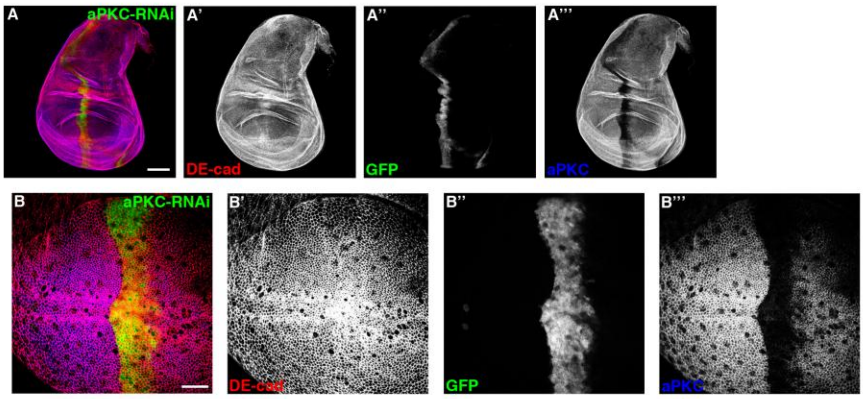

Figure 11

Figure 12. Discs large and Scribble depletion induces JNK-dependent apoptosis, but Discs large, Scribble, and Crumbs do not regulate apoptosis-induced compensatory proliferation

Confocal immunofluorescent localization of DE-cadherin (A, A', B, B'), Discs large (Dlg) (A, A''), and Scribble (Scrib) (B, B'') in larval wing discs expressing Dlg-RNAi (A) and Scrib-RNAi (B) with *ptc-gal4*. Confocal immunofluorescent localization of DE-cadherin (C-F), activated Caspase 3 (C', D'), and β-galactosidase (E') in larval wing discs co-expressing Dlg-RNAi and Scrib-RNAi alone (C), with Puc (D), in a puc^{E69} heterozygous backgroun (E), and with P35 (F) using *ptc-gal4* (C, D, F) and *en-gal4* (E). Confocal immunofluorescent localization of DE-cadherin (G, G', H, I), Crumbs (Crb) (G'''), activated Caspase 3 (H'), and β-galactosidase (I') in larval wing discs expressing Crb-RNAi alone using *ptc-gal4* (G, H) and in a puc^{E69} heterzygous background using *en-gal4* (I). Scale bars represent 100 μm (A-F, H, I) and 10 μm (G).

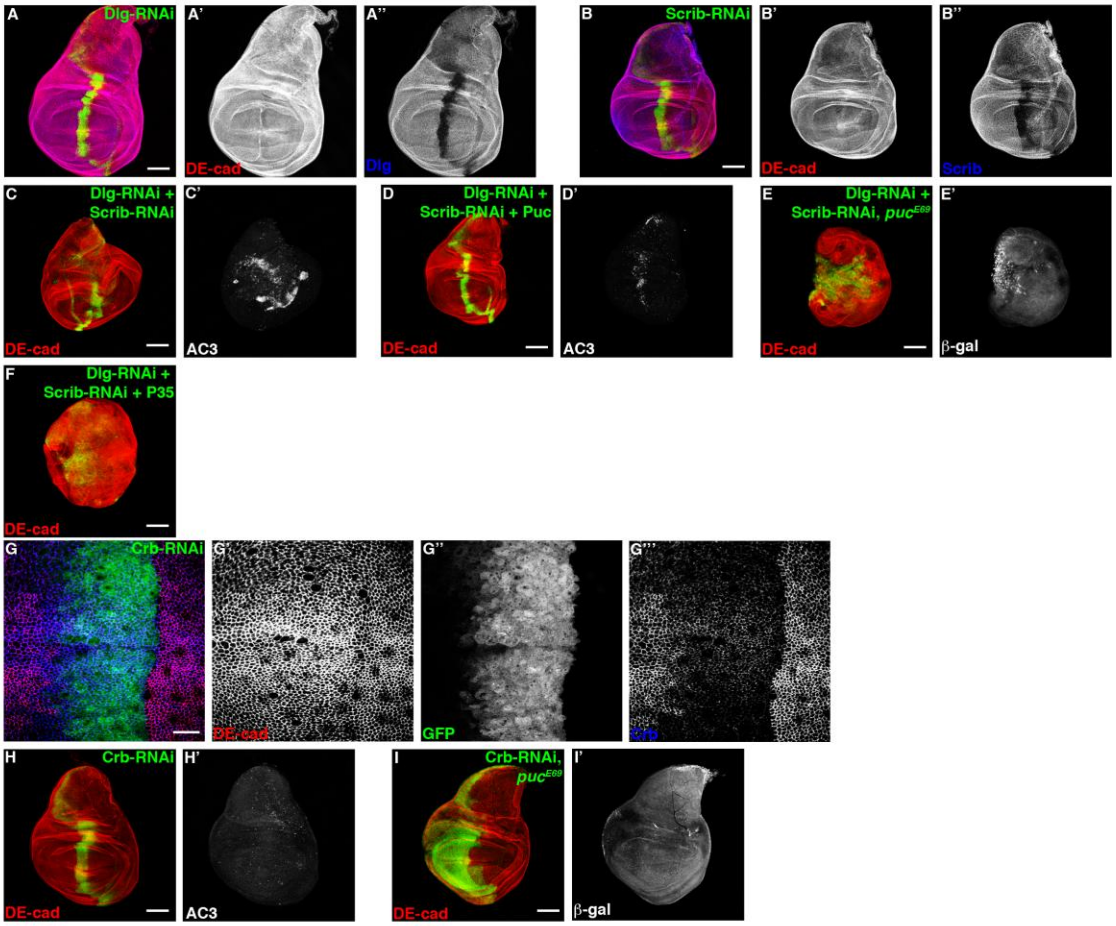
A
Dlg-RNAi
A'
DE-cad
A''
Dlg
B
Scrib-RNAi
B'
DE-cad
B''
Scrib
C
Dlg-RNAi +
Scrib-RNAi
DE-cad
C'
AC3
D
Dlg-RNAi +
Scrib-RNAi + Puc
DE-cad
D'
AC3
E
Dlg-RNAi +
Scrib-RNAi, puc^E69
DE-cad
E'
β-gal
F
Dlg-RNAi +
Scrib-RNAi + P35
DE-cad
G
Crb-RNAi
G'
DE-cad
G''
GFP
G'''
GFP
H
Crb-RNAi
DE-cad
H'
AC3
I
Crb-RNAi,
puc^E69
DE-cad
I'
β-gal

Figure 12

Figure 13. Blocking apoptosis in Cdc42 depleted cells promotes epithelial remodeling, independent of hyperproliferation

Confocal immunofluorescent localization of DE-cadherin (A-F, A'-F') and phalloidin staining (A-F, A'''-F''') in larval wing discs co-expressing Cdc42-RNAi and P35 alone (A, B), with Puc (C, D), and in a *Zip*^{1} heterozygous background (E, F) with *ptc-gal4*. Boxes (A, C, E) identify where higher magnification images (B, D, F) where taken. Scale bars represent 100 μm (A, C, E) and 20 μm (B, D, F).

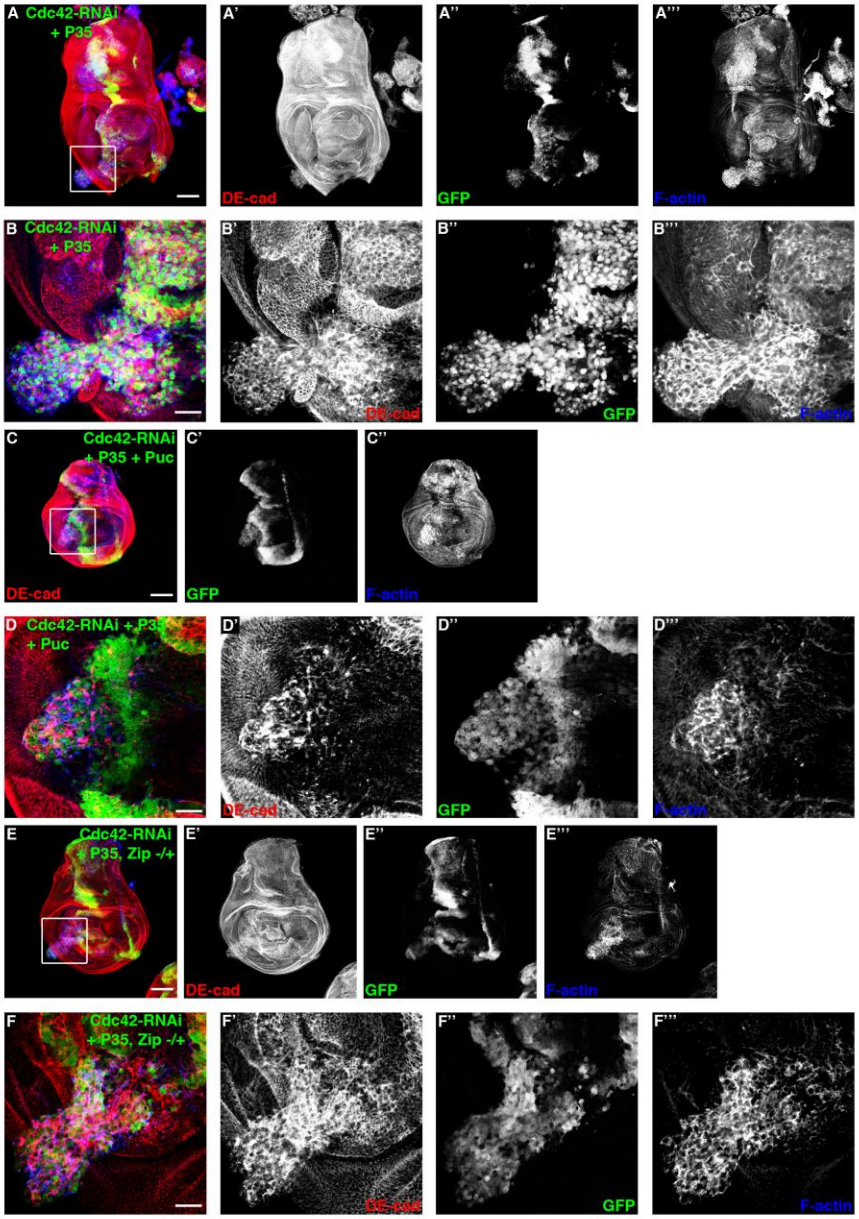
A Cdc42-RNAi + P35
A'
DE-cad
A''
GFP
A'''
F-actin
B Cdc42-RNAi + P35
B'
DE-cad
B''
GFP
B'''
F-actin
C Cdc42-RNAi + P35 + Puc
DE-cad
C'
GFP
C''
F-actin
D Cdc42-RNAi + P35 + Puc
D'
DE-cad
D''
GFP
D'''
F-actin
E Cdc42-RNAi + P35, Zip -/+
E'
DE-cad
E''
GFP
E'''
F-actin
F Cdc42-RNAi + P35, Zip -/+
F'
DE-cad
F''
GFP
F'''
F-actin

Figure 13

Table

Table 1. Larval wing disc area quantification

Genotype	Wing disc area mean	Std dev	N	P
***ptc*>P35**	222477	47004	11	0.00050
***ptc*>Cdc42-RNAi, P35**	303210	91518	35	N/A
***ptc*>Cdc42-RNAi, P35, Puc**	212704	45805	6	0.0024
***ptc*>Cdc42-RNAi, P35, JNK-RNAi**	177726	30046	11	0.000000012
***ptc*>Cdc42-RNAi, P35, *Rho1*^{72F} +/-**	237669	55241	10	0.0096
***ptc*>Cdc42-RNAi, P35, *Zip*^{1} +/-**	176040	45860	9	0.0000035

Quantification of larval wing disc area. Larval wing disc areas were measured by outlining wing discs and determining the number of pixels within the outline. Quantifications were performed using ImageJ v1.38. P-values were calculated using an unpaired, two-sided Student's t-test against *ptc*>Cdc42-RNAi, P35. N/A: not applicable.

CHAPTER 5

Conclusion

Roles of Rho1 and Cdc42 during epithelial morphogenesis

The genetic tractability of *Drosophila* has allowed us to isolate and explore three major functions for Rho GTPases Rho1 and Cdc42 in larval and pupal epithelial cells. First, Rho1 functions in AJ maintenance of post-mitotic pupal PECs by inhibiting E-cadherin endocytosis in a Cdc42/Par6-dependent manner. Whether Rho1 can directly function in E-cadherin endocytosis or whether Rho1 indirectly regulates E-cadherin endocytosis through inhibition of Cdc42/Par6 remains to be determined. Also, whether Rho1 specifically regulates E-cadherin endocytosis, or, more likely, regulates endocytosis in general is an unanswered question. Furthermore, as opposed to the E-cadherin containing AJs of PECs, the N-cadherin containing AJs of the cone cells do not require Rho1 for maintenance. How Rho1 regulates E-cadherin containing AJs differently from N-cadherin containing AJs is an important question for future studies.

Second, Rho1 is necessary for sustaining apical cell tension in pupal PECs by activating Rok and myosin, independent of its AJ regulation. Cdc42 can negatively regulate Rho1 activity at AJs and inhibit apical cell tension, which is mediated through Cdc42's interaction with Par6 and aPKC and subsequent localization of the Cdc42/Par6/aPKC complex to AJs. Since the Cdc42/Par6/aPKC complex also inhibited apical cell tension in *Drosophila* pupal notum epithelial cells, it would be interesting to determine if this was also a result of increased Rho1 activity at AJs.

Third, in proliferating larval eye and wing epithelial cells, Cdc42 negatively regulates apoptosis-induced compensatory proliferation in a JNK-dependent manner, also through its interaction with Par6/aPKC at AJs. Like in the pupal PECs, the

Cdc42/Par6/aPKC complex inhibits Rho1, which promotes apoptosis-induced compensatory proliferation by activating a Rok/myosin/JNK cascade, independent of promoting F-actin assembly. While Cdc42 and aPKC negatively regulates apoptosis-induced compensatory proliferation as a result of irradiation, whether this complex also regulates this phenomenon in response to other stresses (e.g. heat shock, injury) remains to be determined. Also, whether similar events occur in epithelial cancer states where polarity is disrupted and apoptosis is misregulated should be addressed.

Mediation of Rho GTPase crosstalk by GTPase regulators

A dominant theme of all three studies presented here is the opposition between the functions of Rho1 and Cdc42. In addition to the unresolved points raised above, an outstanding question from all three studies is how the opposing crosstalk between Rho1 and Cdc42 in epithelial morphogenesis is mediated. One possibility is that Rho1 and Cdc42 inhibit each other's activities by direct association; although, since no direct associations between any Rho GTPase family member has been reported, this seems unlikely.

Another possibility for how Rho1 and Cdc42 crosstalk with one another is through the upstream regulators of GTPase activity, RhoGAPs, RhoGEFs, and RhoGDIs. In other examples of crosstalk between Rho GTPase family members, these regulators of GTPase activity are often involved. For example, activated, GTP-bound Rac1 can bind directly to p190RhoGAP and localize it to the membrane where it inhibits RhoA activity (Wildenberg et al., 2006). Also, RhoG can form a ternary complex with Elmo and the

Rac1 GEF DOCK180, resulting in increased Rac1 activation (Katoh and Negishi, 2003). Furthermore, Pak1, a Cdc42 effector, can directly phosphorylate RhoGDI, leading to dissociation of Rac1-RhoGDI complexes and activation of Rac1 (DerMardirossian et al., 2004). Therefore, possibly similar interactions with one or multiple RhoGAPs, RhoGEFs, and/or RhoGDI mediate the negative crosstalk between Rho1 and Cdc42 in *Drosophila*.

In an attempt to address this possibility, we used two different approaches. In the first and more directed approach, based on reports in mammalian systems that implicated two specific GTPase regulators in crosstalk, RhoGDI and p190RhoGAP (DerMardirossian et al., 2004; Wildenberg et al., 2006), we determined what function *Drosophila* RhoGDI and p190RhoGAP had in epithelia. As opposed to three RhoGDI paralogs and two p190RhoGAP paralogs in mammals, *Drosophila* have only one predicted ortholog for each protein. Because no mutations in *Drosophila* RhoGDI or p190RhoGAP have been reported, we generated null alleles of RhoGDI and p190RhoGAP by creating deletions that remove the entire coding region of each gene using recombination between Exelixis FRT insertions flanking the coding regions. Each deletion was confirmed by genomic PCR, demonstrating with multiple primer sets that the respective coding regions were deleted and the deletion break points were as predicted based upon FRT insertion position. Surprisingly, both the RhoGDI and p190RhoGAP deletions were homozygous viable with no gross abnormalities, suggesting that RhoGDI and p190RhoGAP do not have significant functions in *Drosophila* development.

Demonstrating that *Drosophila* null for RhoGDI or p190RhoGAP develop normally suggests that they are not major regulators of Rho GTPase function in *Drosophila* since directly modulating Rho1 or Cdc42 results in major phenotypes during development. However, this does not completely eliminate the possibility that RhoGDI and p190RhoGAP may function in Rho1 and Cdc42 crosstalk to some extent. To more specifically address the question of whether RhoGDI or p190RhoGAP function in Rho1 and Cdc42 crosstalk, we determined whether elimination of RhoGDI or p190RhoGAP modulated phenotypes from expression of Rho1-RNAi or Cdc42-RNAi in the *Drosophila* eye. Our data suggests that Rho1-RNAi expression in pupal eye PECs disrupts AJs as a result of increased Cdc42 activity, and Cdc42-RNAi expression in pupal eye PECs causes apical constriction as a result of increased Rho1 activity. Therefore, if RhoGDI or p190RhoGAP were mediating this inhibitory crosstalk between Rho1 and Cdc42 causing increased activation of Rho1 when Cdc42 was depleted or activation of Cdc42 when Rho1 was depleted, then eliminating RhoGDI or p190RhoGAP should rescue these eye phenotypes. However, when Rho1-RNAi or Cdc42-RNAi were expressed in the *Drosophila* eye in RhoGDI or p190RhoGAP null backgrounds, no significant modifications of the adult eye phenotype were seen, suggesting that RhoGDI and p190RhoGAP do not contribute significantly to the opposing crosstalk between Rho1 and Cdc42.

While this first approach to determine if Rho GTPases regulators were mediators of Rho1 and Cdc42 crosstalk specifically ruled out RhoGDI and p190RhoGAP, our second approach was broad. Mammalian genomes are predicted to encode 72 RhoGAPs

and 83 RhoGEFs (Sanz-Moreno et al., 2008), while *Drosophila* are predicted to have 21 RhoGAPs and 24 RhoGEFs. We initiated a comprehensive screen to specifically query whether any of these 45 Rho GTPase regulators are involved in Rho1-Cdc42 crosstalk. We co-expressed two independent sets of RNAi's to individual RhoGAPs or RhoGEFs with either Rho1-RNAi or Cdc42-RNAi in the *Drosophila* eye, and determined whether these RhoGAP or RhoGEF RNAi's modulated the adult eye phenotypes from Rho1-RNAi or Cdc42-RNAi expression. While no RhoGEF or RhoGAP RNAi dramatically modulated the Rho1-RNAi or Cdc42-RNAi phenotypes, several slightly or moderately modified the phenotypes. While further work is needed to determine how depletion of these RhoGEFs and RhoGAPs modified the Rho1-RNAi and Cdc42-RNAi phenotypes, these data highlight the possibility that perhaps several Rho GTPase regulators are involved in crosstalk between Rho1 and Cdc42.

Another possibility for how Rho1 and Cdc42 have opposing functions in *Drosophila* epithelia also involves regulators of Rho GTPase activity but in a more passive manner than that suggested above where RhoGAP, RhoGEF, or RhoGDI function was directly affected downstream of one Rho protein, which then regulated the activity of another Rho protein. The main experimental approach we used in our studies was loss-of-function analysis, where Rho1 or Cdc42 protein was depleted either by genetic mutation or by RNAi expression. Because Rho proteins often share common upstream GTPase regulators, perhaps these manipulations depleting a Rho protein offset a tight balance of GTPase regulation by upstream RhoGAPs, RhoGEFs, and RhoGDI. For example, if a single RhoGEF normally activates both Rho1 and Cdc42 in an

epithelial cell and Cdc42 is depleted from that cell, then the fraction of the RhoGEF that normally activates Cdc42 can now activate Rho1, causing increased Rho1 activation. Likewise, if Rho1 is depleted from that cell, then the RhoGEF can activate Cdc42 more. While the RhoGEF and RhoGAP RNAi screen described above would identify candidate RhoGEFs and RhoGAPs for this model, experiments to distinguish between this latter "passive" model and the former "active" model would be difficult in an *in vivo* system. Most likely, biochemical studies facilitated in an *in vitro* tissue culture system would be necessary.

Potential endocytic regulation of Rho GTPase crosstalk

Yet another possibility for how Rho1 and Cdc42 crosstalk with one another is that they do so independently of upstream Rho GTPase regulators, but rather through downstream functions within the cell. With Rho proteins having such pleiotropic effects within cells, many hypothetical situations could be imagined where the downstream functions of one Rho protein could indirectly affect the activity of another Rho protein. However, one more likely possibility stems from a recent report identifying Rab5-mediated endocytosis as a means to regulate and localize Rac activity in migrating cells (Palamidessi et al., 2008). This study demonstrated that Rac and the RacGEF Tiam1 are recruited to Rab5-containing early endosomes where Rac is activated. Subsequent recycling of active Rac to the plasma membrane results in spatial restriction of Rac1 activity, which is critical for directed actin polymerization and cell migration. Relating this model to our studies, others and we have suggested that Cdc42 promotes Rab5-

mediated endocytosis (Georgiou et al., 2008; Leibfried et al., 2008). In addition, our data suggests that Cdc42 negatively regulates Rho1 activity at AJs and that Rho1 also localizes to Rab5-containing endosomes. Perhaps Rho1, like Rac, can be activated in Rab5-containing endosomes, and when Cdc42 promotes endocytosis of Rab5-containing endosomes, it removes Rho1 from AJs where active Rho1 normally interacts with effector proteins. Therefore, upon Cdc42 depletion, more active Rho1 localizes to AJs, resulting in increased interactions of Rho1 with effector proteins. Again, an *in vitro* system more amenable to biochemistry would be advantageous to test this model.

Implications for Rho GTPase and cell biology

Taken together, the three studies presented here have several implications for Rho GTPase biology and cell biology in general. First, a technical point regarding studies of Rho GTPases, which is also relevant to studies with other enzymes, is that the use of dominant negative proteins should not be used as a reliable method to determine Rho protein function. With the widespread availability of RNA-interference techniques, directed depletion of a specific Rho GTPase should replace use of dominant negative proteins in ascertaining the function of a specific Rho protein. Even though this point is beginning to be recognized, the use of dominant negative Rho proteins is still common in the literature.

Another implication raised here is the possible underappreciated interconnectivity of Rho GTPase regulation. In mammals, about 155 RhoGAPs and RhoGEFs regulate 16 proteins with Rho GTPase activity. Promiscuity in affinities of RhoGAPs and RhoGEFs

for Rho GTPases, coupled with shared effectors downstream of active Rho GTPases, creates an extensive number of possible signaling pathways. More importantly, this also suggests that modulating one specific Rho protein will likely affect the activity of other Rho proteins due to changes in availability of RhoGAPs, RhoGEFs, and effectors that normally bind to the Rho protein in question. In mammalian systems, the effect on the activities of other Rho proteins may be subtle and difficult to recognize since changes can be dispersed across multiple Rho proteins. In *Drosophila*, with only 5 Rho proteins, the possible change in activities of other Rho proteins upon depletion of a specific Rho protein is much greater. This is especially true in the pupal eye PECs, where depletion of the three Rac proteins, Rac1, Rac2, and Mtl, had no significant effect, leaving only two Rho GTPases with functional activity in these cells, Rho1 and Cdc42. Perhaps because of this unique situation in the *Drosophila* pupal eye PECs where only two Rho GTPases are functional, we were able to uncover this opposing crosstalk between Rho1 and Cdc42. In most other cell systems, with more than two Rho GTPases functional, possibly the effects on RhoGAPs, RhoGEFS, and RhoGDIs will be more "diluted" and difficult to detect functionally or biochemically. Regardless, these studies highlight the possibility that experiments designed to affect the activity of one Rho GTPase will likely affect the activities of other Rho GTPases.

Extensions into cancer biology

Rho GTPases have been implicated in several human disease states, including vascular hypertension and cancer. While our results have more direct relevance to Rho

GTPase function in developmental and cell biology, extrapolations can be made to human disease states, especially carcinomas. The post-mitotic pupal eye is unique from other developmental and tissue culture systems, which are most often proliferating, and in this way is more similar to human epithelia such as in the intestine and skin, where differentiated epithelial cells are also post-mitotic. In the pupal eye, we found that Rho1 and Cdc42 are critical for both AJ maintenance and apical cell tension. Both of these processes are often prominently misregulated during carcinoma development (D'Souza-Schorey, 2005; Olson and Sahai, 2009), especially as carcinoma cells undergo epithelial-to-mesenchymal transition and begin to metastasize (Klymkowsky and Savagner, 2009).

In addition, our studies with Rho1 and Cdc42 in the proliferating larval epithelial cells also have parallels to carcinoma development. A requirement for carcinoma cell survival is to block apoptosis (Hanahan and Weinberg, 2000), similar to our experiments where cells express P35. Demonstrating that Cdc42 and Rho1 can regulate proliferation of epithelial cells specifically when apoptosis is blocked suggests that they may also play a role in the proliferation of carcinoma cells where apoptosis is misregulated. To more directly address the role of Rho and Cdc42 in carcinoma development, conditional knockouts of Cdc42 and Rho in the context of carcinoma mouse models would be useful.

References

Adams, C.L., Y.T. Chen, S.J. Smith, and W.J. Nelson. 1998. Mechanisms of epithelial cell-cell adhesion and cell compaction revealed by high-resolution tracking of E-cadherin-green fluorescent protein. *J Cell Biol*. 142:1105-19.

Aranda, V., M.E. Nolan, and S.K. Muthuswamy. 2008. Par complex in cancer: a regulator of normal cell polarity joins the dark side. *Oncogene*. 27:6878-87.

Assemat, E., E. Bazellieres, E. Pallesi-Pocachard, A. Le Bivic, and D. Massey-Harroche. 2008. Polarity complex proteins. *Biochim Biophys Acta*. 1778:614-30.

Atwood, S.X., C. Chabu, R.R. Penkert, C.Q. Doe, and K.E. Prehoda. 2007. Cdc42 acts downstream of Bazooka to regulate neuroblast polarity through Par-6 aPKC. *J Cell Sci*. 120:3200-6.

Bao, S., and R. Cagan. 2005. Preferential adhesion mediated by Hibris and Roughest regulates morphogenesis and patterning in the Drosophila eye. *Dev Cell*. 8:925-35.

Bao, S., and R. Cagan. 2006. Fast cloning inverted repeats for RNA interference. *RNA*. 12:2020-4.

Bilder, D. 2004. Epithelial polarity and proliferation control: links from the Drosophila neoplastic tumor suppressors. *Genes Dev*. 18:1909-25.

Bishop, A.L., and A. Hall. 2000. Rho GTPases and their effector proteins. *Biochem J*. 348 Pt 2:241-55.

Bos, J.L., H. Rehmann, and A. Wittinghofer. 2007. GEFs and GAPs: critical elements in the control of small G proteins. *Cell*. 129:865-77.

Braga, V.M., L.M. Machesky, A. Hall, and N.A. Hotchin. 1997. The small GTPases Rho and Rac are required for the establishment of cadherin-dependent cell-cell contacts. *J Cell Biol*. 137:1421-31.

Bruinsma, S.P., R.L. Cagan, and T.J. Baranski. 2007. Chimaerin and Rac regulate cell number, adherens junctions, and ERK MAP kinase signaling in the Drosophila eye. *Proc Natl Acad Sci U S A*. 104:7098-103.

Bryant, D.M., and J.L. Stow. 2004. The ins and outs of E-cadherin trafficking. *Trends Cell Biol*. 14:427-34.

Burridge, K., and K. Wennerberg. 2004. Rho and Rac take center stage. *Cell*. 116:167-79.

Cagan, R.L., and D.F. Ready. 1989. The emergence of order in the Drosophila pupal retina. *Dev Biol*. 136:346-62.

Capaldo, C.T., and I.G. Macara. 2007. Depletion of E-cadherin disrupts establishment but not maintenance of cell junctions in Madin-Darby canine kidney epithelial cells. *Mol Biol Cell*. 18:189-200.

Carramusa, L., C. Ballestrem, Y. Zilberman, and A.D. Bershadsky. 2007. Mammalian diaphanous-related formin Dia1 controls the organization of E-cadherin-mediated cell-cell junctions. *J Cell Sci*. 120:3870-82.

Carthew, R.W. 2005. Adhesion proteins and the control of cell shape. *Curr Opin Genet Dev*. 15:358-63.

Chen, J., D. Godt, K. Gunsalus, I. Kiss, M. Goldberg, and F.A. Laski. 2001. Cofilin/ADF is required for cell motility during Drosophila ovary development and oogenesis. *Nat Cell Biol*. 3:204-9.

Clark, K., M. Langeslag, C.G. Figdor, and F.N. van Leeuwen. 2007. Myosin II and mechanotransduction: a balancing act. *Trends Cell Biol*. 17:178-86.

Classen, A.K., K.I. Anderson, E. Marois, and S. Eaton. 2005. Hexagonal packing of Drosophila wing epithelial cells by the planar cell polarity pathway. *Dev Cell*. 9:805-17.

Conti, M.A., and R.S. Adelstein. 2008. Nonmuscle myosin II moves in new directions. *J Cell Sci*. 121:11-8.

Corrigall, D., R.F. Walther, L. Rodriguez, P. Fichelson, and F. Pichaud. 2007. Hedgehog signaling is a principal inducer of Myosin-II-driven cell ingression in Drosophila epithelia. *Dev Cell*. 13:730-42.

Coso, O.A., M. Chiariello, J.C. Yu, H. Teramoto, P. Crespo, N. Xu, T. Miki, and J.S. Gutkind. 1995. The small GTP-binding proteins Rac1 and Cdc42 regulate the activity of the JNK/SAPK signaling pathway. *Cell*. 81:1137-46.

D'Souza-Schorey, C. 2005. Disassembling adherens junctions: breaking up is hard to do. *Trends Cell Biol*. 15:19-26.

DerMardirossian, C., A. Schnelzer, and G.M. Bokoch. 2004. Phosphorylation of RhoGDI by Pak1 mediates dissociation of Rac GTPase. *Mol Cell*. 15:117-27.

Diaz-Meco, M.T., M.M. Municio, S. Frutos, P. Sanchez, J. Lozano, L. Sanz, and J. Moscat. 1996. The product of par-4, a gene induced during apoptosis, interacts selectively with the atypical isoforms of protein kinase C. *Cell*. 86:777-86.

Dow, L.E., and P.O. Humbert. 2007. Polarity regulators and the control of epithelial architecture, cell migration, and tumorigenesis. *Int Rev Cytol*. 262:253-302.

Eaton, B.A., and G.W. Davis. 2005. LIM Kinase1 controls synaptic stability downstream of the type II BMP receptor. *Neuron*. 47:695-708.

Etienne-Manneville, S. 2008. Polarity proteins in migration and invasion. *Oncogene*. 27:6970-80.

Fan, Y., and A. Bergmann. 2008a. Apoptosis-induced compensatory proliferation. The Cell is dead. Long live the Cell! *Trends Cell Biol*. 18:467-73.

Fan, Y., and A. Bergmann. 2008b. Distinct mechanisms of apoptosis-induced compensatory proliferation in proliferating and differentiating tissues in the Drosophila eye. *Dev Cell*. 14:399-410.

Furuse, M., and S. Tsukita. 2006. Claudins in occluding junctions of humans and flies. *Trends Cell Biol*. 16:181-8.

Gates, J., and M. Peifer. 2005. Can 1000 reviews be wrong? Actin, alpha-Catenin, and adherens junctions. *Cell*. 123:769-72.

Georgiou, M., E. Marinari, J. Burden, and B. Baum. 2008. Cdc42, Par6, and aPKC regulate Arp2/3-mediated endocytosis to control local adherens junction stability. *Curr Biol*. 18:1631-8.

Gumbiner, B., B. Stevenson, and A. Grimaldi. 1988. The role of the cell adhesion molecule uvomorulin in the formation and maintenance of the epithelial junctional complex. *J Cell Biol*. 107:1575-87.

Gumbiner, B.M. 2005. Regulation of cadherin-mediated adhesion in morphogenesis. *Nat Rev Mol Cell Biol*. 6:622-34.

Habas, R., Y. Kato, and X. He. 2001. Wnt/Frizzled activation of Rho regulates vertebrate gastrulation and requires a novel Formin homology protein Daam1. *Cell*. 107:843-54.

Hajra, K.M., and J.R. Liu. 2004. Apoptosome dysfunction in human cancer. *Apoptosis*. 9:691-704.

Hakeda-Suzuki, S., J. Ng, J. Tzu, G. Dietzl, Y. Sun, M. Harms, T. Nardine, L. Luo, and B.J. Dickson. 2002. Rac function and regulation during Drosophila development. *Nature*. 416:438-42.

Hakem, A., O. Sanchez-Sweatman, A. You-Ten, G. Duncan, A. Wakeham, R. Khokha, and T.W. Mak. 2005. RhoC is dispensable for embryogenesis and tumor initiation but essential for metastasis. *Genes Dev*. 19:1974-9.

Hall, A. 2005. Rho GTPases and the control of cell behaviour. *Biochem Soc Trans*. 33:891-5.

Hanahan, D., and R.A. Weinberg. 2000. The hallmarks of cancer. *Cell*. 100:57-70.

Harden, N., M. Ricos, Y.M. Ong, W. Chia, and L. Lim. 1999. Participation of small GTPases in dorsal closure of the Drosophila embryo: distinct roles for Rho subfamily proteins in epithelial morphogenesis. *J Cell Sci*. 112 (Pt 3):273-84.

Harder, J.L., and B. Margolis. 2008. SnapShot: tight and adherens junction signaling. *Cell*. 133:1118, 1118 e1-2.

Harris, K.P., and U. Tepass. 2008. Cdc42 and Par proteins stabilize dynamic adherens junctions in the Drosophila neuroectoderm through regulation of apical endocytosis. *J Cell Biol*. 183:1129-43.

Hay, B.A., T. Wolff, and G.M. Rubin. 1994. Expression of baculovirus P35 prevents cell death in Drosophila. *Development*. 120:2121-9.

Hayashi, T., and R.W. Carthew. 2004. Surface mechanics mediate pattern formation in the developing retina. *Nature*. 431:647-52.

Haynie, J.L., and P.J. Bryant. 1977. The effects of X-rays on the proliferation dynamics of cells in the imaginal disc of *Drosophila melanogaster*. *Rouxs Arch. Dev. Biol.* 183:85-100.

Heasman, S.J., and A.J. Ridley. 2008. Mammalian Rho GTPases: new insights into their functions from in vivo studies. *Nat Rev Mol Cell Biol*. 9:690-701.

Henrique, D., and F. Schweisguth. 2003. Cell polarity: the ups and downs of the Par6/aPKC complex. *Curr Opin Genet Dev*. 13:341-50.

Ho, T.T., S.D. Merajver, C.M. Lapiere, B.V. Nusgens, and C.F. Deroanne. 2008. RhoA-GDP regulates RhoB protein stability. Potential involvement of RhoGDIalpha. *J Biol Chem*. 283:21588-98.

Hollande, F., A. Shulkes, and G.S. Baldwin. 2005. Signaling the junctions in gut epithelium. *Sci STKE*. 2005:pe13.

Homem, C.C., and M. Peifer. 2008. Diaphanous regulates myosin and adherens junctions to control cell contractility and protrusive behavior during morphogenesis. *Development*. 135:1005-18.

Hutterer, A., J. Betschinger, M. Petronczki, and J.A. Knoblich. 2004. Sequential roles of Cdc42, Par-6, aPKC, and Lgl in the establishment of epithelial polarity during Drosophila embryogenesis. *Dev Cell*. 6:845-54.

Igaki, T., R.A. Pagliarini, and T. Xu. 2006. Loss of cell polarity drives tumor growth and invasion through JNK activation in Drosophila. *Curr Biol*. 16:1139-46.

Igaki, T., J.C. Pastor-Pareja, H. Aonuma, M. Miura, and T. Xu. 2009. Intrinsic tumor suppression and epithelial maintenance by endocytic activation of Eiger/TNF signaling in Drosophila. *Dev Cell*. 16:458-65.

Ito, K., W. Awano, K. Suzuki, Y. Hiromi, and D. Yamamoto. 1997. The Drosophila mushroom body is a quadruple structure of clonal units each of which contains a virtually identical set of neurones and glial cells. *Development*. 124:761-71.

Jacinto, A., S. Woolner, and P. Martin. 2002. Dynamic analysis of dorsal closure in Drosophila: from genetics to cell biology. *Dev Cell*. 3:9-19.

Jeanes, A., C.J. Gottardi, and A.S. Yap. 2008. Cadherins and cancer: how does cadherin dysfunction promote tumor progression? *Oncogene*. 27:6920-9.

Johndrow, J.E., C.R. Magie, and S.M. Parkhurst. 2004. Rho GTPase function in flies: insights from a developmental and organismal perspective. *Biochem Cell Biol*. 82:643-57.

Katoh, H., and M. Negishi. 2003. RhoG activates Rac1 by direct interaction with the Dock180-binding protein Elmo. *Nature*. 424:461-4.

Klymkowsky, M.W., and P. Savagner. 2009. Epithelial-mesenchymal transition: a cancer researcher's conceptual friend and foe. *Am J Pathol*. 174:1588-93.

Knust, E., and O. Bossinger. 2002. Composition and formation of intercellular junctions in epithelial cells. *Science*. 298:1955-9.

Kobielak, A., H.A. Pasolli, and E. Fuchs. 2004. Mammalian formin-1 participates in adherens junctions and polymerization of linear actin cables. *Nat Cell Biol*. 6:21-30.

Kondo, S., N. Senoo-Matsuda, Y. Hiromi, and M. Miura. 2006. DRONC coordinates cell death and compensatory proliferation. *Mol Cell Biol*. 26:7258-68.

Larson, D.E., Z. Liberman, and R.L. Cagan. 2008. Cellular behavior in the developing Drosophila pupal retina. *Mech Dev*. 125:223-32.

Le Borgne, R., and F. Schweisguth. 2003. Unequal segregation of Neuralized biases Notch activation during asymmetric cell division. *Dev Cell*. 5:139-48.

Lee, T., and L. Luo. 1999. Mosaic analysis with a repressible cell marker for studies of gene function in neuronal morphogenesis. *Neuron*. 22:451-61.

Leibfried, A., R. Fricke, M.J. Morgan, S. Bogdan, and Y. Bellaiche. 2008. Drosophila Cip4 and WASp define a branch of the Cdc42-Par6-aPKC pathway regulating E-cadherin endocytosis. *Curr Biol*. 18:1639-48.

Liu, A.X., N. Rane, J.P. Liu, and G.C. Prendergast. 2001. RhoB is dispensable for mouse development, but it modifies susceptibility to tumor formation as well as cell

adhesion and growth factor signaling in transformed cells. *Mol Cell Biol*. 21:6906-12.

Magie, C.R., M.R. Meyer, M.S. Gorsuch, and S.M. Parkhurst. 1999. Mutations in the Rho1 small GTPase disrupt morphogenesis and segmentation during early Drosophila development. *Development*. 126:5353-64.

Marinissen, M.J., M. Chiariello, T. Tanos, O. Bernard, S. Narumiya, and J.S. Gutkind. 2004. The small GTP-binding protein RhoA regulates c-jun by a ROCK-JNK signaling axis. *Mol Cell*. 14:29-41.

Martin-Belmonte, F., A. Gassama, A. Datta, W. Yu, U. Rescher, V. Gerke, and K. Mostov. 2007. PTEN-mediated apical segregation of phosphoinositides controls epithelial morphogenesis through Cdc42. *Cell*. 128:383-97.

Martin-Blanco, E., A. Gampel, J. Ring, K. Virdee, N. Kirov, A.M. Tolkovsky, and A. Martinez-Arias. 1998. puckered encodes a phosphatase that mediates a feedback loop regulating JNK activity during dorsal closure in Drosophila. *Genes Dev*. 12:557-70.

Matusek, T., A. Djiane, F. Jankovics, D. Brunner, M. Mlodzik, and J. Mihaly. 2006. The Drosophila formin DAAM regulates the tracheal cuticle pattern through organizing the actin cytoskeleton. *Development*. 133:957-66.

McEwen, D.G., and M. Peifer. 2005. Puckered, a Drosophila MAPK phosphatase, ensures cell viability by antagonizing JNK-induced apoptosis. *Development*. 132:3935-46.

Minden, A., A. Lin, F.X. Claret, A. Abo, and M. Karin. 1995. Selective activation of the JNK signaling cascade and c-Jun transcriptional activity by the small GTPases Rac and Cdc42Hs. *Cell*. 81:1147-57.

Montell, D.J. 2008. Morphogenetic cell movements: diversity from modular mechanical properties. *Science*. 322:1502-5.

Montesano, R., G. Schaller, and L. Orci. 1991. Induction of epithelial tubular morphogenesis in vitro by fibroblast-derived soluble factors. *Cell*. 66:697-711.

Mukai, H. 2003. The structure and function of PKN, a protein kinase having a catalytic domain homologous to that of PKC. *J Biochem*. 133:17-27.

Mulinari, S., M. Padash Barmchi, and U. Hacker. 2008. DRhoGEF2 and Diaphanous Regulate Contractile Force during Segmental Groove Morphogenesis in the Drosophila Embryo. *Mol Biol Cell*.

Nagaraj, R., and U. Banerjee. 2007. Combinatorial signaling in the specification of primary pigment cells in the Drosophila eye. *Development*. 134:825-31.

Nakayama, M., T.M. Goto, M. Sugimoto, T. Nishimura, T. Shinagawa, S. Ohno, M. Amano, and K. Kaibuchi. 2008. Rho-kinase phosphorylates PAR-3 and disrupts PAR complex formation. *Dev Cell*. 14:205-15.

Nejsum, L.N., and W.J. Nelson. 2009. Epithelial cell surface polarity: the early steps. *Front Biosci*. 14:1088-98.

Niessen, C.M. 2007. Tight junctions/adherens junctions: basic structure and function. *J Invest Dermatol*. 127:2525-32.

Niwa, R., K. Nagata-Ohashi, M. Takeichi, K. Mizuno, and T. Uemura. 2002. Control of actin reorganization by Slingshot, a family of phosphatases that dephosphorylate ADF/cofilin. *Cell*. 108:233-46.

O'Brien, L.E., T.S. Jou, A.L. Pollack, Q. Zhang, S.H. Hansen, P. Yurchenco, and K.E. Mostov. 2001. Rac1 orientates epithelial apical polarity through effects on basolateral laminin assembly. *Nat Cell Biol*. 3:831-8.

Olson, M.F., and E. Sahai. 2009. The actin cytoskeleton in cancer cell motility. *Clin Exp Metastasis*. 26:273-87.

Palamidessi, A., E. Frittoli, M. Garre, M. Faretta, M. Mione, I. Testa, A. Diaspro, L. Lanzetti, G. Scita, and P.P. Di Fiore. 2008. Endocytic trafficking of Rac is required for the spatial restriction of signaling in cell migration. *Cell*. 134:135-47.

Perez-Garijo, A., F.A. Martin, and G. Morata. 2004. Caspase inhibition during apoptosis causes abnormal signalling and developmental aberrations in Drosophila. *Development*. 131:5591-8.

Perez-Garijo, A., E. Shlevkov, and G. Morata. 2009. The role of Dpp and Wg in compensatory proliferation and in the formation of hyperplastic overgrowths caused by apoptotic cells in the Drosophila wing disc. *Development*. 136:1169-77.

Ridley, A.J. 2006. Rho GTPases and actin dynamics in membrane protrusions and vesicle trafficking. *Trends Cell Biol*. 16:522-9.

Ryoo, H.D., T. Gorenc, and H. Steller. 2004. Apoptotic cells can induce compensatory cell proliferation through the JNK and the Wingless signaling pathways. *Dev Cell*. 7:491-501.

Sahai, E., and C.J. Marshall. 2002. ROCK and Dia have opposing effects on adherens junctions downstream of Rho. *Nat Cell Biol*. 4:408-15.

Sanz-Moreno, V., G. Gadea, J. Ahn, H. Paterson, P. Marra, S. Pinner, E. Sahai, and C.J. Marshall. 2008. Rac activation and inactivation control plasticity of tumor cell movement. *Cell*. 135:510-23.

Schwamborn, J.C., and A.W. Puschel. 2004. The sequential activity of the GTPases Rap1B and Cdc42 determines neuronal polarity. *Nat Neurosci*. 7:923-9.

Simoes, S., B. Denholm, D. Azevedo, S. Sotillos, P. Martin, H. Skaer, J.C. Hombria, and A. Jacinto. 2006. Compartmentalisation of Rho regulators directs cell invagination during tissue morphogenesis. *Development*. 133:4257-67.

Somogyi, K., and P. Rorth. 2004. Evidence for tension-based regulation of Drosophila MAL and SRF during invasive cell migration. *Dev Cell*. 7:85-93.

Sotiropoulos, A., D. Gineitis, J. Copeland, and R. Treisman. 1999. Signal-regulated activation of serum response factor is mediated by changes in actin dynamics. *Cell*. 98:159-69.

Symons, M., and N. Rusk. 2003. Control of vesicular trafficking by Rho GTPases. *Curr Biol*. 13:R409-18.

Takaishi, K., T. Sasaki, H. Kotani, H. Nishioka, and Y. Takai. 1997. Regulation of cell-cell adhesion by rac and rho small G proteins in MDCK cells. *J Cell Biol*. 139:1047-59.

Tanos, B., and E. Rodriguez-Boulan. 2008. The epithelial polarity program: machineries involved and their hijacking by cancer. *Oncogene*. 27:6939-57.

Tepass, U., and K.P. Harris. 2007. Adherens junctions in Drosophila retinal morphogenesis. *Trends Cell Biol*. 17:26-35.

Uhlirova, M., and D. Bohmann. 2006. JNK- and Fos-regulated Mmp1 expression cooperates with Ras to induce invasive tumors in Drosophila. *EMBO J*. 25:5294-304.

Uhlirova, M., H. Jasper, and D. Bohmann. 2005. Non-cell-autonomous induction of tissue overgrowth by JNK/Ras cooperation in a Drosophila tumor model. *Proc Natl Acad Sci U S A*. 102:13123-8.

Valentin-Vega, Y.A., H. Okano, and G. Lozano. 2008. The intestinal epithelium compensates for p53-mediated cell death and guarantees organismal survival. *Cell Death Differ*. 15:1772-81.

Vega, F.M., and A.J. Ridley. 2007. SnapShot: Rho family GTPases. *Cell*. 129:1430.

Verdier, V., C. Guang Chao, and J. Settleman. 2006. Rho-kinase regulates tissue morphogenesis via non-muscle myosin and LIM-kinase during Drosophila development. *BMC Dev Biol*. 6:38.

Wang, H.R., Y. Zhang, B. Ozdamar, A.A. Ogunjimi, E. Alexandrova, G.H. Thomsen, and J.L. Wrana. 2003. Regulation of cell polarity and protrusion formation by targeting RhoA for degradation. *Science*. 302:1775-9.

Wang, L., and Y. Zheng. 2007. Cell type-specific functions of Rho GTPases revealed by gene targeting in mice. *Trends Cell Biol*. 17:58-64.

Warner, S.J., and G.D. Longmore. 2009a. Distinct functions for Rho1 in maintaining adherens junctions and apical tension in remodeling epithelia. *J Cell Biol*. 185:1111-1125.

Warner, S.J., and G.D. Longmore. 2009b. Distinct functions for Rho1 in maintaining adherens junctions and apical tension in remodeling epithelia. *J Cell Biol*. In press.

Wennerberg, K., and C.J. Der. 2004. Rho-family GTPases: it's not only Rac and Rho (and I like it). *J Cell Sci*. 117:1301-12.

Wheeler, A.P., and A.J. Ridley. 2004. Why three Rho proteins? RhoA, RhoB, RhoC, and cell motility. *Exp Cell Res*. 301:43-9.

Wildenberg, G.A., M.R. Dohn, R.H. Carnahan, M.A. Davis, N.A. Lobdell, J. Settleman, and A.B. Reynolds. 2006. p120-catenin and p190RhoGAP regulate cell-cell adhesion by coordinating antagonism between Rac and Rho. *Cell*. 127:1027-39.

Wilkinson, S., H.F. Paterson, and C.J. Marshall. 2005. Cdc42-MRCK and Rho-ROCK signalling cooperate in myosin phosphorylation and cell invasion. *Nat Cell Biol*. 7:255-61.

Wodarz, A., and I. Nathke. 2007. Cell polarity in development and cancer. *Nat Cell Biol*. 9:1016-24.

Wolff, T., and D.F. Ready. 1991. The beginning of pattern formation in the Drosophila compound eye: the morphogenetic furrow and the second mitotic wave. *Development*. 113:841-50.

Xu, T., and G.M. Rubin. 1993. Analysis of genetic mosaics in developing and adult Drosophila tissues. *Development*. 117:1223-37.

Yamada, S., and W.J. Nelson. 2007. Localized zones of Rho and Rac activities drive initiation and expansion of epithelial cell-cell adhesion. *J Cell Biol*. 178:517-27.

Yang, L., L. Wang, and Y. Zheng. 2006. Gene targeting of Cdc42 and Cdc42GAP affirms the critical involvement of Cdc42 in filopodia induction, directed migration, and proliferation in primary mouse embryonic fibroblasts. *Mol Biol Cell*. 17:4675-85.

Yap, A.S., M.S. Crampton, and J. Hardin. 2007. Making and breaking contacts: the cellular biology of cadherin regulation. *Curr Opin Cell Biol*. 19:508-14.

Yu, W., A.M. Shewan, P. Brakeman, D.J. Eastburn, A. Datta, D.M. Bryant, Q.W. Fan, W.A. Weiss, M.M. Zegers, and K.E. Mostov. 2008. Involvement of RhoA, ROCK I and myosin II in inverted orientation of epithelial polarity. *EMBO Rep*. 9:923-9.

Zhan, L., A. Rosenberg, K.C. Bergami, M. Yu, Z. Xuan, A.B. Jaffe, C. Allred, and S.K. Muthuswamy. 2008. Deregulation of scribble promotes mammary tumorigenesis and reveals a role for cell polarity in carcinoma. *Cell*. 135:865-78.

Zhang, H., and I.G. Macara. 2008. The PAR-6 polarity protein regulates dendritic spine morphogenesis through p190 RhoGAP and the Rho GTPase. *Dev Cell*. 14:216-26.

Zhang, J., K.L. Schulze, P.R. Hiesinger, K. Suyama, S. Wang, M. Fish, M. Acar, R.A. Hoskins, H.J. Bellen, and M.P. Scott. 2007. Thirty-one flavors of Drosophila rab proteins. *Genetics*. 176:1307-22.